POLITECNICO DI TORINO

Collegio di Ingegneria Chimica e dei Materiali

Corso di Laurea Magistrale
in Ingegneria Chimica e dei Processi Sostenibili

Tesi di Laurea Magistrale

Processi di elettrofilatura di polimeri fluorurati per la preparazione di membrane microfibrose

Electrospinning processes of fluorinated polymers for the preparation of microfibrous membranes

Relatori
Ing. *Alessandra Vitale*
Prof.ssa *Roberta Maria Bongiovanni*

Candidato
Mariagrazia Di Falco

Marzo 2020

Lo scopo di questo lavoro di tesi di laurea Magistrale è di produrre membrane fibrose fluorurate attraverso il versatile metodo dell'elettrofilatura e di studiare l'effetto del processo sui prodotti ottenuti. Il lavoro è illustrato in questo manoscritto attraverso tre capitoli principali che sono seguiti da una conclusione riassuntiva raggruppante le riflessioni relative ai risultati ottenuti e gli sviluppi futuri.
Il primo capitolo introduce il processo di elettrofilatura cercando di esporre il metodo e le sue principali applicazioni al giorno d'oggi, in aggiunta descrive i materiali fluorurati sottoposti a questo processo.
L'elettrofilatura è una tecnica semplice ma versatile per la preparazione di fibre polimeriche con diametri compresi tra i nanometri e i micrometri. Risulta adatta ad una vasta gamma di materiali polimerici ed offre una combinazione unica di alto tasso di produzione, basso costo, ampia applicabilità dei prodotti ottenuti e qualità costante delle fibre.
L'Elettrospinning è un processo unico per la sintesi di micro-o-nanofibre a partire da soluzioni polimeriche o da fusi e desta sempre più interesse. Il principio di funzionamento è legato alla formazione di una carica elettrostatica su una gocciolina di soluzione polimerica trattenuta sulla punta di una siringa (un ago), la quale agisce come elettrodo. Un elevato campo elettrico viene applicato alla gocciolina del fluido e nel momento in cui la forza elettrostatica supera la tensione superficiale trattenente la gocciolina, quest'ultima fuoriesce dalla punta della siringa, si deforma in un cono detto cono di Taylor. Dall'apice del cono di Taylor, un getto elettricamente carico viene espulso, quindi, accelerato dal campo elettrico, migra verso un controelettrodo detto collettore. Il getto si estende in direzione del campo elettrico verso tale collettore, inizialmente in linea retta, poi subisce vigorosi movimenti in prossimità del collettore e solidifica rapidamente su di esso, portando alla deposizione di fibre solide. Durante il tragitto in cui le fibre coprono la distanza di percorrenza tra i due elettrodi, se vi è solvente, esso evapora gradualmente portando alla formazione di una fibra solida sul collettore. Il collettore può essere un piano o un tamburo rotante su cui si depositano le fibre prodotte in continuo, quindi esso può essere stazionario o dinamico. Quando si utilizza un piano, si ha la formazione di un mat, ovvero un tessuto/non tessuto formato dalle fibre in ordine casuale. È documentato che la produzione di fibre elettrofilate è influenzata dalle caratteristiche legate alla soluzione e alle condizioni di processo, in particolare.
1. variando la concentrazione del polimero nel solvente (cioè la viscosità della soluzione) il diametro delle fibre e la dimensione dei pori delle membrane risultanti possono essere ottimizzati.
2. la velocità di alimentazione, la tensione applicata, la distanza tra la punta e il collettore relative al processo agiscono sui diametri delle fibre e sulla morfologia delle membrane ottenute.
Sono state prodotte per elettrofilatura fibre di diversa composizione destinate a diversi usi come possiamo trovare in letteratura, esempi tipici sono fibre caratterizzate da proprietà smart o fibre utili per processi con scopi ambientali o ancora utilizzate in elettronica per batterie o in catalisi. In molti casi sono utilizzate anche in ambito biomedico o per la separazione di sostanze come ad esempio acqua e olio da un'emulsione, tale caso specifico potrebbe essere il fine ultimo dei copolimeri fluorurati studiati in questo lavoro.
I polimeri fluorurati sono stati processati tramite elettrofilatura ed in particolare sono validi per la produzione di membrane utili in applicazioni quali filtrazione, applicazioni biomediche o dispositivi elettronici.
I polimeri fluorurati sono interessanti per la loro versatilità, certamente i copolimeri P(VDF) sono polimeri semicristallini con eccezionale resistenza chimica, dielettrici unici, piroelettrici e piezoelettrici. I fluoropolimeri ad alto contenuto di fluoro presentano un'elevata resistenza termica e chimica, un'eccellente inerzia ai solventi, agli idrocarburi, agli acidi e agli alcali, una bassa energia superficiale, basse costanti dielettriche, bassa infiammabilità, basso indice di

rifrazione e assorbimento dell'umidità. Inoltre, la presenza del forte legame C-F ha un impatto fondamentale sull'elevata resistenza all'ossidazione e alla stabilità idrolitica.
I copolimeri del P(VDF) legati all'esafluoropropilene (HFP) e al trifluoroetilene (TrFE) sono ottimi esempi di polimeri elettroattivi dielettrici e mostrano un forte comportamento piezoelettrico e ferroelettrico. Questi polimeri sono versatili per applicazioni quali la desalinazione oppure vengono utilizzati in sensori, batterie, telefoni cellulari ed inoltre risultano essere validi per applicazioni biomediche.
Il P(VDF) rappresenta il più grande volume di fluoropolimeri utilizzati, per l'eccellente combinazione di proprietà e lavorabilità. Parliamo di un materiale di particolare interesse scientifico e tecnologico per le sue eccellenti qualità, tra cui resistenza chimica, buone proprietà meccaniche e in particolare proprietà elettriche come piezo-, piro- e ferroelettricità.
Questo polimero è tipicamente cristallino al 50-70%, caratterizzato da tre principali polimorfi cristallini denominati:
- α, non elettroattiva, non polare; fase ottenuta direttamente dalla fusione alla cristallizzazione dove atomi di idrogeno e fluoro si alternano in modo regolare;
- β, la fase più polare, la conformazione delle catene polimeriche può indurre un significativo momento di dipolo; mostra le migliori proprietà piezo, piro e ferroelettriche, derivanti dalla forte polimerizzazione originata dai legami C-F e dall'orientamento spontaneo dei dipoli nella fase cristallina;
- γ, i dipoli CH_2-CF_2 sono orientati parallelamente l'uno all'altro in modo da avere una conformazione polare intermedia non centrosimmetrica, ottenuta quando il polimero è moderatamente sollecitato o quando si applica la ricottura ad alte temperature.
Le proprietà elettroattive del P(VDF) dipendono fortemente dal contenuto di fase β, dalla microstruttura e dal grado di cristallinità dei campioni, che a loro volta dipendono dalle condizioni di lavorazione. A partire da questo, l'elettrofilatura sembra essere una tecnica preferita per lo sviluppo di membrane elettroattive da P(VDF) poichè agisce sulla struttura cristillina e grazie all'allungamento durante il processo incrementa la fase β.
Il poli (fluoruro di vinilidene-co-esafluoropropilene) P(VDF-HFP) rispetto al fluoruro di polivinilidene P(VDF), presenta ottime proprietà, tra le quali una maggiore solubilità, una maggiore idrofobicità e una migliore resistenza meccanica, grazie alla combinazione con l'HFP.
L'incorporazione della fase amorfa di HFP sull'omopolimero P(VDF) migliora il comportamento meccanico, la resistenza chimica e le proprietà piezoelettriche con una certa riduzione della cristallinità complessiva rispetto al P(VDF). Le unità HFP vengono per lo più escluse dalla struttura cristallina a causa delle loro grandi dimensioni che si spiegano con la presenza dei gruppi CF_3; è inopportuno aumentare il contenuto di HFP di oltre il 5 % molare poiché la cristallinità diminuisce significativamente e le proprietà ferroelettriche finirebbero per scomparire. In particolare nel nostro caso in esame la quantità di HFP presente è al 3,3 % molare.
I copolimeri poli (VDF-co-TrFE) non sono disponibili in commercio, ma vengono sintetizzati ed essi cristallizzano direttamente con una conformazione planare a zig-zag a catena lunga, riproducendo una struttura chimica molto simile alla fase β del P(VDF), dove i forti dipoli risultanti dai gruppi CF_2 aggiunti vengono tutti allineati nella stessa direzione.
Il P(VDF-TrFE-HFP) è un terpolimero semicristallino, caratterizzato da interessanti proprietà elettroattive, risulta un copolimero speciale che forma automaticamente la fase ferroelettrica β attiva senza orientamento meccanico, particolarmente importante per le applicazioni coating che utilizzano processi dove non si impone una orientazione al materiale.
I terpolimeri poli (VDF-co-TrFE-co-MAF) presentano l'unità trifluorometacrilica e hanno interessanti proprietà superficiali con idrofobicità modulabile, ma al contempo mostrano un'ottima adesione su substrati di vetro e metallo. Gli esteri contenenti MAF sono stati

copolimerizzati con successo con le catene di poli (VDF-co-TrFE) tramite tecniche di polimerizzazione radicale in soluzione.
L'aggiunta di MAF ai fluorocopolimeri elettroattivi migliora l'adesione, e apre la strada ad una migliore incorporazione di film sottili elettroattivi da utilizzare in sistemi multistrato per dispositivi elettronici flessibili. La presenza di catene di copolimeri alternati poli (VDF-co-MAF) non influisce sulle proprietà elettroattive dei materiali finali e neanche sulla cristallinità del materiale essendo tali catene amorfe.
Nel capitolo due viene illustrato il lavoro sperimentale eseguito. Sono stati usati questi copolimeri:

1) Il poli (fluoruro di vinilidene-co-esafluoropropilene) indicato come P(VDF-HFP) è un copolimero casuale contenente il comonomero HFP al 5,7% in peso acquistato da Aldrich in forma di pellet.
2) Il terpolimero poli (viniliden fluoruro-Trifluoroetilene-Esafluoropropilene) indicato con l'acronimo P(VDF-TrFE-HFP), sintetizzato tramite terpolimerizzazione in sospensione dei tre in percentuale accurata 65/31/4 (rapporto molare).
3) Il terpolimero fluoruro di vinilidene (VDF) trifluoroetilene (TrFE), acido 2-(trifluorometil) acrilico (MAF) ottenuto con un rapporto molare 66/32/2 tra i monomeri tramite terpolimerizzazione in soluzione.

A partire dai copolimeri esposti sono state ottenute le soluzioni da sottoporre al processo di electrospinning. Tali soluzioni sono state preparate singolarmente miscelando il singolo copolimero, P(VDF-HFP) al 15% in peso in una soluzione DMSO:Acetone 50:50 in peso per un'intera notte a 70 °C e 300 rpm. Per quanto riguarda i terpolimeri, P(VDF-TrFE-HFP) e P(VDF-TrFE-MAF), sono state preparate due soluzioni una al 15% in peso e l'altra al 20% in peso per ogni terpolimero separatamente.
1,00 g di ognuna delle diverse soluzioni preparate è stato utilizzato per produrre film, ottenuti versando la quantità su un vetrino e lasciati essiccare in forno a 40 °C per un giorno.
I film essiccati sono stati utilizzati per le analisi FT-IR e XRD e per la valutazione dei diversi angoli di contatto dei materiali usando acqua ed esadecano come liquidi di contatto.
A partire dalle soluzioni preparate sono state ottenere fibre tramite elettrofilatura analizzando diversi parametri di influenza sul processo al fine di raggiungere i migliori risultati possibili nella produzione delle fibre, riassunti in tabella 1:

Parametri di influenza	**Unità di misura**	**Valori**
Voltage	*kV*	*7* *10* *15* *20*
Distanza tra ago e collettore	*cm*	*10* *15* *20*
Velocità di alimentazione	*ml/h*	*1* *1.5*
Concentrazione del polimero in soluzione	*% wt*	*15* *20*

Tabella 1: Parametri influenti sull'elettrospinning

Tutti i materiali prodotti per elettrofilatura sono stati esaminati tramite microscopio ottico analizzando per ogni copolimero l'azione della tensione, della velocità di avanzamento e della distanza tra i collettori, nel caso di produzione di fibre sono state valutate le distribuzioni delle dimensioni delle fibre. Nella tabella 2 riassumiamo tutti i casi studiati indicando dove e come sono state ottenute le fibre:

ELECTROSPINNING CONDITIONS						
Tensione	*kV*	***10***	***15***			***20***
Distanza	*cm*	***15***	***10***	***15***	***20***	***15***
Velocità di alimentazione	*ml/h*	***1.5***				
P(VDF-HFP) 15% wt		*Sì*	*Sì ma presenta bolle*	*Sì*	*Sì*	*no*
P(VDF-TrFE-HFP) 15% wt		*Sì*	*no*	*Sì*	*no*	*no*
P(VDF-TrFE-MAF) 15% wt		*no*	*no*	*Sì ma presenta bolle*	*Sì*	*no*
P(VDF-TrFE-HFP) 20% wt		*no*	*no*	*Sì*	*no*	*no*
P(VDF-TrFE-MAF) 20% wt		*no*	*no*	*Sì ma presenta bolle*	*no*	*no*
Velocità di alimentazione	*ml/h*	***1***				
P(VDF-HFP) 15% wt		*no*	*no*	*Sì*	*no*	*no*
P(VDF-TrFE-HFP) 15% wt		*no*	*no*	*no*	*no*	*no*
P(VDF-TrFE-MAF) 15% wt		*no*	*no*	*Sì*	*no*	*no*

Tabella 2: riassunto delle condizioni di electrospinning analizzate

Facendo un resoconto dei risultati ottenuti raggruppati nella tabella 2, risulta come condizione migliore per tutti e tre i copolimeri, considerando una concentrazione del polimero in soluzione al 15 %wt, quella caratterizzata dalle suddette condizioni di processo: tensione=15kV; distanza di lavoro=15cm; velocità di avanzamento=1.5ml/h.

Sono inoltre analizzate le diverse distribuzioni delle dimensioni delle fibre come riportiamo nell'istogramma riassuntivo, figura 1. Si evince che i campioni P(VDF-TrFE-HFP) e P(VDF-TrFE-MAF) sono caratterizzati da una distribuzione omogenea delle fibre con diametro medio di circa 1µm invece la distribuzione delle fibre del P(VDF-HFP) è molto più ampia come confermano le immagini al FESEM.

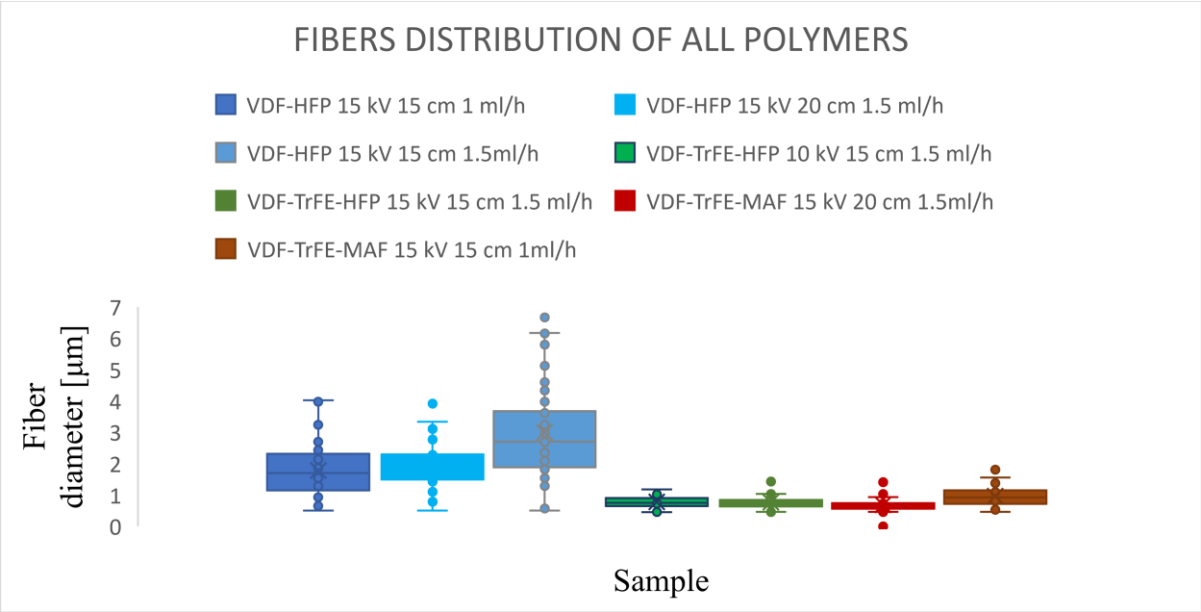

Figura 1:riassunto delle distribuzioni delle dimensioni delle fibre analizzate

Le membrane fibrose ottenute sotto le condizioni operative scelte come migliori sono state osservate al microscopio elettronico a scansione ad emissione di campo (FESEM) e sottoposte ad analisi specifiche al fine di ottenere una caratterizzazione delle superfici e una conoscenza della loro composizione. La spettroscopia infrarossa a trasformata di Fourier (FT-IR) e la diffrattometria a raggi X (XRD) sono state impiegate al fine di conoscere la struttura chimica e la morfologia dei tre polimeri e delle rispettive fibre ottenute. L'analisi termica e il comportamento termico a decomposizione dei materiali sono stati studiati tramite Calorimetria differenziale a scansione (DSC) e analisi termogravimetrica (TGA). Per concludere le fibre ottenute sono state testate a trazione meccanica e le proprietà superficiali sono state analizzate mediante la misura dell'angolo di contatto.

Nel capitolo tre sono riportati i risultati sperimentali. Le fibre ottenute dai risultati migliori (tensione= 15 kV, distanza=15 cm e velocità di alimentazione=1.5ml/h con concentrazione del polimero in soluzione al 15%) sono presentate in Figura 2.

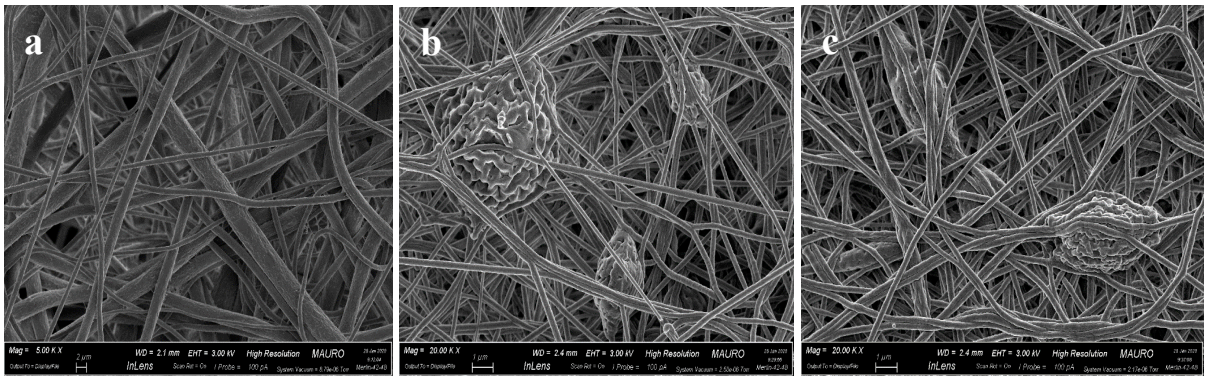

Figura 2: Morfologia dei copolimeri P(VDF-HFP) (a), P(VDF-TrFE-HFP) (b), P(VDF-TrFE-MAF) (c) rispettivamente ad 1 µm, immagini ottenute al FESEM.

La distribuzione delle dimensioni delle fibre del P(VDF-HFP), sulla sinistra (a), risulta essere eterogenea, riscontriamo infatti per la maggior parte dimensioni dell'ordine di 2 µm ma le dimensioni possono variare da 1 a 7 µm. Tale risultato può essere legato all'instabilità dei getti durante la filatura a sua volta causata dalla tensione del processo o dalla soluzione utilizzata per

la filatura. La matrice fibrosa dei terpolimeri, P(VDF-TrFE-HFP) e P(VDF-TrFE-MAF), è invece caratterizzata dalla presenza di bolle di accumulo del materiale, nonostante ciò la distribuzione delle fibre di questi terpolimeri risulta essere omogenea con dimensioni delle fibre di circa 1 micrometro. Tale comportamento, più pronunciato nel caso del P(VDF-TrFE-MAF), potrebbe essere legato a diversi fattori quali: utilizzo di tensioni basse, basse concentrazioni del polimero nella soluzione, presenza di contaminazioni nel polimero o nella soluzione prodotta.
Per migliorare la struttura delle fibre si è deciso di sottoporre ad un preliminare trattamento la soluzione da elettrofiltrare utilizzando filtri di carta Whatman 542 oppure incrementare la concentrazione del polimero al 20% in peso all'interno della soluzione. In entrambi i casi si ottiene un miglioramento nella matrice fibrosa del P(VDF-TrFE-HFP) la quale nei risultati presenta una minore quantità di bolle, sotto le specifiche condizioni di processo scelte (nuovamente 15 cm - 15 kV e 1.5 ml/h).
La struttura del P(VDF-TrFE-MAF) invece presenta anche in questo caso un'ingente quantità di bolle di accumulo sulla matrice fibrosa. In un futuro potrebbe essere utile aumentare oltre il 20% la concentrazione del polimero in soluzione oppure utilizzare diversi valori di tensione per ovviare a tale problema.

Sulle fibre ottenute sono state svolte delle analisi atte a identificare la struttura chimica dei copolimeri.
Dalle analisi ottenute tramite XRD possiamo dire che per quanto riguardo il P(VDF-HFP) come polimero grezzo si riscontrano due segnali riconducibili principalmente alla fase α del P(VDF). La fase α del P(VDF) si ottiene direttamente durante la cristallizzazione, nella trasformazione durante la fase di raffredddamento del materiale a partire dalla fusione. È una fase che presenta un materiale con caratteristiche non polari e non ferroelettriche, tuttavia, se il materiale viene deformato, mostra maggiori proprietà elettriche, legate al gradiente di deformazione. Per quanto riguarda invece il film P(VDF-HFP) essendo stato sottoposto a miscelazione in soluzione e a riscaldamento esso ha già subito un cambiamento di fase presenta infatti valori di 2θ caratterizzanti le fasi gamma e beta come si evince dai dati della letteratura (riportati in tabella 3.8).
La fase α può essere trasformata in altre forme polimorfe sotto l'azione di un campo elettrico o di sollecitazioni meccaniche, è per questo che le fibre del P(VDF-HFP) sono caratterizzate principalmente dalla fase β del P(VDF). La fase β, solitamente ottenuta è attualmente il polimorfo più importante del P(VDF) utilizzato ampiamente per applicazioni piezoelettriche e piroelettriche.
Per questo motivo se esaminiamo la curva delle fibre P(VDF-HFP) individuiamo un solo picco a 2θ=20.24°. Il valore in letteratura rappresenta principalmente la fase β quindi durante la filatura la fase β prevale sulla fase α, a causa del campo elettrico e dell'allungamento meccanico a cui è sottoposto il polimero.
Per quanto riguarda i terpolimeri, l'introduzione di un comonomero trifluoroetilene nella struttura, formando fluoruro di polivinilidene - trifluoroetilene, P(VDF-TrFE), permette la cristallizzazione spontanea in fase β. I legami dati dal monomero TrFE portano ad una ricombinazione della struttura riconducibile alla fase β del P(VDF).
I risultati del P(VDF-TrFE-HFP) pervenuti dall'XRD confermano questo comportamento, difatti sotto forma di fibra, film e polimero grezzo identifichiamo picchi con valori 2θ di circa 20°, caratterizzanti il normale copolimero ferroelettrico P(VDF-TrFE) principalmente in fase β.
Nel terpolimero P(VDF-TrFE-MAF), il monomero MAF amorfo agisce come difetto casuale nel copolimero P(VDF-TrFE) in modo che la spaziatura tra le catene sia più grande di quest'ultimo. I risultati delle fibre P(VDF-TrFE-MAF) in figura 3.20(a) presentano nella prima parte un ampio picco associabile alla parte amorfa del polimero, invece il picco caratteristico a 2θ= 20° rappresenta la fase beta ma in questo caso essa presenta un'intensità inferiore rispetto

a quella degli altri copolimeri a causa della quantità di catene amorfe presenti. Dai valori 2θ relativi a film e polimero grezzo notiamo la presenza delle fasi β e γ con valori paragonabili al P(VDF-co-TrFE): film(3.20b)=19,6°, polimero grezzo(3.20c)=19,29°.
In conclusione di questa analisi possiamo dire che le membrane fibrose, ottenute a partire dai tre copolimeri, sono caratterizzate principalmente dalla fase β, presentano quindi buone proprietà piezo e ferroelettriche da renderle valide per future applicazioni.
Le fibre ottenute sono sottoposte a FT-IR, analisi specifica al fine di avvalorare i risultati ottenuti per quanto concerne l'analisi della struttura cristallina delle membrane. I risultati riportati in figura 3.21, 3.23, 3.26 nell'elaborato, mostrano gli spettri dei polimeri a temperatura ambiente confrontando direttamente il polimero di partenza (curva arancione) con le fibre ottenute da esso (curva blu). Il confronto degli spettri relativi alle due forme del polimero mostra un andamento molto simile tra copolimero e fibre ma applicando uno zoom della regione 1450 cm^{-1}-550 cm^{-1}, comprendente secondo la letteratura le bande spettroscopiche delle fasi cristalline del P(VDF), è possibile concludere che la fase cristallina β relativa al P(VDF) è maggiormente evidente all'interno delle fibre essendo esse sottoposte a stiro durante l'electrospinning.
Dall'analisi sui copolimeri contenenti TrFE, riscontriamo due picchi caratteristici 1288 cm^{-1} e 850 cm^{-1} assegnati a CF_2 e CH_2 relativi alla fase ferroelettrica cristallina della catena (VDF-co-TrFE), riscontrati in entrambi gli spettri dei terpolimeri.
In aggiunta, nel copolimero P(VDF-TrFE-MAF) gli spettri FT-IR in figura 3.26 sia per il polimero che per le fibre mostrano una banda di assorbimento a 1740 cm^{-1} assegnata al legame carbonilico del MAF. La caratterizzante presenza della fase β nelle fibre dei copolimeri li rende particolarmente ferroelettrici e piezoelettrici per le successive applicazioni.

Studiando il materiale dal punto di vista termico tramite l'analisi al DSC, si individuano le temperature di cristallizzazione e di fusione di ogni materiale. I risultati mostrano che le proprietà termiche e la percentuale di cristallinità presentano valori simili nei polimeri grezzi e sotto forma di fibre rispettivamente per ogni copolimero. Considerando la presenza dei domini ferroelettrici caratteristici, la loro composizione e morfologia nei terpolimeri [P(VDF-TrFE-HFP) e P(VDF-TrFE-MAF)] si determina la temperatura di transizione di Curie, come riportato nelle tabelle rispettivamente 3.11 e 3.12. dove sono presenti anche le temperature di fusione e cristallizzazione e le percentuali di cristallinità di ogni campione.

Le temperature ed entalpie mostrano lievi variazioni tra polimeri e fibre ma possiamo vedere una lieve riduzione della percentuale di cristallinità nelle fibre di ogni rispettivo copolimero.
Per quanto riguarda il comportamento a decomposizione termica viene analizzato tramite la TGA in un intervallo da 25 °C a 800 °C con una velocità di riscaldamento di 10 °C/min, in atmosfera inerte di azoto.
Nella tabella 3 vengon riassunti i risultati ottenuti dai grafici riportando in particolare la temperatura di degradazione alla quale abbiamo la perdita del 5% del materiale, la T alla quale abbiamo la perdita del 10% del materiale, la quantità di materiale residuo alla fine della degradazione termica ed in aggiunta il picco di degradazione riportato nei grafici D-TGA relativi ai polimeri e alle rispettive fibre.

Campioni	T[°C] at 5%	T[°C] at 10%	Materiale residuo	T relativa alla massima degradazione[°C]
POLIMERI				
P(VDF-HFP)	455.2	458.5	12.82%	481.5
P(VDF-TrFE-HFP)	456.3	467.5	2.35%	496.6
P(VDF-TrFE-MAF)	403.3	435	7.55%	486
FIBRE				
P(VDF-HFP)	418.5	458	16.24%	496
P(VDF-TrFE-HFP)	433	461.4	4.93%	487
P(VDF-TrFE-MAF)	401.7	430.9	7.56%	487

Tabella 3: Informazioni generali dell'analisi TGA relative ai polimeri e alle fibre (prima-dopo ES)

Analizzando il comportamento delle fibre si osserva una temperatura di inizio degradazione termica leggermente inferiore per ciascuno dei tre copolimeri, una caratteristica che risulta maggiormente evidente nelle fibre ottenute dai terpolimeri. Questo comportamento potrebbe essere legato alla presenza iniziale di una quantità di solvente non completamente evaporato nelle fibre, condizione più accentuata nel P(VDF-TrFE-MAF).

Al fine di avere una panoramica delle proprietà meccaniche dei materiali sono state svolte prove di trazione a temperatura ambiente, alla velocità di 5 mm/min, sulle membrane fibrose di ogni copolimero. Per ogni verifica sono stati testati almeno tre campioni al fine di avere un risultato accurato e per ogni membrana sono stati calcolati il modulo di Young e l'allungamento a rottura.
Dalle analisi si riscontra che le fibre P(VDF-TrFE-MAF) hanno il più alto modulo di Young sappiamo inoltre che più alto è il valore del modulo di Young, meno deformabile è il materiale.

I risultati vengono riportati in figura 3 dove abbiamo il confronto tra i tre materiali:

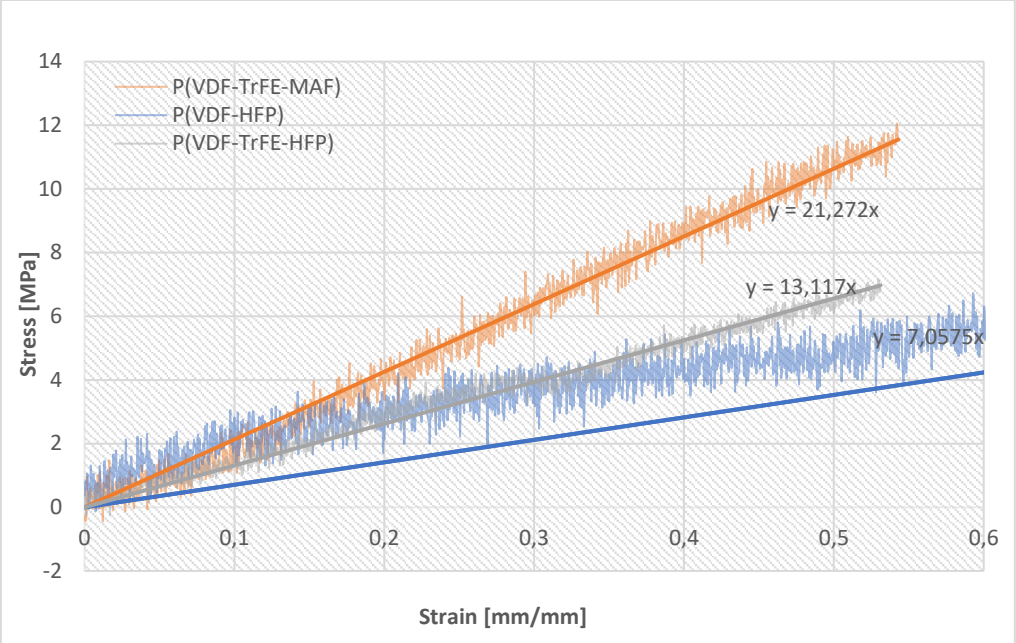

Figura 3: confronto del comportamento meccanico tra i 3 polimeri

In aggiunta è stata analizzata la bagnabilità del materiale calcolando l'angolo di contatto per le fibre e per i film polimerici. Esso viene generalmente misurato al fine di determinare la bagnabilità della superficie, nell'analisi i liquidi scelti per la misurazione dell'angolo sono stati acqua ed esadecano.
I valori degli angoli di contatto di vari campioni sono raggruppati in tabella 4.

ANGOLI DI CONTATTO				
Campioni	***Acqua***		***Esadecano***	
	Fibre	Film essiccati	Fibre	Film essiccati
P(VDF-HFP)	$111° \pm 1°$	$101° \pm 1°$	*0°*	$26° \pm 2°$
P(VDF-TrFE-HFP)	$115.7° \pm 5°$	$107° \pm 5°$	*0°*	$41° \pm 3°$
P(VDF-TrFE-MAF)	$114.5° \pm 5°$	$108° \pm 3°$	*0°*	$40.5° \pm 3°$

Tabella 4: Angoli di misura a contatto determinati su film e fibre

Essi indicano che sia i film sia le fibre sono idrofobici, mentre nei confronti di liquidi apolari la repellenza è esibita solo dai film continui e non dalle membrane fibrose le quali risultano lipofile.
Le membrane fibrose elettrofilate ottenute dai copolimeri fluorurati potrebbero essere di interesse nella separazione delle emulsioni acqua-in-olio.

Table of contents

List of figures and tables

Introduction

The aim of this M.Sc. final year project is to manufacture fluorinated fibrous membranes by electrospinning and to investigate the effect of electrospinning on the properties of the fluorinated materials. This report is composed of three main chapters which are followed by general conclusions summarizing the the results obtained.
Chapter 1 introduces the electrospinning process, describing the method and its main applications nowadays. Electrospinning is a straightforward yet versatile technique for the preparation of polymeric nanofibers with diameters in the range from nanometers to micrometers.[1] The first chapter also deals with fluorinated polymers focusing on their ferroelectric electroactive properties, in order to show the reasons for choosing these polymers for making fibers and fibrous membranes by electrospinning.
Chapter 2 contains the experimental section, it describes the materials and methods for the preparation of the electrospun membranes made of the fluorinated polymers.
Chapter 3 collects the results and reports the investigation on the influence of the different process parameters on the morphology of the fluorinated samples after electrospinning. The first part mainly gathers the images obtained by optical microscopy of the fibers produced; the fibers size distribution is estimated; the identification of the phases and chemical structures that characterize the fibers by FT-IR is reported. Moreover, the results of the physical and chemical properties and the thermal and mechanical characterization of each sample are shown.

1 Background

1.1 Electrospinning

Electrospinning has proven to be a unique method for the preparation of micro/nanofibers from polymer solutions. [2] Suitable for a wide range of polymeric materials, it offers a unique combination of easy fabrication, low cost, wide material suitability, and consistent nanofiber quality, therefore gaining interest over the years.[3]
The resulting fibers with controllable diameters ranging from nanometer to micrometer scale possess unique properties such as a high surface area-to-volume, low density, and high pore volume. These properties make materials more advantageous than conventional materials in energy harvesting, energy conversion, and storage devices. Electrospinning method proves to be suitable for a wide range of polymeric materials, for nanostructured fibers of biopolymers, metals, metal oxides, hydrocarbons, composites. [2] The process can give different results in fiber production and fiber sizes by acting on the process parameters, including applied voltage, power feed rate, collector type, tip to collector distance etc.[4]

1.2 Principle of Electrospinning

Electrospinning involves an electrodynamic process, during which a liquid droplet is electrified to generate a jet, followed by stretching and elongation to obtain fibers.[2]
Electrospinning is a process of fiber formation characterized by an operating principle linked to the electrostatic charge of a droplet of polymer solution held at the tip of a fine capillary that manages to overcome the surface tension that holds it. [2] A high electric field is applied, the solution is extruded from the spinneret producing a droplet, which comes out of the tip, it acts as one of the electrodes. This leads to the deformation of the droplet and finally to the expulsion

of a charged jet from the tip of the cone which accelerates towards the counterelectrode leading to the formation of continuous fibers.
A general electrospinning setup consists of three primary components: a high voltage power supply (usually in the kV range), a syringe with a metallic needle (usually, a needle with blunt tip), that represent the conductive collector and another grounded collector where takes place the deposition of solid fibers [3] as shown in Figure 1.1:

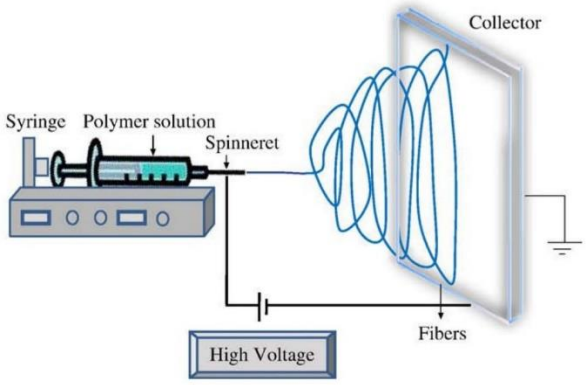

Figure 1.1: Scheme of the electrospinning process. Image from[3].

The shape of the droplet depends on the properties of the liquid. When using a viscous liquid, the tension must reach a critical value capable of generating an electrostatic repulsion strong enough to overcome both the surface tension and the viscoelastic force of the liquid. [2]
During electrification, the electrostatic repulsion between surface charges with the same mark deforms the droplet into a Taylor cone, from which a charged jet is generated. [2] The Taylor cone, in figure 1.2, indicates the start of an electrospinning process, the use of which ensures successful preparation. [4] From the apex of the Taylor cone, the electrically charged jet is ejected, then accelerated by the electric field migrates to the grounded collector. [5] The jet extends in the direction of the electric field towards the collector, initially in a straight line then undergoes vigorous whiplash movements, as in figure 1.2, due to instability. It extends with finer diameters near the collector and rapidly solidifies on it, leading to the deposition of solid fibers.[2]

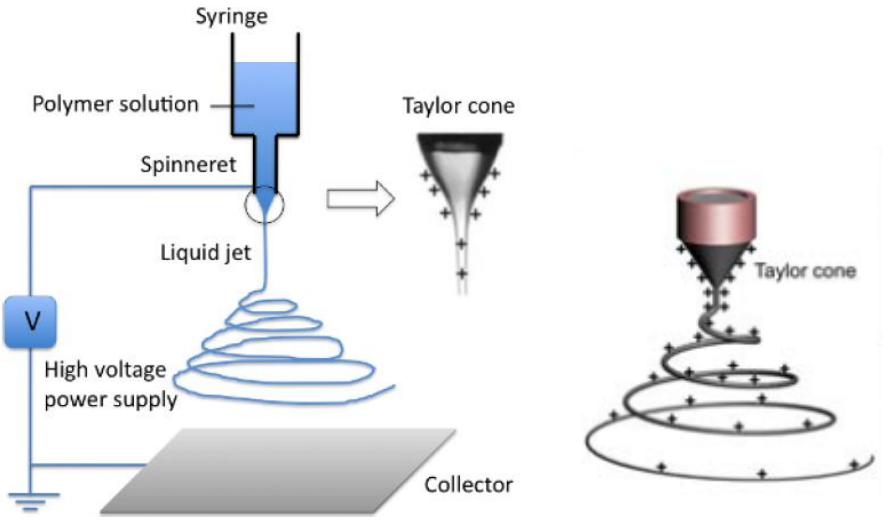

Figure 1.2: A schematic diagram showing the Taylor cone. Image from [6]

During electrospinning, the liquid is typically fed through the spinneret at a constant and controllable rate using a syringe pump. When the voltage rises to the critical voltage required

to generate the jet, more charges start to accumulate on the tip; by increasing the density of the surface charges due to the electrostatic repulsion the shape of the drops starts to deform. The mean radius of curvature of the surface can be represented by the spinneret's internal radius.[6] These parameters utilized to characterize Taylor cone should have a certain relationship with the final nanofibers' diameter, and thus in turn, these electrospinning characteristics can be useful tools for predicting the nanofibers' diameter, for manipulating the working processes, and for ensuring the creating of high quality nanoproducts. [7] The interactions among the charges residing on the jet and the external electric field coordinate different types of instabilities, which grow at different rates and are controlled by the chemical properties of the liquid and the electrospinning parameters. [8] During the process it is essential to control the electrospinning parameters in order to obtain fibers with desirable diameters and structures [7]. Since electrospinning is a fiber formation process that relies on the formation of a jet once the repulsion forces dominate the surface tension of the solution, also solution parameters become prominent factors on the fibers formation.[9] The spinnability of a polymer solution is highly dependent on the solution properties, particularly viscosity, molecular weight [9], surface tension and conductivity [8].

1.3 Characteristic parameters of Electrospinning

As mentioned before, in general, the success of electrospinning a polymer solution, as well as the structure and morphology of the resultant polymer fibers, is determined by a set of parameters. The parameters are commonly divided into three categories: solution parameters (such as polymer concentration and/or viscosity, solution surface tension, and solution conductivity), process parameters (such as feed rate, applied voltage, and tip to collector distance), and ambient conditions (as temperature and humidity). For example a higher voltage gives a bigger diameter, while instable jets give un heterogeneous distribution of fibers. [5]

1.3.1 Process parameters

1.3.1.1 Feed Rate

The feed rate of the solution is a critical factor which influences the diameter and morphology of the fibers. An increase in feed rate leads to a corresponding increase in the diameter of the fibers, whereas a higher feed rate of the solution involves the formation of beads because the time necessary for the evaporation of the solvent is not guaranteed.[7]
For this reason all treatments have a minimum flow rate of the spinning solution, a lower feed rate is more desirable as the solvent gets enough time for evaporation.[6]

1.3.1.2 Applied Voltage

An increase in applied tension increases the electrostatic force on the solution, which favors the elongation of the jet, leading to the reduction of the fiber diameter.[8] Only if a minimum voltage is applied, the process of fiber formation occurs.[6]
Applied voltage may affect some factors such as mass of polymer fed out from the tip of the needle, elongation level of the jet by the electrical force: in this way it influences the morphology of the jets. [9]
In most cases, a higher voltage causes greater stretching of the solution due to the forces in the jet as well as a stronger electric field, and these effects lead to the reduction in the fiber diameter and also rapid evaporation of solvent from the fibers. A higher voltage at the nozzle can produce a larger average electric field strength which helps producing smaller fiber diameters for the large bending frequency. [10]

In most cases, the applied tension influences the diameter of the fiber, however other parameters such as the concentration of the polymer solution and the distance between the tip and the collector are more relevant.[11]

1.3.1.3 Tip to Collector Distance

This parameter has an influence on fiber diameters and morphology, although with a less noticeable effect than the previous ones. The process requires a minimum distance that allows adequate time for the solvent to evaporate before the fibers reach the grounded collector. Usually thinner fibers are produced for a longer distance, but beads can be produced when the distance is too far or too close. [7]

1.3.1.4 Collector type

The collector design determines morphology of electrospun fibers as the way fibers are assembled into structures.[12] Electrospun nanofibers are usually deposited on a grounded solid collector, a stationary collector is able to modulate the distribution of voltage in an electric field and to drive the deposition of nanofibers. The electrostatic forces stretch transversely forming a high density of aligned fibers perpendicularly.[2]
It is possible to find collectors composed of several heterogeneous layers such as metal and insulating characterized by different conductivities that can alter the distribution of electricity in field and consequently direct the nanofibers to the conductive regions. In addition, there are ring metal electrodes that generate radially aligned nanofibers. Rotating collectors (e.g. disc, drum, wheel, cone conveyor) represent instead a class of mobile; for the rotating drum, the force of rotational speed stretches the fibers, resulting in alignment and reduction in diameter.[12] Other unique collectors, like the rotating funnel and rotating rings, are good to generate nanofibers with specific structures.

1.3.2 Solution parameters

1.3.2.1 Polymer concentration

The concentration of the polymer solution used is a very important parameter that affects the process determining the diameter of fibers. Fibers with a smaller diameter can be obtained by reducing the concentration of the polymer solution; when the solution concentration reaches the entanglement concentration beaded fibers are produced. [7]
At very low concentrations, fibers may not form evenly due to low viscosity, resulting in the formation of droplets, a phenomenon known as spraying. On the other hand, at high concentrations also, formation of fibers is not possible, due to high viscosity. Thus, there will be an optimal concentration range for each polymer at which good fibers will be obtained.[6]

1.3.2.2 Electrical conductivity

Solution conductivity is a key parameter affecting beads formation and the size of the fibers obtained. These beads can be observed due to the low conductivity of the solution, which results in an insufficient elongation of the jet of electrical force to produce uniform fibers. Instead, a solution with a higher electrical conductivity facilitates electrospinning polymer fibers with a smaller diameter. [13]

1.3.2.3 Polymer molecular weight

The molecular weight of the polymer can have a significant effect on the rheological and electrical properties, i.e. viscosity, electrical conductivity, dielectric strength and surface tension of the solution [7].
The other important solution parameter that plays an important role for the stabilization of the fiber diameter is the molecular weight of the polymer.[11] It influences the morphology of the

electrospun fiber and in general high molecular weight polymer solutions have been used in electrospinning as they can provide the desired viscosity to have the fiber generation[15]. It has been observed that a solution with too low molecular weight tends to form beads rather than fibers and a high molecular weight solution gives fibers with medium to large diameters.

1.3.2.4 Surface tension

Surface tension, which is a function of solvent compositions of the solution, plays a critical role in the electrospinning process; Different solvents may contribute differently to surface tension.[3]The higher the surface tension the lower the area per unit mass: as a consequence the jet can be changed into droplets [15] thus bead fibers are facilitated. Reducing the surface tension of a solution can promote the formation of smooth fibers without beads. [15]

1.3.2.5 Viscosity

The viscosity of the solution plays an important role in determining the range of concentrations from which continuous fibers can be obtained in electrospinning. [17]
It has been found that with very low viscosity there is no continuous fiber formation and with very high viscosity it is difficult to have the ejection of jets from polymer solutions, thus there is a requirement of optimal viscosity for electrospinning.[16]

1.3.3 Envirnomental parameters

1.3.3.1 Humidity

The porosity of the material may be affected by the external environment, including relative humidity: it influences the evaporation time of the solvent during the travelling distance and also the solidification rate of the solid on the collector. [2] In the electrospinning of polymers it is observed the formation of larger pores with increasing relative humidity.[13]

1.3.3.2 Temperature

Since most electrospun fibers are produced from solution, the dry fiber diameter depends on the removal of solvent, which in turn is influenced by temperature.
The viscosity depends on temperature: there is an inverse relationship between viscosity and temperature. Therefore a higher yield of fibers with smaller diameters can be obtained by increasing temperature as it decreases viscosity of the polymer solutions. [3]

1.4 Electrospinning applications

The application of electrical forces to produce polymer filaments began in the early 1930s.
The chemical modification related to electrospinning of polymer nanofibers imparts new characteristics to the materials, thus extending and enhancing their industrial applications.[6]
Nowadays electrospun polymer fibers are widely used as described below.

1.4.1 Electrospun fibers as smart materials

The extremely large surface area of electrospun nanofibers and the high porosity of their nonwoven mats are instrumental to the incorporation of smart properties.
When polymers reacting to stimuli are electrospun into nanofibers, the transfer of the stimulus is greatly accelerated leading to a faster response of the material. If they are used for drug release, release can be accelerated.[18] Shape memory nanofibers are able to transform in response to an external stimulus, as what have been produced using thermoplastic polyurethane (TPU). The nanofiber membrane can show two different shapes: at room temperature, it typically takes its permanent form, while warming up at temperature above its memory-shape

transition temperature the mat becomes a soft elastomer due to the increased mobility of the polymer.[19]
Owing to the high porosity, a nanofiber-based mat offers much quicker and sharper high strain recovery.[20] Therefore, electrospun nanofibers are superior for use in situations that require immediate control of the shape transition.
The shape-memory fiber mats are largely used in a variety of applications, such as tissue engineering and filtration. For example, a shape-memory mat can control the growth of cells via shape transition to mimic the dynamic environment in the human body.[21] The capability of shape-memory nanofibers can be further extended to make composite materials. The nanofiber-based mat with a superhydrophilic surface is often used as a coating layer to produce a self-cleaning material. Three approaches have been employed to obtain hydrophobic surface: directly electrospinning of a hydrophobic polymer, modifying the rough surface with a low-surface-energy material, and roughening the low-surface-energy polymer. In the first case, the superhydrophobicity of the resultant nanofibers is mainly determined by the macromolecular structures and the functional groups of the polymers. In particular, fluorinated polymers are highly hydrophobic; however, these polymers are difficult to dissolve in a solvent for electrospinning. As such, other spinnable polymers are often blended with them to guarantee electrospinning.[2]

1.4.2 Electrospun fibers for the Environment

Membranes based on electrospun nanofibers are used in filtration [22]: they are superior in removing pollutants quickly and effectively and allow the recovery of precious metals with high selectivity, good recyclability and remarkable stability.
The filtration efficiency can be further improved by reducing the diameter of the fibers and the non-woven polymer nanofiber mats are particularly suitable for use as a face mask, due to their light weight and breathable characteristics.[13]
Electrospun nanofiber mats have been widely analysed as filters for water treatment, due to their ability to simultaneously separate and degrade pollutants in waste water. A greater purification capacity can be achieved when nanofibers are integrated with new active adsorbents: the material can be more selective in removing a pollutant by adding a specific capture agent and/or changing the wettability of the surface. For example, a carpet of nanofibers with a low free surface energy and a rough surface structure can selectively remove oil from polluted water, it is used as an efficient means for oil-water separation during the recycling of crude oil. [24]

1.4.3 Electrospun fibers for Catalysis, Energy and Electronics devices

Applications in solar cells, fuel cells, nanogenerators, hydrogen energy harvesting and storage, lithium-ion batteries, and supercapacitors are reviewed in [4]
Ceramic nanofibers are another class of stable and robust solid media for the immobilization of catalytic nanoparticles: unlike carbon nanofibers, they can resist corrosion for use in electrocatalysis, providing the supported metal nanoparticles with improved stability.[14]
In order to efficiently collect, convert and store energy, a wide variety of devices have been developed such as solar cells, rechargeable batteries and supercapacitors. In order to improve performance, electrospun membranes characterized by specific functional groups are used to selectively transport protons in fuel cells while preventing fuel and oxidant permeation. To this use nanofibers of Nafion mixed with P(VDF) have been proposed.[10]

1.4.4 Electrospun fibers for Biomedical Applications

Over the past two decades, electrospun nanofibers have found widespread use in a variety of biomedical applications including cell migration and/or stem cell differentiation to enhance the

repair or regeneration of various types of tissues, thanks to properties such as porosity, surface functionality, good mechanical properties and biodegradability.[2]
In addition, it has been shown that electrospinning is an extremely promising method for the preparation of scaffolds for tissue engineering (TE).[14] The electrospun fiber mats have been used for cardiac tissue regeneration or vascular tissue regeneration, but also musculoskeletal bone or cartilage tissue regeneration.[2]
The easiest way is to coat the nanofibre surface with bioactive agents such as proteins and growth factors to regulate the interaction between the cells and the underlying fibers.[2]
For example, coating with fibronectin where active microorganisms are applied via nanofibres is useful to improve cell adhesion, uniformity of cell distribution, and increase the rate of cell migration to better guide cell migration along a specific direction.[15]
Thanks to their chemical and biological characteristics, electrospun nanofibres can be designed to control the fate of stem cells by providing a combination of physical characteristics and straight migration of tumor cells. With the use of functional polymers and/or biochemical agents, nanofibers can provide a progressive microenvironment to control stem cell proliferation and specific differentiation.[16]
As mentioned in 1.4.1, the reversible changes in volume and/or surface hydrophobicity make the mats made of thermoresponsive nanofibers ideal for applications related to cell culture, drug delivery, and actuating. [17]
Electrospun nanofibers are advantageous in introducing the property of self-healing, developed using nanofibers with a structure similar to an interconnected network.
The response capability of nanofibers is usually achieved through an electro-responsive material. Since nanofibers allow rapid diffusion of healing agents along the edge of damaged fissures, they garantee shorter healing times.[18]
Piezoelectric nanofibers made of poly(vinylidene-fluoride-trifluoroethylene) have been explored to promote neurite extension: due to their piezoelectric nature, an electrical stimulus can be delivered to cells without an external power source. Conductive polymers allow for excellent control of the electrical stimulus : nanofibers made of conductive polymers have been used to promote neurite extension and/or cell growth.[19]
Many natural and synthetic polymers have been electrospun to produce fine fibers, also for protective clothing: polyacrylonitrile (PAN), polyvinyl alcohol (PVA), poly(methyl methacrylate) (PMMA), polyethylene oxide (PEO), polyethylene (PE), and polypropylene (PP). Poly-L-lactic acid PLLA nanofibers have been widely used for cell culture, electronic devices, tissue scaffolds.[20]
PVDF has attracted much attention due to its properties and molecular structure. [9] Some researchers try to modify the properties of the PVDF fibers by blending with other polymers with varying amounts to fabricate fiber mats for use in lithium batteries or electrospun scaffolds for wound healing or electrospun membranes for distillation but also in biomedical applications. [19]

1.5 Fluorinated polymers

Fluorinated polymers are interesting for their versatility. Fluoropolymers with high fluorine contents exhibit high thermal, chemical, and weather resistance, excellent inertness to solvents, to hydrocarbons, to acids, and to alkali, low surface energy (oil and water repellency), low dielectric constants, low flammability, low refractive index, and moisture absorption. Furthermore, the presence of the strong C-F bond has a powerful impact on the high resistance to oxidation and to hydrolytic stability.[21]
In the following polyvinylidene fluoride, p(VDF), and the p(VDF)-based copolymers used in this work are described in details.

1.5.1 Polyvinylidene fluoride P(VDF)

P(VDF) represents the largest volume of fluoropolymers used because of its excellent combination of properties and processability.[21] P(VDF) is a thermoplastic material [21] of particular scientific and technological interest due to its excellent properties including chemical resistance, good mechanical properties, and, in particular, electrical properties, such as piezo-, pyro-, and ferroelectricity. Its structure is shown in Figure 1.3

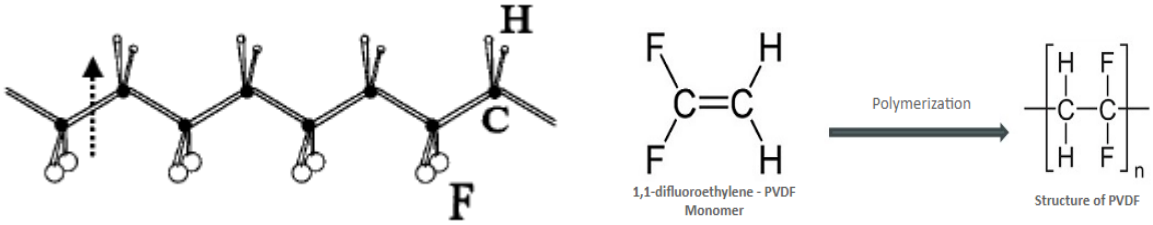

Figure 1.3 : structure of P(VDF). Image from[22]

This polymer is typically 50-70% crystalline with five distinct crystal polymorphs named α, β, γ, δ, and ε; the three main phases are [21]:

- α phase (Figure 1.4) , antiparallel chains, not electroactive, non polar[22], hydrogen and fluorine atoms are alternating in a regular way [21], it is the phase obtained directly from the melt by crystallization;[23]

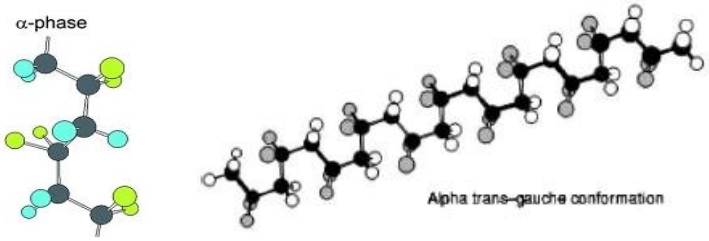

Figure 1.4: α phase where black, white, and gray spheres represent carbon, hydrogen, and fluorine atoms respectively. Image from[21]

- β phase (Figure 1.5), parallel chains where the dipole align, it is the most polar phase, as trans planar zigzag[21]; conformation of the polymeric chains can induce a significant dipole moment; it shows the best piezo-, ferro- and pyroelectric properties,[23] arising from the strong polymerization originating from C-F bonds and the spontaneous orientation of dipoles in the crystalline phase;[21]

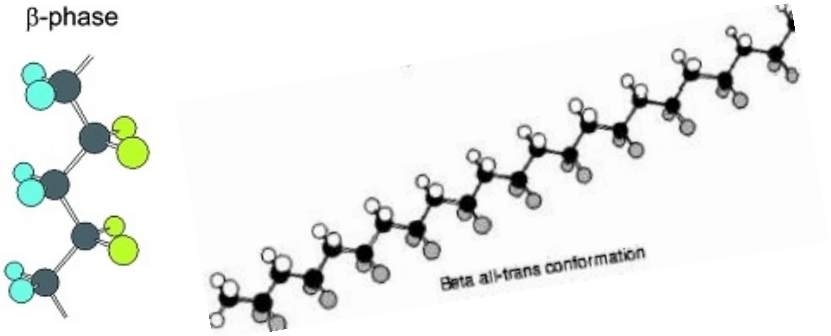

Figure 1.5 : β phase where black, white, and gray spheres represent carbon, hydrogen, and fluorine atoms respectively. Image from[21]

- γ phase, (Figure 1.6) CH_2-CF_2 dipoles are oriented parallel to each other to form a non-centrosymmetric intermediate polar conformation [24] obtained when the polymer is moderately stressed [25] or when high-temperature annealing is applied.

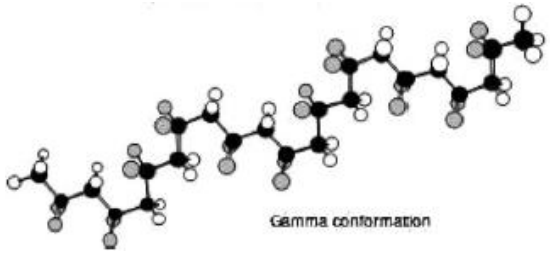

Figure 1.6: γ phase where black, white, and gray spheres represent carbon, hydrogen, and fluorine atoms respectively. Image from[21]

The α form is kinetically the most favorable one because it is formed from the melt directly, while the β form, electroactive, has even superior dielectric permittivity arising from the strong polymerization originating from the C-F bonds and the spontaneous orientation of dipoles in the crystalline phase; it is the most thermodynamically stable form, the transition to the other phases is more difficult.[25] The polar crystalline phase β, which has zigzag (all-trans) conformation of the polymeric chains, is obtained by straining, stretching, or quenching the polymer.
The intermediate polar conformation phase γ is formed when the polymer is moderately stressed or when high-temperature annealing is applied.[20]
The electroactive properties of P(VDF) heavily depend on the β-phase content, microstructure, and degree of crystallinity of the samples, which in turn depend on the processing conditions. Therefore, electrospinning seems to be a suitable technique for the development of electroactive membranes from P(VDF).
Copolymerization usually modifies the symmetry of the polymeric chain and modulates both intramolecular and intermolecular forces so that properties such as melting point, glass transition temperature, crystallinity, stability, elasticity, permeability, and chemical reactivity may be varied within limits.

1.5.2 Polyvinylidene fluoride P(VDF)- Hexafluoropropylene (HFP) copolymer

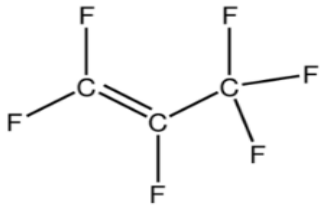

(HFP)

Figure 1.7: Structure of HFP. Image from [26]

Poly(vinylidene fluoride-co-hexafluoropropylene) P(VDF-HFP) is a copolymer obtained by copolymerisation of VDF and HFP (Figure 1.7). Compared with P(VDF), it has better properties, such as higher solubility, higher hydrophobicity and better mechanical strength, owing to the introduction of HFP .[27] Copolymerised with it, the degree of crystallinity is greatly reduced in the chain. [25] In addition, the incorporation of HFP units improves the fluorine content, which results in increased hydrophobicity . [28]

P(VDF-HFP) has been mainly studied for applications in the area of polymer electrolytes, for rechargeable lithium batteries and for the production of membranes for organophilic pervaporation.[23] The incorporation of the amorphous phase of HFP in the PVDF homopolymer improves the mechanical behaviour, chemical resistance and piezoelectric properties with some reduction in overall crystallinity when compared with P(VDF).[29] HFP units are mostly excluded from the crystalline structure because of their large size which is explained by the presence of the CF_3 groups. Usually the HFP content is no more than 5 mol % because the crystallinity decrease significantly and the ferroelectric property eventually disappears.[30]

1.5.3 Polyvinylidene fluoride P(VDF)-Trifluoroethylene (TrFE) copolymer

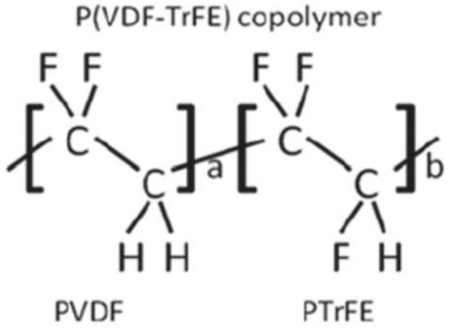

Figure 1.8: Structure of random P(VDF-TrFE). Image from[31]

The P (VDF- TrFE) copolymer (Figure 1.8) is formed by the addition of the trifluoroethylene (TrFE) monomer unit. TrFE increases the steric hindrance favors a higher degree of crystallinity, playing an important role in the phase transition and nucleation behaviors.[27] Random copolymers of VDF and TrFE are semicrystalline thermoplastics, are very good examples of ferroelectric dielectric electroactive polymers. Poly(VDF-co-TrFE) copolymers are not commercially available, but are synthesized in the laboratory; they crystallize directly with an all-trans chain zig-zag planar conformation where the strong dipoles resulting from CF_2 groups are all aligned in the same direction.[32]
P(VDF-TrFE) has a Curie Temperature (T_C) lower than its melting temperature (T_m), which can vary from 55 to 128 °C, depending on the amount of TrFE. [33] : above the Curie temperature, a ferroelectric material becomes paraelectric, losing its most interesting electroactive properties. [30] This F-P phase transition is associated to the crystalline phase change from β to α phase. [21] By comparison, poly(vinylidene fluoride-trifluoroethylene) P(VDF-TrFE), thanks to the bond with TrFE directly crystallizes in the polar β-phase showing a similar conditions to the conditions as PVDF β-phase. The difference in the crystallization behavior is comprehensively investigated between the polymers: PVDF, P(VDF-TrFE), and the resulting blend films. It is found that replacement of the fluoride atom of TrFE monomer in copolymers induces a strong steric obstacle that may alter the crystallization process to become more favorable for nucleation of the PVDF β-phase. [33]

1.5.4 Polyvinylidene fluoride P(VDF)-Trifluoroethylene (TrFE)-Hexafluoropropylene (HFP) copolymer

P(VDF-TrFE-HFP) is a semi-crystalline polymer, characterized by interesting electroactive properties, as it forms the ferroelectric active β phase without mechanical orientation. This is particularly important for applications that use coating process to apply a thin layer of piezoelectric active material on a substrate such as spin coating. On the contrary PVDF, solution processing results in the obtaining of the thermodynamically favored non-polar α-phase.

P(VDF-TrFE-HFP) copolymers are soluble in dimethyl sulfoxide (DMSO), dimethylformammide (DMF) and dimethylacetamide (DMAC), as the PVDF, but also in other solvents, such as methyl ethyl ketone (MEK), cycloexanone and tetrahydrofuran (THF). This large range of solvents is an important advantage for the industrial production processes of the copolymer.

1.5.5 Polyvinylidene fluoride P(VDF)-Trifluoroethylene (TrFE)-2(trifluoromethyl)acrylic acid (MAF) copolymer

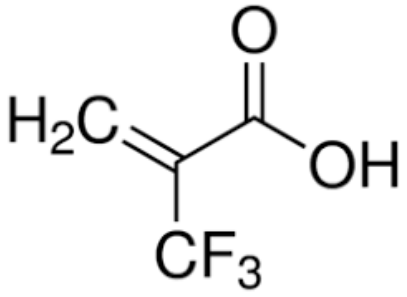

Figure 1.9: Chemical structure of MAF, image from[34]

2-(trifluoromethyl) acrylic acid (MAF) structure is reported in Figure 1.9. MAF-esters have been successfully copolymerized with VDF via radical polymerization in solution.[32]
The poly(VDF-co-TrFE-co-MAF) copolymers present interesting surface properties with tunable hydrophobicity, improving adhesion onto metal and glass substrates, as MAF acts as an adhesion promoting agent.[32] The addition of MAF to electroactive fluorocopolymers improves adhesion and paves the way for better incorporation of fluorinated electroactive thin films in multilayer films for flexible electronic devices.[32]

1.6 Electrospinning of fluorinated (co)polymers and their application

Fluoropolymers have found important developments in modern technologies: construction industry (resistant paints and coatings to UV and graffiti), automotive and aeronautics, petrochemical and chemical engineering (high performance membranes), optical or textile industry and microelectronics.[35]
However, homopolymers are often crystalline, leading to reduced solubility in common organic solvents, they are not easily cross-linked. This is why has increased considerably the generation of fluorinated copolymers (composed of a mixture of comonomers) by inserting (bulky) lateral groups such as to produce clutter in the macromolecule, thus reducing or eliminating the high crystallinity of the homopolymer.[36]
The enhancement of molecular orientation of the P(VDF) micro/nanofibers obtained by electrospinning has attracted the scientific interest. A number of functionalization techniques are available in pilot scale and commercial operation processes that can be economical, profitable, environmentally friendly and reliable in the long term. [8]
Introduction of chemical functional groups into virgin P(VDF) polymer has resulted in novel functional characteristic of significant practical interest. Molecular cross-linking on P(VDF) can be achieved by introducing functional comonomers in order to improve mechanical properties.[24] As nanofibers the production of membranes for various applications, including filtration, biomedical applications, sensors, batteries, cell phones has been proposed. [2] The electrospinning of fluorinated copolymers (for example P(VDF-HFP)[28]) under conditions

suitable to form microparticles interconnected with nanofibers provide a simple single-step method for the formation of superhydrophobic surfaces. [1].
Polyvinylidene fluoride nanofibers are discussed as potential applications of electroactive materials thanks to their properties such as electrical, structural, optical, adhesive and tensile strength, strongly depend on their intrinsic properties and internal molecular structure.
The high thermal stability and mechanical strength of the P(VDF) fibers showed excellent catalytic activity and recycling stability. They, can be embedded or coated with catalyst particles, have thermal stability over a useful temperature range, are inert to many chemical environments, can be superhydrophobic, and thus provide a barrier to aqueous solutions while being porous to gases.
The P(VDF) membranes have potential applications for water treatment, first as a filter but second as a desalination membrane. The inherent dipole charges due to the CH_2-CF_2 repeated monomer units may be useful for separating salt ions from water. [8]
Electrospun polymeric fibers with enhanced molecular orientation, surface textural morphologies, piezo-, pyro-, and ferroelectric properties and high surface-to-volume ratio are potential resources for several novel applications in the fields of micro-nanoscale filtration as water desalination, drug delivery, catalysis, and energy harvesters. [8] P(VDF) membranes are given particular consideration due to their asymmetric morphology which assists in improving the water permeation flux for this reason are also proposed for Membrane distillation. [16]
Batch tests were conducted with Pd supported on P(VDF-HFP) fiber mats were tested as aerosol filter media. Are found to have a remarkable effect during liquid–liquid filtration applications compared to aerosol filtration as the interfacial strength between liquid droplets is much higher in polarized fiber mats compared to relatively smooth fibers.
Blending P(VDF) with inorganic materials to increase adsorption capacity can help in heavy metal ion removal.

2 Materials and Methods

2.1 Materials

2.1.1 Poly (vinylidene fluoride-co-hexafluoropropylene) P(VDF-HFP)

Poly(vinylidene fluoride-co-hexafluoropropylene) random copolymer (Figure 2.1), with 3.3% mol HFP comonomer (5.7% wt), was purchased from Aldrich in pellet form.

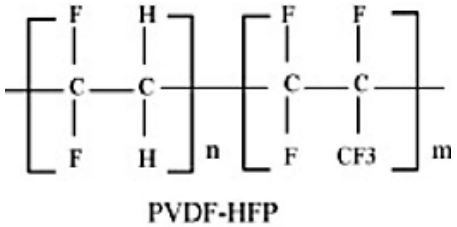

PVDF-HFP

Figure 0.1: polymerization scheme to obtain P(VDF-HFP). Image taken from[37].

2.1.2 Polyvinylidene fluoride- Trifluoroethylene -Hexafluoropropylene P(VDF-TrFE-HFP)

The terpolymer P(VDF-TrFE-HFP) was synthesized by Ameduri's team at Institut Charles Gerhardt, Ecole Nationale Supérieure de Chimie de Montpellier (France), following the procedure described in [30]. It was produced by suspension terpolymerization of VDF, TrFE and HFE monomers in accurate percentage 65/31/4 (molar ratio).[30] The simplified structure is in Figure 2.2.

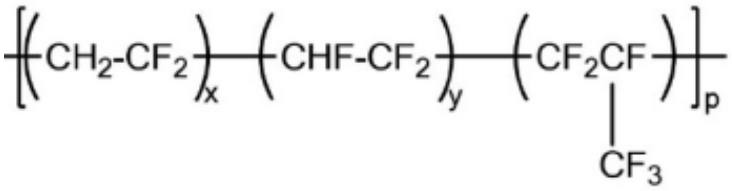

Figure 0.2: Structure of P(VDF-TrFE-HFE). Image taken from [30].

2.1.3 Polyvinylidene fluoride P(VDF)-Trifluoroethylene (TrFE)-(trifluoromethyl)acrylic acid (MAF)

The terpolymer P(VDF-TrFE-MAF) (Figure 2.3) was synthesized by Ameduri's team at Institut Charles Gerhardt, Ecole Nationale Supérieure de Chimie de Montpellier (France), following the procedure described in [32]VDF and TrFE were terpolymerized with 2 mol % of MAF as an adhesion-promoting monomer. The terpolymer was synthesised with a 66/32/2 molar ratio among monomers. The radical terpolymerization of VDF, TrFE, and MAF was performed in solution in DMC. [32]

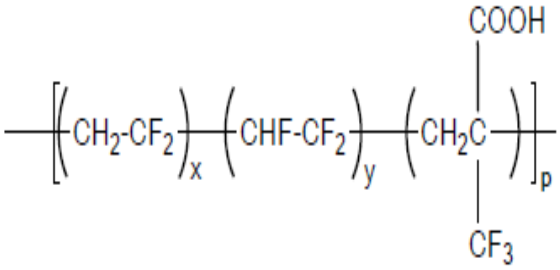

Figure 0.3: Structure of P(VDF-TrFE–MAF), obtained by radical solution. Image taken from [32]

2.1.4 Solvents

The fluorinated polymers, prior to electrospinning, are dissolved in different solvents purchased from Sigma-Aldrich and used as received:DMSO,a highly polar organic reagent that has exceptional solvent properties for organic and inorganic chemicals.[38]
Acetone (CH_3COCH_3), also called 2-propanone or dimethyl ketone, which is an organic solvent of industrial and chemical significance, the simplest and most important of the aliphatic (fat-derived) ketones. Pure acetone is a colourless, somewhat aromatic, flammable, mobile liquid that boils at 56.2 °C (133 °F). [39]
All other chemicals were purchased from Sigma-Aldrich.

2.2 Preparation of polymer solutions

The polymers are added to a solution of DMSO-Acetone [50:50] in weight (wt:wt). In order to obtain the solutions for the electrospinning process, polymer and solvents are mixed together continuously at 300 rpm at a temperature of 70 °C overnight in a glass beaker sealed with parafilm, until complete polymer dissolution (i.e., until a homogeneous and transparent solution is obtained). P(VDF-HFP) copolymer is dissolved in the solvents with 15% wt concentration.
Meanwhile two different solution concentrations are used with the other two copolymers, P(VDF-TrFE-HFP) and P(VDF-TrFE-MAF): 15% wt and 20 wt% concentration.

2.3 Film preparation

Casted films were prepared to compare the electrospinning process effects on polymers properties. The polymer solutions were poured onto a glass slide and let them dried in the oven at 40 °C for one day.

2.4 Fibers preparation by electrospinning

E-fiber electrospinning system SKE apparatus (Figure 2.4) was employed in horizontal setup, with high voltage power supply, a programmable syringe pump (syringe tip diameter of 1 mm) and a stationary collector. The experiments were done in a range of voltage between 7 to 20 kV, with a constant feed rate of 1.5 ml/h or 1 ml/h. In addition three different distances between the needle tip and the collector were tested: 10 cm, 15 cm and 20 cm.
The concentration of the polymer in the solution was 15% wt or 20% wt, in order to evaluate how much it affected on the formation of the fibers and the fibers size distribution. All conditions used are listed in Table 2.1.

Figure 0.4: Electrospinner SKE

Parameters	Units	Value
Voltage	*kV*	*7* *10* *15* *20*
Distance	*cm*	*10* *15* *20*
Feed rate	*ml/h*	*1* *1.5*
Concentration of polymer in solution	*% wt*	*15* *20*

Table 0.1: Process conditions used for electrospinning experiments

2.5 Characterization methods

2.5.1 Optical microscopy

The morphology of the electrospun polymer mats was controlled through the optical microscope Olympus BX53M (figure 2.5).

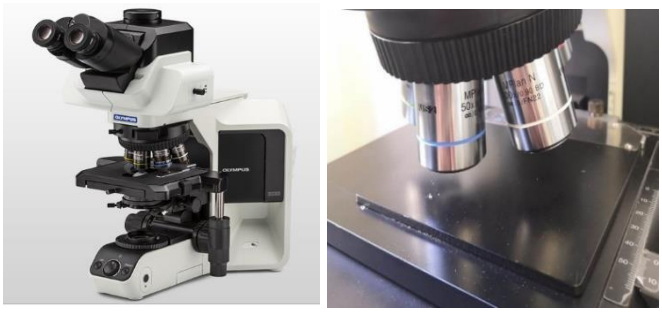

Figure 0.5: Optical microscope OLYMPUS BX53M

The size distribution of the fibers was evaluated by taking at least 60 measurements on three samples, using 50X magnification.

2.5.2 Field Emission Scanning Electron Microscope (FESEM)

The morphology of the fibrous membranes was examined by a ZEISS Merlin FESEM instrument (figure 2.6). Prior to FESEM examination samples were coated with a thin Cr film via sputtering, carried out by QUORUM Q150T ES.

Figure 0.6: ZEISS Merlin FESEM

2.5.3 X-ray Diffraction (XRD)

X-ray PANAlytical X'Pert diffractometer using CuKα1 radiation produce the overall orientation of crystallographic planes of the samples in the range of angles between 0° and 30°, (figure 2.7).

Figure 0.7 : X' Pert ray diffractometer. Image from [40]

We analyse the raw material, film and fibers to obtain the characterization of the crystalline phases of all copolymers to study the crystallinity. The crystalline phases are identify thanks to 2θ and correlated to specific crystalline phase thank to literature; In addition starting from these value it is possible to calculate the interchain spacing (d) using Bragg's law:

$$d = \frac{n\lambda}{2\,sen(\theta)}$$

Where λ is the wavelength and θ angle of diffraction.[41]

2.5.4 IR spectroscopy

The Fourier transform infrared (FT-IR) analysis were performed on a ThermoScientific Nicolet iS50-FTIR spectrometer equipped with a Smart ITX Diamond Attenuated Total Reflection (ATR) accessory, (figure 2.8).

Figure 0.8: Thermo Scientific iS50 FTIR

The polymer spectra are obtained at room temperature in the 4000–450 cm^{-1} range, with 32 scans per spectrum.

2.5.5 Differential Scanning Calorimetry (DSC)

The thermal properties were examined by DSC-Differential Scanning Calorimetry (model DSC1 STARe), figure 2.9.

Figure 0.9: DSC (Mettler Toledo)

DSC measurements are performed on 10-15 mg samples of original polymer and its fibers. The conditions for analysis are as follows: the sample, initially at -50°C, is heated up to 200 °C with a rate of 10°C/ min and kept at this temperature for 5 min; then it is cooled down to -50° C with the same rate used in the first step, 10°C/min, and kept at this temperature for 5 min; in a second cycle the temperature of the sample is increased until the value of 200 °C, with a rate of 10 °C/min, then is decreased to room temperature.
The maximum endothermic value related to the DSC is assumed to be the melting temperature of the sample individuate by T_m from the integrate under the curve of this peak we calculate the enthalpy of fusion (H_m). In the same way the maximum exothermic value is related to crystallization temperature T_{CR} [42] and under the curve related to this peak we calculate the integrate to abtian the crystallization enthalpy (H_{CR}). The results of DSC for terpolymers containing TrFE shows also the passage between ferro to paraelectric material and vice versa individuate thanks to the Curie transition temperature, another peak of graph and when we integrate the area under this peak we obtain H_C
In addition with the fusion enthalpy obtained from each sample and the ΔH_{100} evaluated to the specific material 100% crystalline it is possible to calculate the percentage of crystallinity using the following formula:

$$X_c\ (\%) = \frac{\Delta H_f}{\Delta H_{100}} * 100\%$$

2.5.6 Thermogravimetric Analysis (TGA)

Figure 0.10: TGA METTLER TOLEDO

Thermogravimetric Analysis (TGA) were carried out on 10-15 mg samples of original polymer and its fibers on a TGA/SDTA851 apparatus from METTLER TOLEDO instruments in a range from 25 °C to 800 °C with a heating rate of 10 °C/min, under nitrogen flow rate of 60 ml/min.

2.5.7 Mechanical properties

The mechanical properties of the fibers of the copolymers prepared were investigated using an Instron dynamometer (model 3366), figure 2.11, at room temperature in tensile mode at a tensile speed of 5 mm/min.

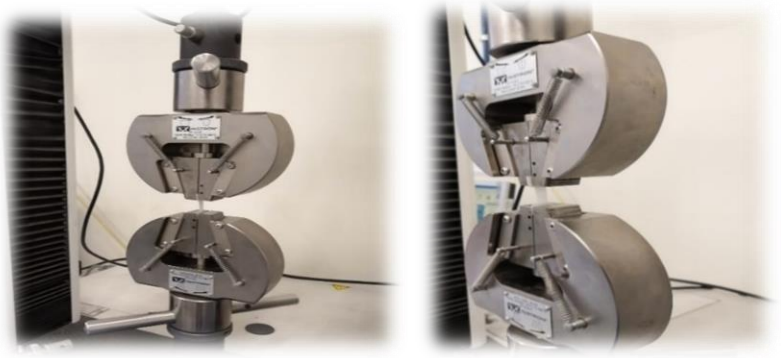

Figure 0.11: INSTRON MODEL 3366

For tensile tests samples were carefully peeled off from the electrospinning collector. They were cut in rectangles with length of 20 mm and 10 mm width. For each polymer at least three replicates were tested.

2.5.8 Contact angle measuring

The contact angle that a liquid drop establishes on a solid surface characterizes the solid's wetting behavior with said liquid. Static contact angle measurements were carried out with FTA 1000 (First Ten Angstroms) drop shape instrument (Figure 2.12)

Figure 0.12: FTA 1000 drop shape instrument

Measurements were carried out with (triply distilled) water and hexadecane on sample as fibers and films, at room temperature. The volume of the drop was maintained as 5 µl in all cases using a microsyringe and a release rate of 2.5 µl/s was used. Measurements were repeated three times within the same sample to check the accuracy.

3 Results and discussion

This chapter reports the investigation on the influence of the different process parameters on the properties of the fluoro-copolymers electrospun membranes. During the electrospinning process different process parameters, such as voltage and working distance, which are considered as the most important parameters for the properties control of the studied polymers subjected to electrospinning according to the articles in the literature [32], were examined. Moreover, the feed rate was modified to evaluate its effect on the size fiber distribution.
The fibrous mats are analysed by optical microscopy; the fibers size distribution is estimated; the identification of the phases and chemical structures that characterize the fibers by FT-IR is reported, and XRD analyses are carried out to investigate the stretching-induced behaviour of the copolymers during electrospinning. [30]
In addition the results of the physical and chemical properties and the thermal and mechanical characterization of the fluorinated electrospun membranes are shown.

3.1 Fibers morphology and size distribution: the effect of spinning conditions

By electrospinning under pre-established conditions, fibers from fluorinated copolymers are obtained; in order to choose the optimum process conditions, we analyze the fibrous membranes under microscope (i.e., optical microscope and FESEM), investigating their morphology.

3.1.1 P(VDF-HFP) fibers

Solutions of P(VDF-HFP) 15%wt are used for the electrospinning experiments; to find the best spinning conditions, we change the applied voltage, the working distance (between the needle tip and the collector) and the feed rate, as reported in Table 2.1.

i. Effect of voltage

Keeping the working distance and the feed rate at 15 cm and 1.5 ml/h, respectively, the voltage is varied between 7 and 20 kV. When a voltage of 7 kV is applied, electrospinning is not feasible as the jet is not constant and fibers cannot be obtained, therefore we can assume that the use of voltages lower than 10 kV cannot assure electrospinning. Instead in figure 3.1 we can compare the fibers obtained with an applied voltage of 10, 15 and 20 kV.

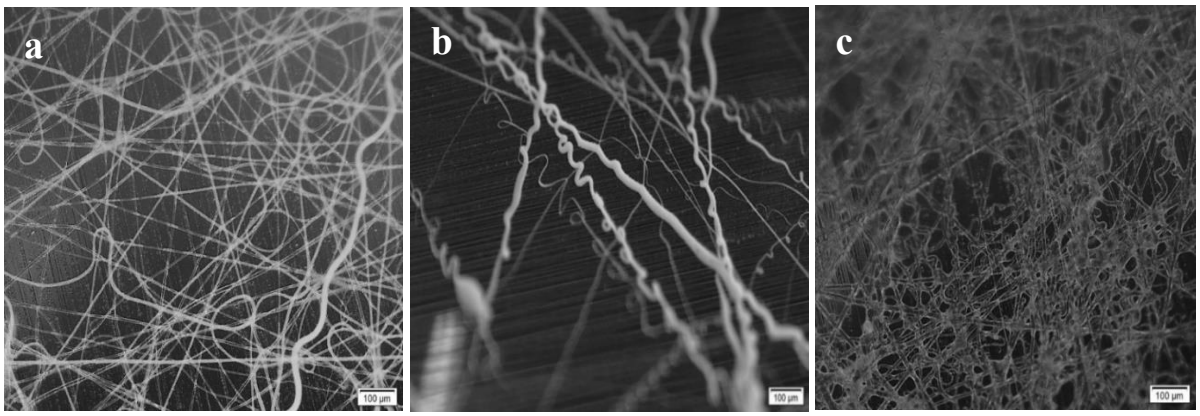

Figure 3.1: Optical microscope images of P(VDF-HFP) fibers electrospun with different voltage conditions: a) 10 kV, b) 15 kV, c) 20 kV, keeping fixed working distance = 15cm, feed rate = 1.5 ml/h and solution concentration = 15%wt

The experiments carry out with a voltage of 10 kV and 15 kV seem to be the best because the production of well-defined fibers is assured. Instead, when 20 kV are applied, a membrane with fuzzy fibers is obtained.

ii. Effect of distance between needle and collector

Keeping the voltage at 15 kV and the feed rate at 1.5 ml/h, the effect of the working distance (10 or 20 cm) is analysed. As shown in Figure 3.2, it can be deduced that the working distance of 20 cm gives wider fibers, but defect-free and homogeneous membranes. In fact, when 10 cm are set, defects, especially in the form of beads, are obtained.

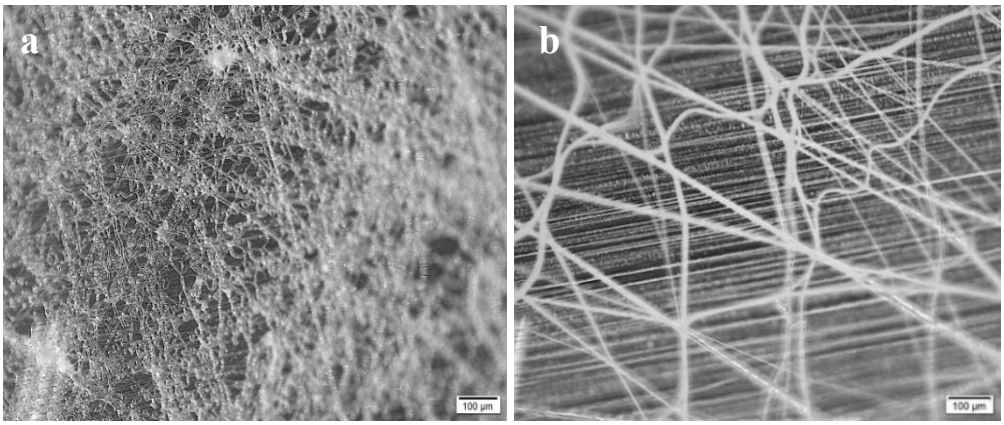

Figure 3.2: Optical microscope images of P(VDF-HFP) fibers electrospun with different working distances: a) 10 cm, b) 20cm, keeping fixed voltage = 15 kV, feed rate = 1.5 ml/h and solution concentration = 15%wt

iii. Effect of feed rate

Keeping the voltage at 15 kV and the working distance at 15 cm, the effect of the feed rate on the electrospun fibers is analysed. The production of regular fibers can also be obtained reducing the feed rate to 1 ml/h, as can be observed in figure 3.3.

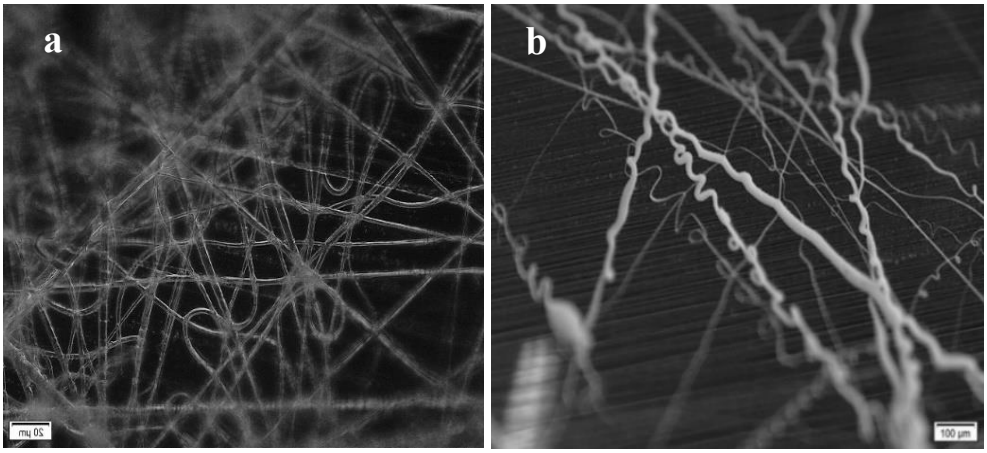

Figure 3.3: Optical microscope images of P(VDF-HFP) fibers electrospun with different feed rate: a) 1ml/h, b) 1.5 ml/h, keeping fixed voltage = 15 kV, working distance = 15 cm and solution concentration = 15%wt

iv. Fibers size distribution

After analysing the effect of the different process parameters on fibers production, the fibers size distribution is evaluated in order to define the best electrospinning conditions. In figure 3.4

we can observe the size distribution of the P(VDF-HFP) fibers obtained under different electrospinning conditions. While table 3.2 summarises the measured average size of the different fibers obtained under different electrospinning conditions.

a)

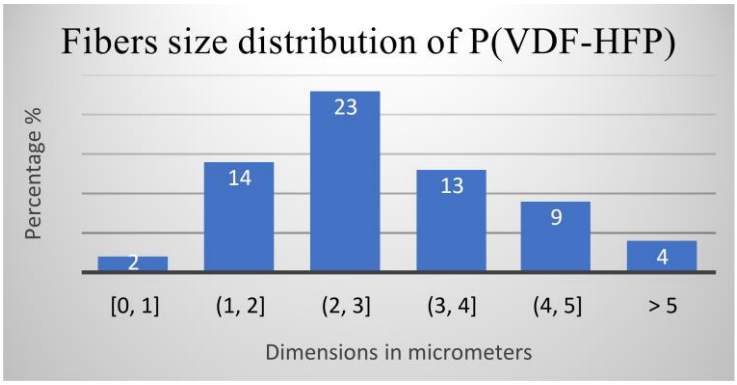

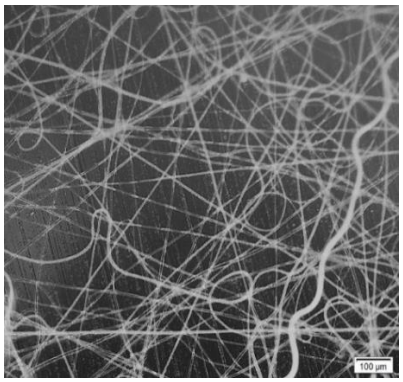

b)

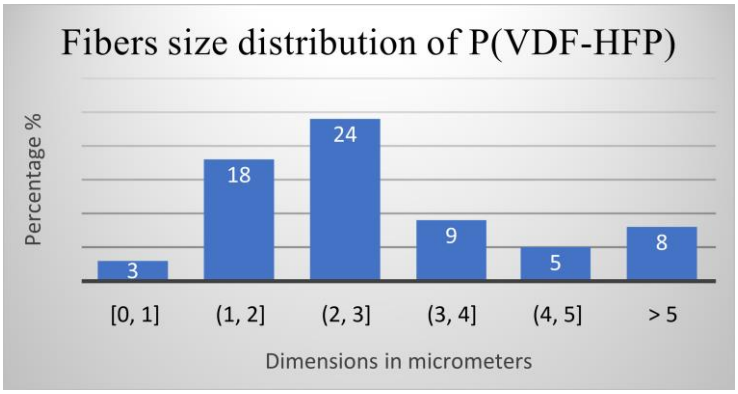

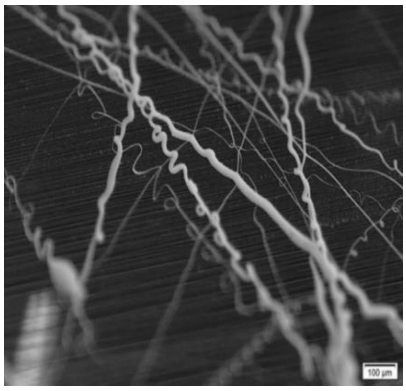

c)

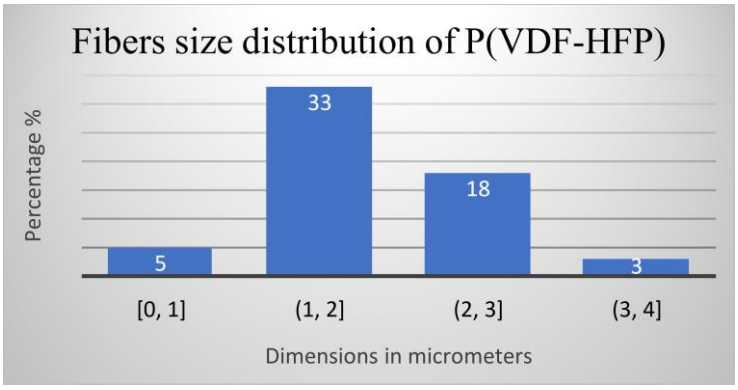

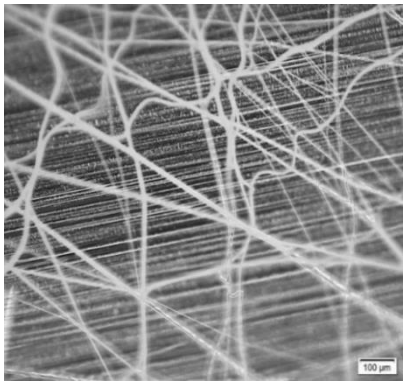

d)

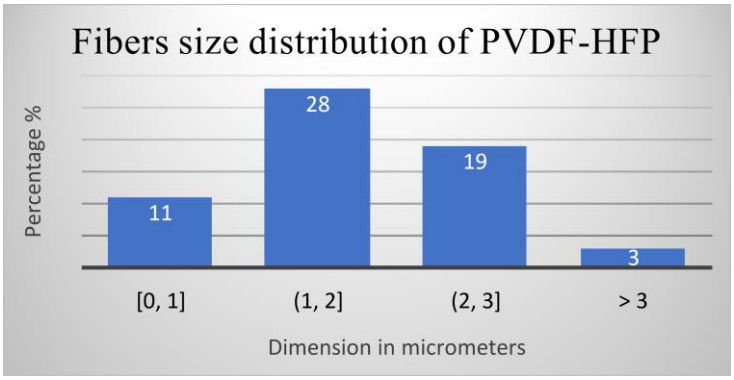

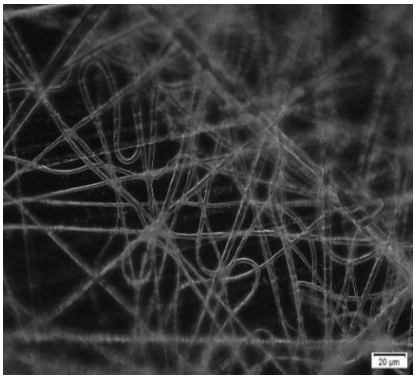

Figure 3.4: Morphology of the P(VDF-HFP) fibrous membranes and size distribution of electospun fibers obtained with: (a) voltage of 10 kV, working distance of 15cm, feed rate of 1.5 ml/h, (b) voltage of 15 kV, working distance of 15 cm, feed rate of 1.5 ml/h, (c) voltage of 15

kV, working distance of 20 cm, feed rate of 1.5 ml/h, (d) voltage of 15 kV, working distance of 15 cm, feed rate of 1 ml/h

Electrospinning conditions	**10kV-15cm-1.5ml/h**	**15kV-15cm-1.5ml/h**	**15kV-20cm-1.5ml/h**	**15kV-15cm-1ml/h**
Average size	$1.8 \pm 1\mu m$	$2.9 \pm 0{,}5\mu m$	$2 \pm 0.5\mu m$	$2.95 \pm 0{,}2\ \mu m$

Table 3.1: Comparison between the P(VDF-HFP) fibers size obtained with different electrospinning conditions

From data reported in figure 3.4 and table 3.1 it can be deduced that the best conditions also in terms of fibers size distribution are the two at 15 kV and 1.5 ml/h with a travelling distance of 15 cm or 20 cm, and also the one with a feed rate of 1 ml/h. In these conditions we can assure constant electrospinning and efficient production of fibers of P(VDF-HFP) with a good fibers size distribution. The optimum electrospinning conditions for P(VDF-HFP) are listed in table 3.2.

Distance between needle tip and collector	15 cm	20 cm	15 cm
Feed rate	1.5 ml/h	1.5 ml/h	1 ml/h
Voltage	15 kV	15 kV	15 kV

Table 3.2: The best electrospinning conditions for P(VDF-HFP)

v. FESEM analyses

The morphology of the fibrous membranes is confirmed by FESEM analyses (figure 3.5). By using a feed rate of 1.5 ml/h, a voltage of 15 kV, a working distance of 15 cm and solution concentration of 15%wt, P(VDF-HFP) generates fine fibers without producing accumulations or beads on the membrane. However, probably due to the unstable jet during the spinning process, an heterogeneus distribution of fibers is generated. Most fibers are about 2 μm, but there are also smaller or larger fibers up to 7 μm.

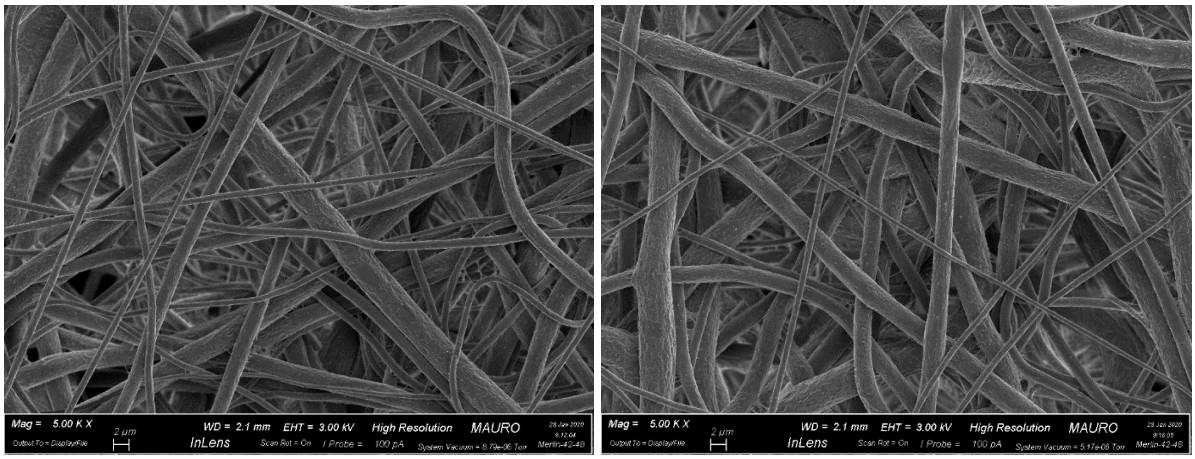

Figure 3.5: P(VDF-HFP) electrospun membrane morphology obtained by FESEM. Electrospinning conditions: feed rate = 1.5 ml/h, voltage = 15 kV, working distances = 15cm and solution concentration = 15%wt

3.1.2 P(VDF-TrFE-HFP) fibers

Similarly, the electrospinnng of P(VDF-TrFE-HFP) copolymer using different process conditions (table 2.1) is conducted and the membrane morphology is analysed by microscopy.

i. Effect of voltage

Figure 3.6 represents the fibers of P(VDF-TrFE-HFP) obtained using a feed rate of 1.5 ml/h, a distance between the needle and the collector of 15 cm and a voltage of 10 kV, 15 kV and 20kV respectively.

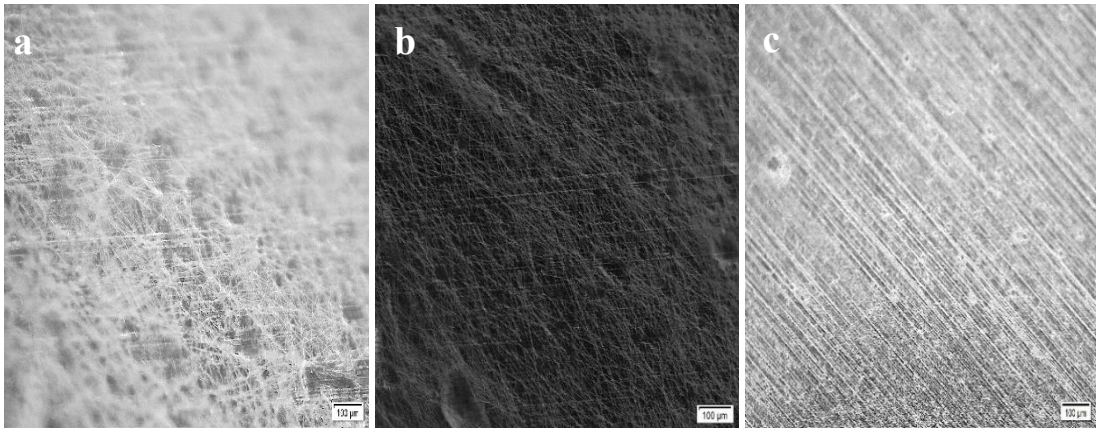

Figure 3.6 : Optical microscope images of P(VDF-TrFE-HFP) fibers electrospun with different voltage conditions: a) 10 kV, b) 15 kV, c) 20 kV, keeping fixed working distance = 15 cm, feed rate = 1.5 ml/h and solution concentration = 15%wt

From the images of figure 3.6 we can observe that the production of regular fibers is obtained using two different voltage condition :10 kV and 15 kV. Instead electrospinning cannot be assured in the case a voltage of 20 kV is used.
The same results are obtained also when different working distances or different feed rates are employed.

ii. Fibers size distribution

In figure 3.7 the fiber size distribution analysis for the two efficient electrospinning conditions that give production of fibers (i.e., working distance of 15 cm, feed rate of 1.5 ml/h, voltage of 10 and 15 kV) is reported.

a)

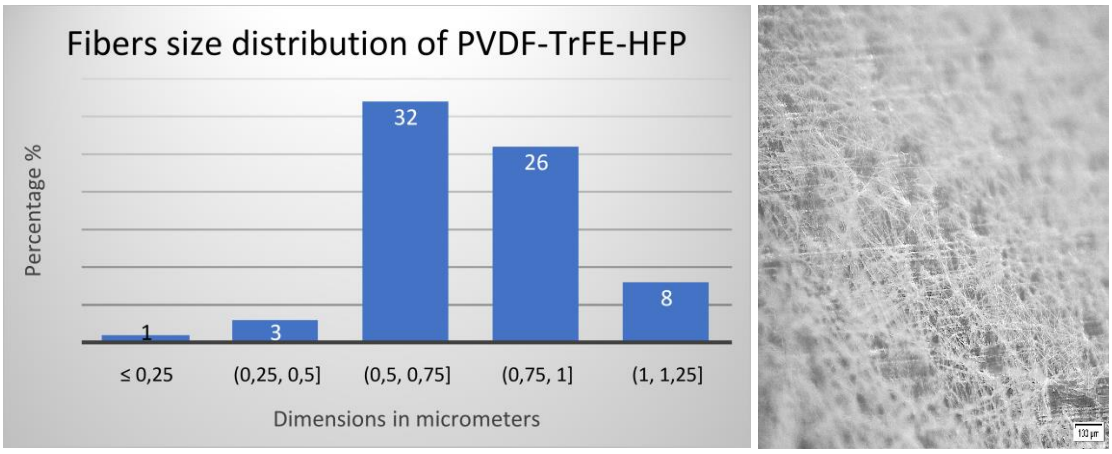

b)

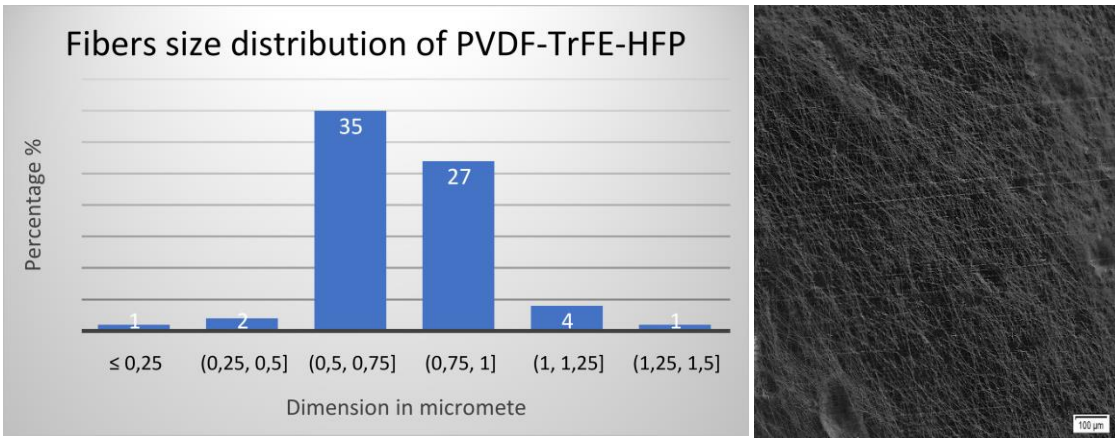

Figure 3.7: Morphology of P(VDF-TrFE-HFP) fibrous membranes and size distribution of electrospun fibers obtained with: (a) voltage of 10 kV, working distance of 15 cm, feed rate of 1.5 ml/h, (b) voltage of 15 kV, working distance of 15 cm, feed rate of 1.5 ml/h

Analyzing the size distribution it can be deduced the average size of the fibers, as reported in table 3.3.

Electrospinning conditions	**10kV-15cm-1.5ml/h**	**15kV-15cm-1.5ml/h**
Average size	$from\ 0.8 \pm 0.2\mu m$	$from\ 0.7 \pm 0.5\mu m$

Table 3.3: Comparison between the P(VDF-TrFE-HFP) fibers size obtained with different electrospinning conditions

Both conditions used for the production of P(VDF-TrFE-HFP) fibers ensure good results in terms of electrospun fibers and fibers size distribution, they are collected in table 3.4. However, as also shown in figure 3.7, in some areas of the membrane it is possible to find defects in the form of beads.

Distance between needle tip and collector	15 cm	15 cm
Feed rate	1.5 ml/h	1.5 ml/h
Voltage	10 kV	15 kV
Concentration of polymer in solution	15% wt	15% wt

Table 3.4: The best electrospinning conditions for P(VDF-TrFE-HFP)

iii. FESEM analyses

In figure 3.8 the FESEM analyses of the P(VDF-TrFE-HFP) electrospun membrane obtained using a feed rate of 1.5 ml/h, a voltage of 15 kV, a working distance of 15 cm and a solution concentration of 15%wt are reported. A problem related to the production of these fibers can be observed. In fact, in some areas of the membrane it is possible to find beads and this could be related to a low concentration of polymer in the solution, a too high applied tension, some accumulation in the solution, or a residue of previous processing in the polymer. For this reason some modifications have been applied in order to try to reduce these defects.

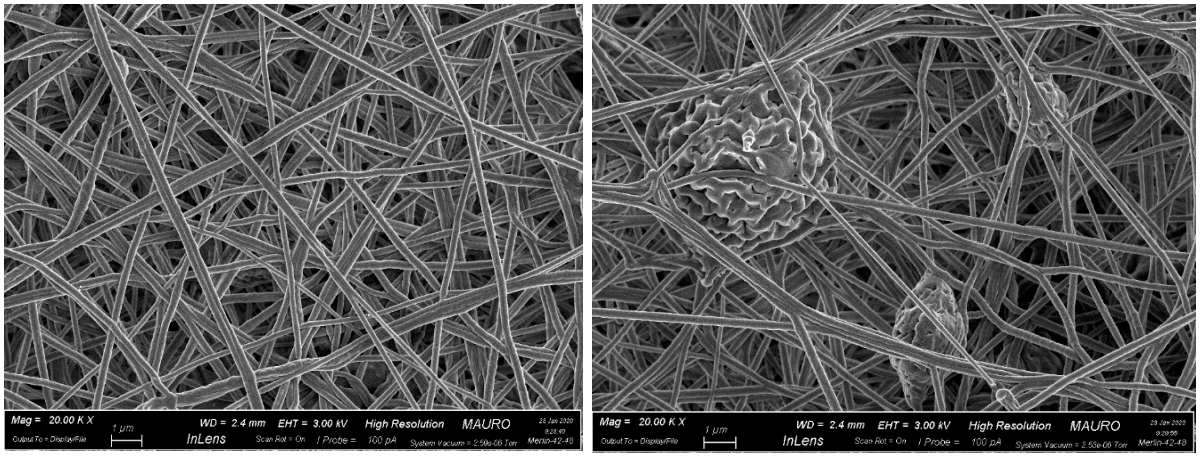

Figure 3.8: P(VDF-TrFE-HFP) electrospun membrane morphology obtained by FESEM. Electrospinning conditions: feed rate = 1.5 ml/h, voltage = 15 kV, working distances =15 cm and solution concentration = 15%wt

iv. Effect of solution filtration and solution concentration

In order to obtain electrospun mats without beads and thus improve the fibrous membranes producted, two ways could be tested:

1. filter the copolymer solution before electrospinning by using a filter paper (Whatman, 542)
2. increase the weight concentration of copolymer in the solution (to 20 % wt)

Since in the P(VDF-TrFE-HFP) electrospun membranes the presence of beads is significant, the first strategy is attempted. Thanks to the solution filtration, we get a clear improvement of the P(VDF-TrFE-HFP) membranes, as homogeneous fiber membranes with less beads are formed (figure 3.9). Moreover, the fiber size distribution remains similar with respect to the non-filtered samples.

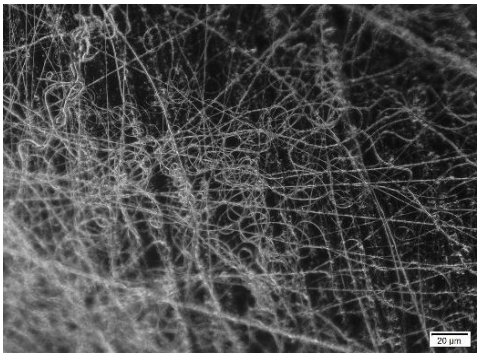

Figure 3.9: Optical microscope image of P(VDF-TrFE-HFP) fibers electrospun with 1.5 ml/h, 15 cm and 15 kV spinning conditions using a filtered polymer solution.

The second strategy (i.e., increase the concentration of the copolymer in the solution to 20 %wt) is attempted. As shown in figure 3.10, where the concentration is increased to 20%wt, also in this case a significant improvement in the membrane uniformity is obtained. Moreover, the size distribution of the fibers remains homogeneous with values in the order of 1µm.

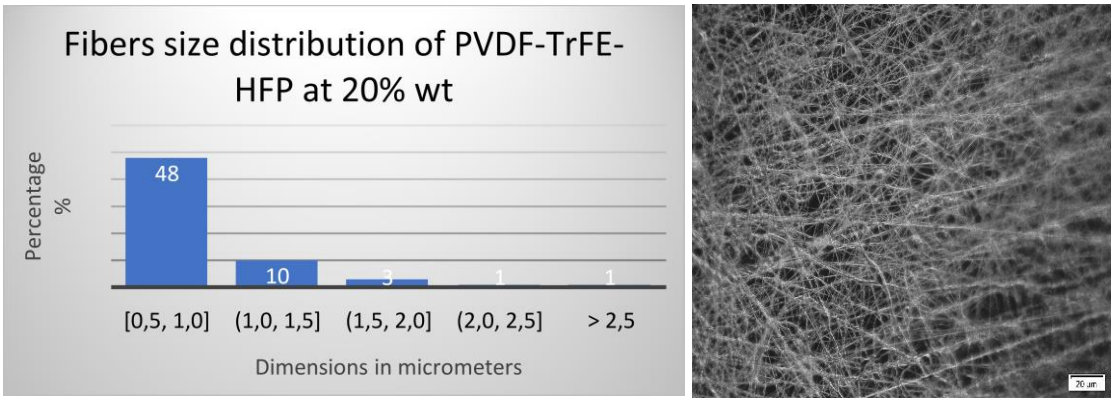

Figure 3.10: Morphology of P(VDF-TrFE-HFP) fibrous membranes and size distribution of electrospun fibers obtained with voltage of 15 kV, working distance of 15 cm, feed rate of 1.5ml/h, and a solution concentration of 20 % wt

3.1.3 P(VDF-TrFE-MAF) fibers

The electrospinning of the P(VDF-TrFE-MAF) copolymer is conducted at the conditions reported in table 2.1.
The P(VDF-TrFE-MAF) polymer require more analyses to find good spinning conditions because in many cases a consistent amount of beads was produced.

i. Effect of voltage

Starting from a distance between the needle and the collector of 15 cm as in the previous cases and a feed rate of 1.5 ml/h, a voltage between 10 and 20 kV is tested. In figure 3.11 we observe that the use of voltages of 10 kV and 20 kV does not assure electrospinning, as fibers cannot be formed. Instead the condition of 15 kV gives fibers, even though on the membrane there is a consistent presence of beads.

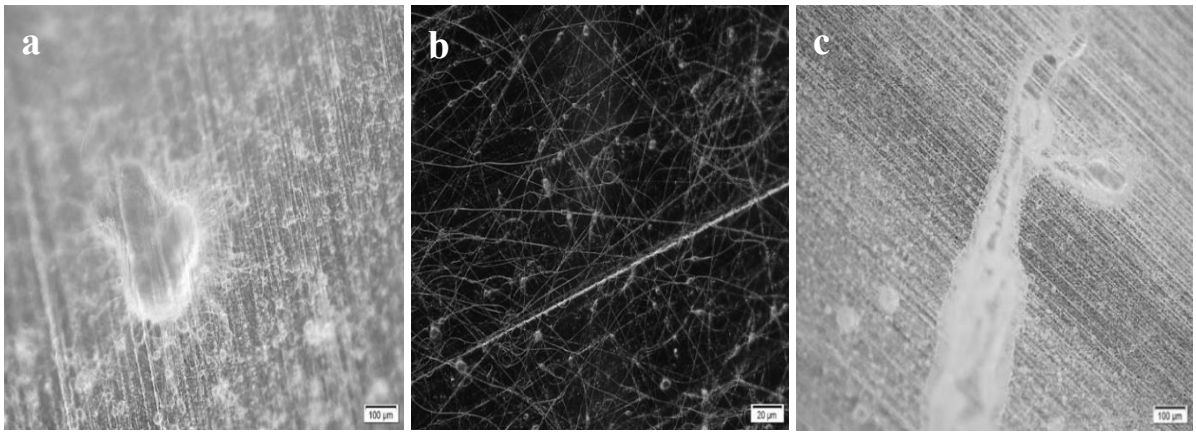

Figure 3.11: Optical microscope images of P(VDF-TrFE-MAF) fibers electrospun with different voltage conditions: a) 10 kV, b) 15 kV, c) 20 kV, keeping fixed working distance = 15 cm, feed rate = 1.5 ml/h and solution concentration = 15%wt

ii. Effect of distance between needle and collector and feed rate

For the P(VDF-TrFE-MAF) copolymer, the feed rate and the working distance are also changed. Figure 3.12 reports three conditions under which fibers formation is achieved, but the membranes also include the presence of beads in all cases.

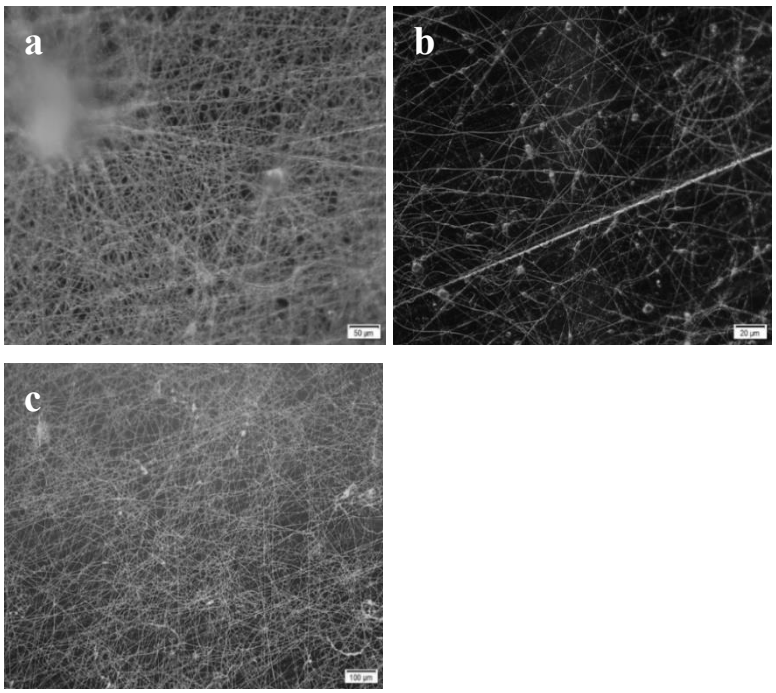

Figure 3.12: Optical microscope images of P(VDF-TrFE-MAF) fibers electrospun with different working distance: a) 15 cm, b) 20 cm, keeping fixed voltage = 15 kV, feed rate = 1.5 ml/h and solution concentration = 15%wt. In c) feed rate = 1 ml/h, voltage = 15 kV, working distance = 15cm, solution concentration = 15%wt

iii. Fibers size distribution

The fiber size distributions are analysed for the conditions that guarantee the production of fibrous mats and the results shown in figure 3.13 are obtained. The average fiber size values are summarised in table 3.5.

a)

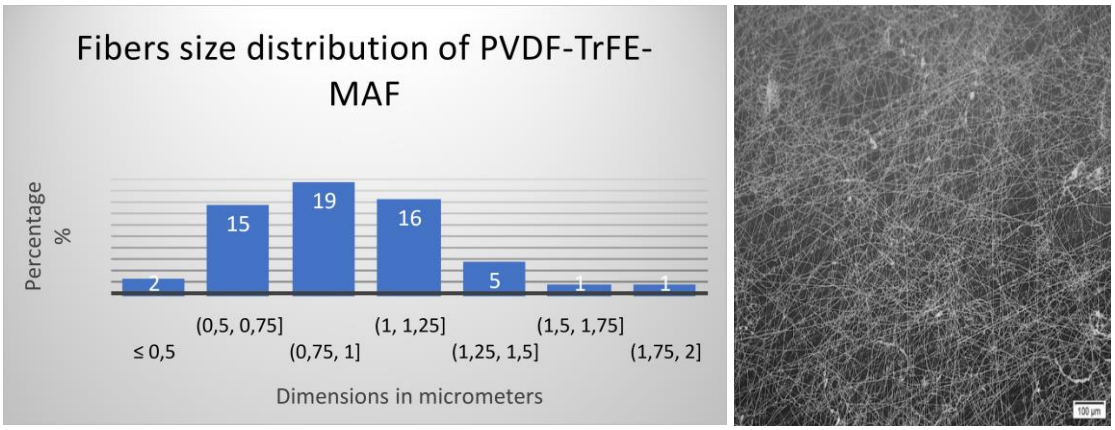

b)

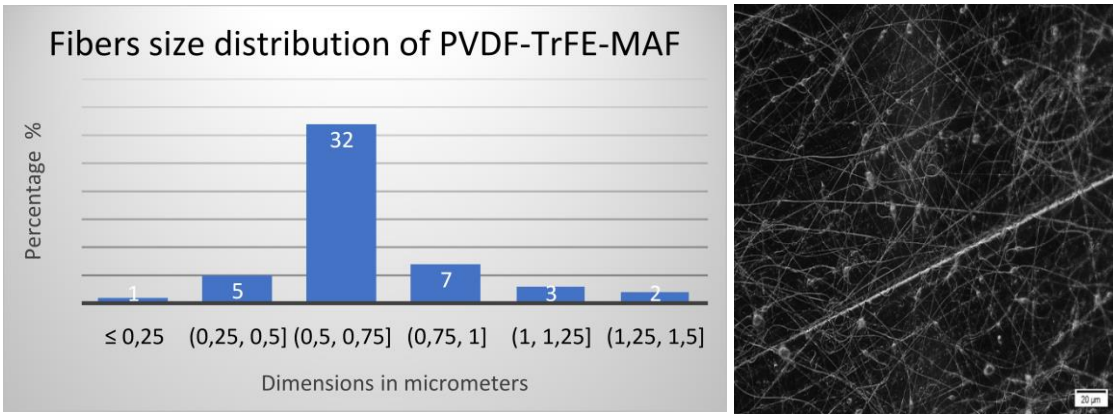

c)

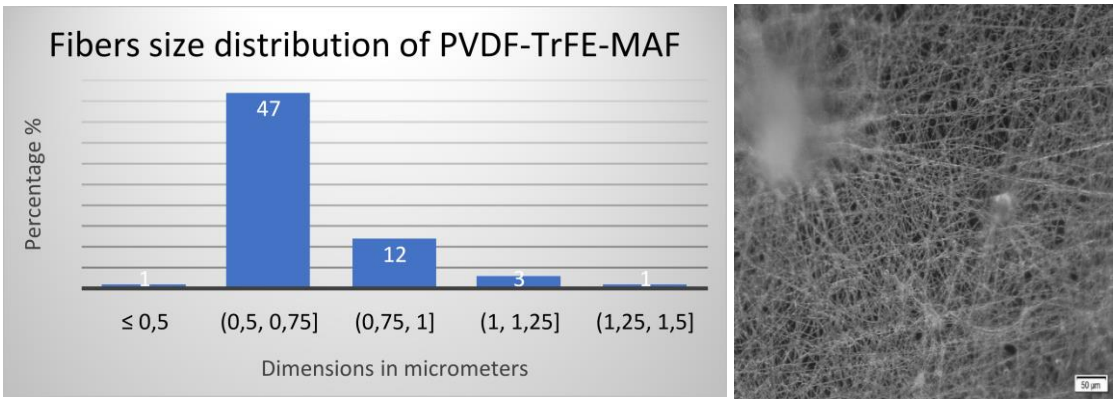

Figure 3.13: Morphology of P(VDF-TrFE-MAF) fibrous membranes and size distribution of electospun fibers obtained with: a) voltage of 15 kV, working distance of 15 cm, feed rate of 1 ml/h, b) voltage of 15 kV, working distance of 15 cm, feed rate of 1.5 ml/h, c) voltage of 15 kV, working distance of 20 cm, feed rate of 1.5 ml/h

Electrospinning conditions	**15kV-15cm-1ml/h**	**15kV-15cm-1.5ml/h**	**15kV-20cm-1.5ml/h**
Average size	1 ± 0.5 µm	$from\ 0.75 \pm 0.25$ µm	$from\ 0.5 \pm 0.25$ µm

Table 3.5: Comparison between the P(VDF-TrFE-MAF) fibers size obtained with different electrospinning conditions

These results suggest that the presence of both defects fine and uniform fibers is obtained by electrospinning P(VDF-TrFE-MAF) terpolymer.

For the P(VDF-TrFE-MAF) polymer the best process conditions are summarized in table 3.6.

Distance between needle tip and collector	15 cm	20 cm
Range of feed rate	1 ml/h	1.5 ml/h
Voltage	15 kV	15 kV
Concentration of polymer in solution	15% wt	15% wt

Table 3.6: The best electrospinning conditions for P(VDF-TrFE-MAF)

iv. FESEM analyses

From the results of FESEM analyses shown in figure 3.14, we can see that P(VDF-TrFE-MAF) mats are characterized by an homogeneous distribution of fibers, but the presence of beads can clearly be noticed.

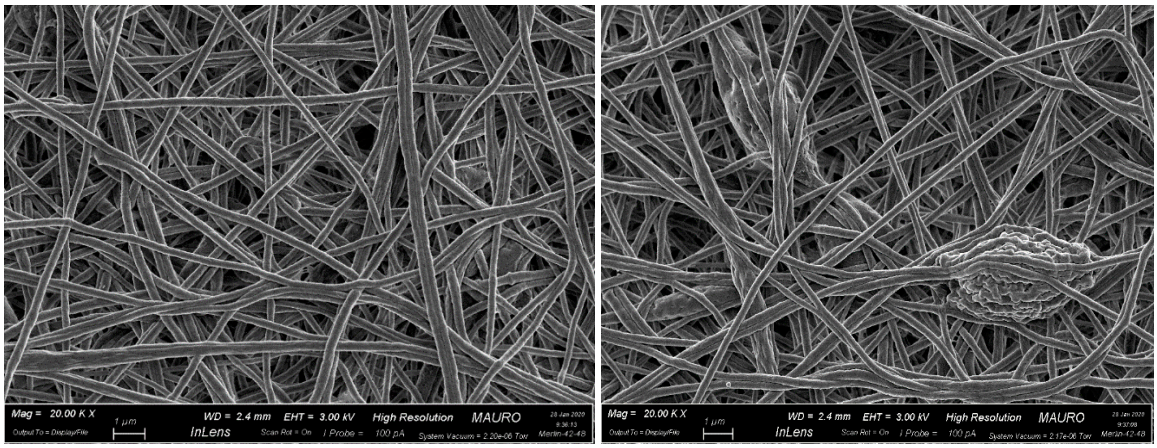

Figure 3.14: P(VDF-TrFE-MAF) electrospun membrane morphology obtained by FESEM. Electrospinning conditions: feed rate = 1.5ml/h, voltage = 15 kV, working distances = 15 cm and solution concentration = 15%wt

v. Effect of solution filtration and solution concentration

In order to reduce the presence of beads on the membranes, the solution is filtered prior to electrospinning. However, even if filtration is applied, the P(VDF-TrFE-MAF) electrospun mats present beads, as can be seen in figure 3.15.

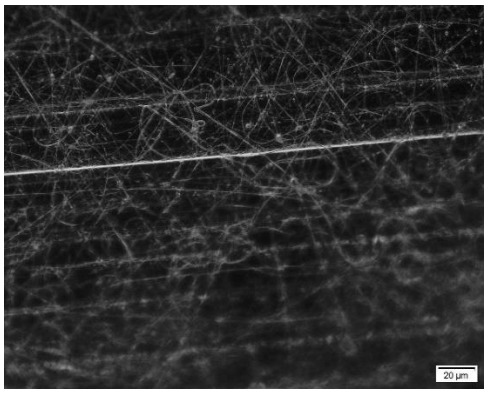

Figure 3.15 : Optical microscope image of P(VDF-TrFE-HFP) fibers electrospun with 1.5 ml/h, 15 cm and 15 kV spinning conditions using a filtered polymer solution

As an alternative strategy to reduce the beads on the membranes, the solution concentration is increased until 20 % in weight. In this case we obtain similar results (i.e., presence of beads), as shown in figure 3.16. However, the fibrous membranes obtained exhibit an homogeneous fibers size distribution.

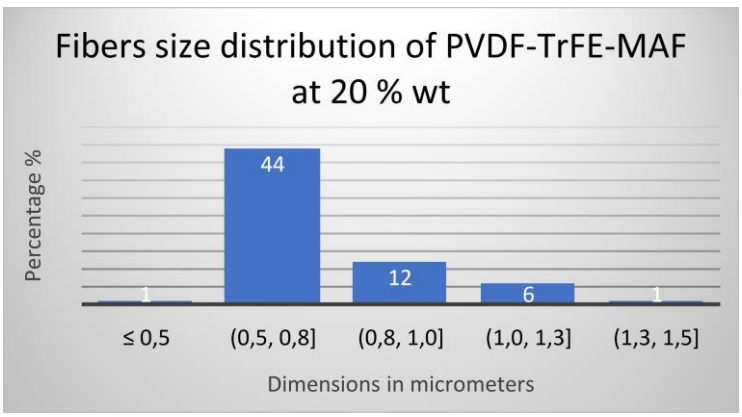

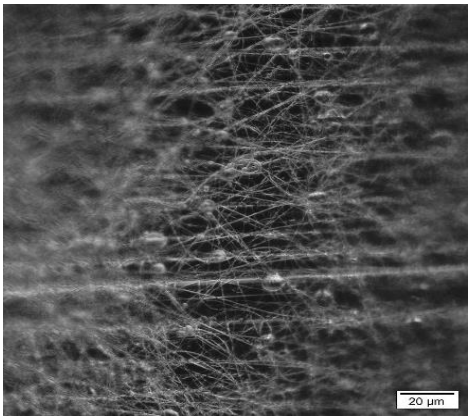

Figure 3.16: Morphology of P(VDF-TrFE-MAF) fibrous membranes and size distribution of electospun fibers obtained with voltage of 15 kV, working distance of 15cm, feed rate of 1.5 ml/h and a polymer concentration of 20 % wt in solution

3.1.4 Summary of spinning conditions and fibers size

In order to have a complete overview of the analyses conducted on all copolymers and to explain which are the best conditions for each of them, the results have been briefly summarized in table 3.7 and a single histogram containing the fiber size distributions in the best conditions of spinning has been produced (figure 3.17).

ELECTROSPINNING CONDITIONS						
VOLTAGE	kV	**10**	**15**			**20**
DISTANCE	cm	**15**	**10**	**15**	**20**	**15**
FEED RATE	ml/h	**1.5**				
P(VDF-HFP) 15% wt		*YES*	*YES but with beads*	*YES*	*YES*	*no*
P(VDF-TrFE-HFP) 15% wt		*YES*	*no*	*YES*	*no*	*no*
P(VDF-TrFE-MAF) 15% wt		*no*	*no*	*YES but with beads*	*YES*	*no*
P(VDF-TrFE-HFP) 20% wt		*no*	*no*	*YES*	*no*	*no*
P(VDF-TrFE-MAF) 20% wt		*no*	*no*	*YES but with beads*	*no*	*no*
FEED RATE	ml/h	***1***				
P(VDF-HFP) 15% wt		*no*	*no*	*YES*	*no*	*no*
P(VDF-TrFE-HFP) 15% wt		*no*	*no*	*no*	*no*	*no*
P(VDF-TrFE-MAF) 15% wt		*no*	*no*	*YES*	*no*	*no*

Table 3.7: Summary of operative conditions for electrospinning

It is therefore deduced that the generally valid process condition for the investigated fluoropolymers is related to a potential of 15 kV, a distance between needle and collector of 15 cm and a feed rate of 1.5 ml/h, even if P(VDF-HFP) shows good production of fibers also with other conditions of voltage and distance between needle and collector. In the case of P(VDF-TrFE-MAF) electrospinning can be assured in different conditions but in all these cases we have the presence of beads on the fibrous membranes. In figure 3.17, the overall fibers size

distribution is grouped in a single histogram where the distributions related to the same polymer are identified with the same colour.

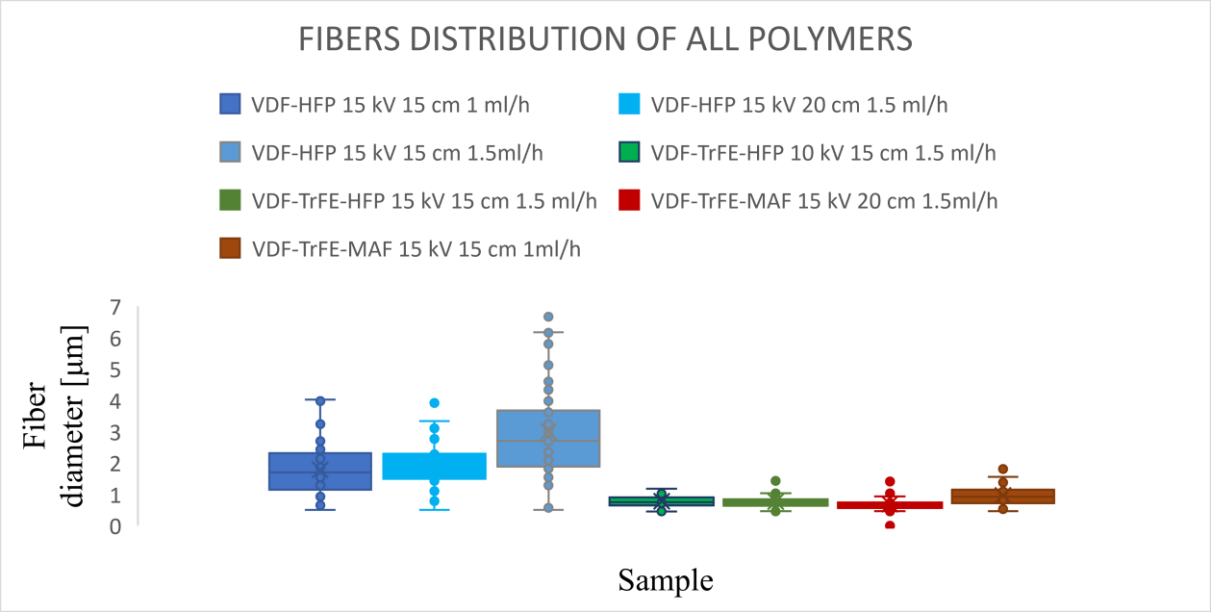

Figure 3.17: Summary of fibers size distribution of each polymer at its best process condition

From the histogram of figure 3.17 it can be seen that P(VDF-TrFE-HFP) and P(VDF-TrFE-MAF) samples are characterized by an homogeneous distribution of fibers with average diameter close to 1 µm. Instead the fiber distribution relative to P(VDF-HFP) is much wider and the fiber diameter is around 2-3 µm, with larger fibers up to 7 µm.

3.2 Copolymer crystalline morphology characterization

3.2.1 X-Ray-Diffraction analysis before and after electrospinning

XRD analyses are performed on the investigated polymers to evaluate if their crystalline morphology is varied during electrospinning. In particular, samples in the form of solid polymer as received, casted film and fibrous membrane obtained by the best conditions of electrospinning are analysed. From the XRD spectra, the copolymers crystalline phases are identified thanks to the 2θ peaks and their correlation to specific crystalline phases according to the literature. In addition, starting from the 2θ values, it is possible to calculate the interchain spacing (d) using Bragg's law, as described in Chapter 2.
These information are collected in table 3.8.

Crystalline phases	*2θ (°)*	*d (Å)*
α	17.66 18.30 19.90 26.56	5.018 4.844 4.458 3.353
β	20.26	4.38
γ	17.66 19.30 20.04 26.56	5.018 4.484 4.427 3.353

Table 3.8: Values of 2θ and the respective d spacing observed in the XRD diffractograms

3.2.1.1 XRD analyses of P(VDF-HFP)

Analyzing the P(VDF-HFP) XRD diffractograms (figure 3.18), when the copolymer is in the pellet form, a double peak and a trend that mainly resembles the α phase of P(VDF) can be detected, as shown in figure 3.18c. The α phase of PVDF is directly obtained by crystallization from the melt. [43] It is nonpolar and not ferroelectric, however, when deformed, it displays a large electric effect, related to strain gradient. [44]
Even if we have some external noises in film(b) diffrattogram, it is possible deduced that are represented beta/gamma phases as we can prove thanks to 2θ in table 3.8 and as we see also in FT-IR results.
The α phase, present in pellets, can be transformed into other polymorphic forms under an action of electrical field, mechanical stress or heat. The β phase is presently the most important polymorph of P(VDF), as can be used extensively for piezoelectric and pyroelectric applications.
Generally, an all-trans molecular conformation of P(VDF) is responsible for its ferroelectric properties, but in P(VDF-HFP) copolymer the fluorine atoms are too big to allow a simple all-trans conformation, and for this reason a zig-zag conformation is present. In fact, if we examine the XRD spectrum of P(VDF-HFP) fibers (figure 3.18a), only one peak at 2θ= 20.24° can be detected. [43] This value in the literature is mainly correlated to the β phase. Therefore, we can assume that after electrospinning the β phase prevails on the α phase, due to the large mechanical elongation to which the polymer is subjected.[43]

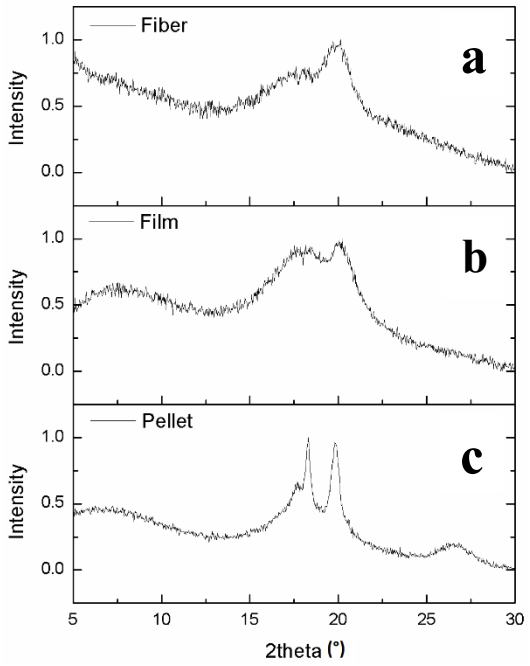

Figure 3.18 : XRD patterns of P(VDF-HFP) as electrospun fibers (a), casted film (b) and pellets (c)

3.2.1.2 XRD analyses of P(VDF-TrFE-HFP)

Figure 3.19 displays the XRD spectra of P(VDF-TrFE-HFP) in the form of fibers, casted film and raw polymer. The introduction of a trifluoroethylene comonomer in the structure, forming polyvinylidene fluoride - trifluoroethylene, P(VDF-TrFE), allows spontaneous crystallization in phase β. In all three spectra a characteristic peak near 20° is detected, representing the ferroelectric copolymer P(VDF-TrFE) in phase β.[44] Due to the copolymerization with TrFE that induces a strong steric obstacle, P(VDF-TrFE-HFP) allows a crystallization similar to the β-phase P(VDF). In figure 3.19 all the forms of copolymer show the β-phase but in the film and in the neat material we could find also the γ-phase as we see in FT-IR. [45]

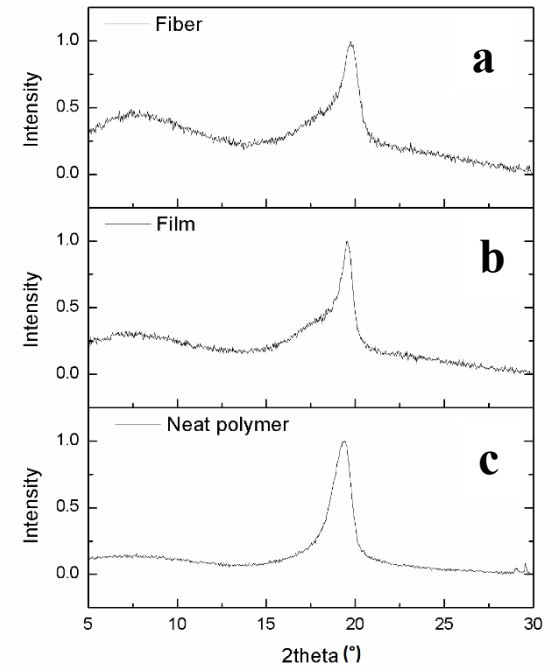

Figure 3.19: XRD patterns of P(VDF-TrFE-HFP) as electrospun fibers (a), casted film (b) and neat polymer (c)

3.2.1.3 XRD analyses of P(VDF-TrFE-MAF)

In P(VDF-TrFE-MAF) terpolymer, the monomer MAF is known to act as random defects in the P(VDF-TrFE) copolymer so that the interchain spacing is larger than that of P(VDF-TrFE) copolymer, and thus, polar phases in P(VDF-TrFE) copolymers transform into nonpolar nanophases in P(VDF-TrFE-MAF) terpolymer. [46]

As shown in figure 3.20, the 2θ values of the XRD spectra of P(VDF-TrFE-MAF) casted film (2θ = 19.6°) and raw polymer (2θ = 19.29°) can be associated to P(VDF-coTrFE). Instead the spectrum of P(VDF-TrFE-MAF) fibers (figure 3.20a) presents external interferences: in the first part the broad peak can be associated to the amorphous part of the terpolymer, while the characteristic peak at 2θ= 20° represents the β phase also in this case, but the intensity is lower than for the other copolymers.

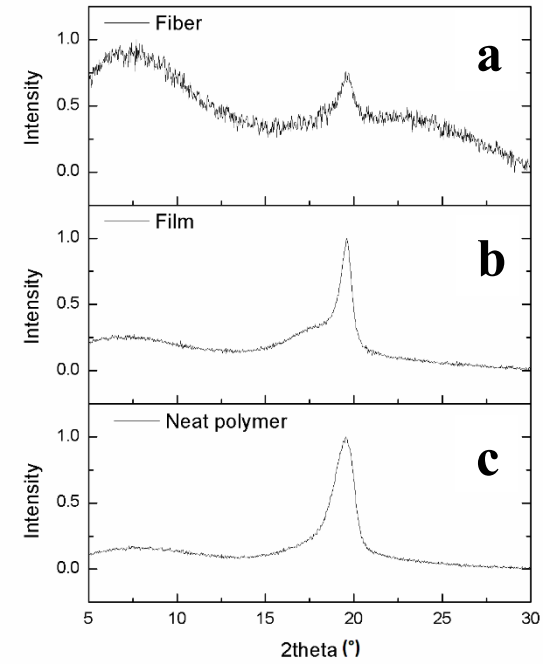

Figure 3.20: XRD patterns of P(VDF-TrFE-MAF) as electrospun fibers (a), casted film (b) and neat polymer(c)

3.2.2 *ATR-FT-IR* spectroscopy before and after electrospinning

The FT-IR spectra of the different polymers are analysed both as pure solid polymer as received and as electrospun fibers in order to evaluate if the chemical structure and the characteristic phases may be subject to variations during spinning.
Table 3.11 summarizes the FT-IR peaks associated to different phases in P(VDF).

Wavenumber (cm^{-1})	*Crystalline phases*
532 -763-795-854-976- 1120-1149-1393 cm^{-1}	α
510-745-840 -881 -1071 -1176 1234 -1275 -1289-1401 cm^{-1}	β
776-811-833-1117 1233-1429 cm^{-1}	γ

Table 3.9: FT-IR characteristic peaks of different crystallinity phases of P(VDF). Data from [43]

3.2.2.1 ATR spectra of P(VDF-HFP)

Figure 3.21 compares the spectra of the raw polymer P(VDF-HFP) as pellets, its fibers obtained with the chosen best conditions of electrospinning, and the copolymer in the form of film. We can observe that the three spectra are very similar.

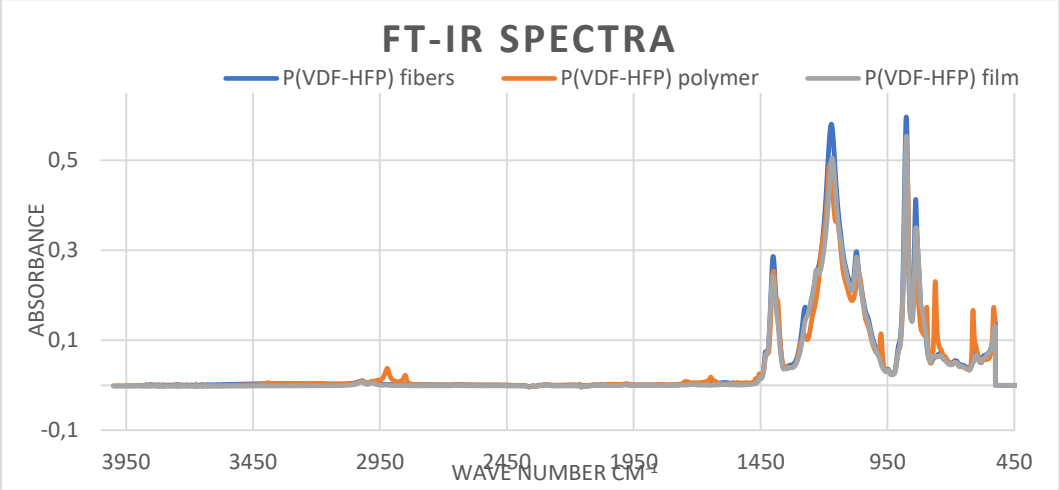

Figure 3.21: FT-IR spectra of P(VDF-HFP) in the form of pellets, casted film and electrospun fibers

The peaks in the range 1100-1200 cm^{-1} as well as 1172 cm^{-1} represent C–F vibrations of the P(VDF) block. [39]
Figure 3.22 represents a zoom of the region 550 cm^{-1} -1450 cm^{-1}, where according to the literature we can find the spectroscopic bands of the P(VDF) phases which are listed in table 3.9. Instead HFP in percentage till 5 % mol does not show great influence on the polymer crystallinity phases. In the specific P(VDF-HFP) copolymer analysed in this thesis there is 3.3% mol of HFP.[44]

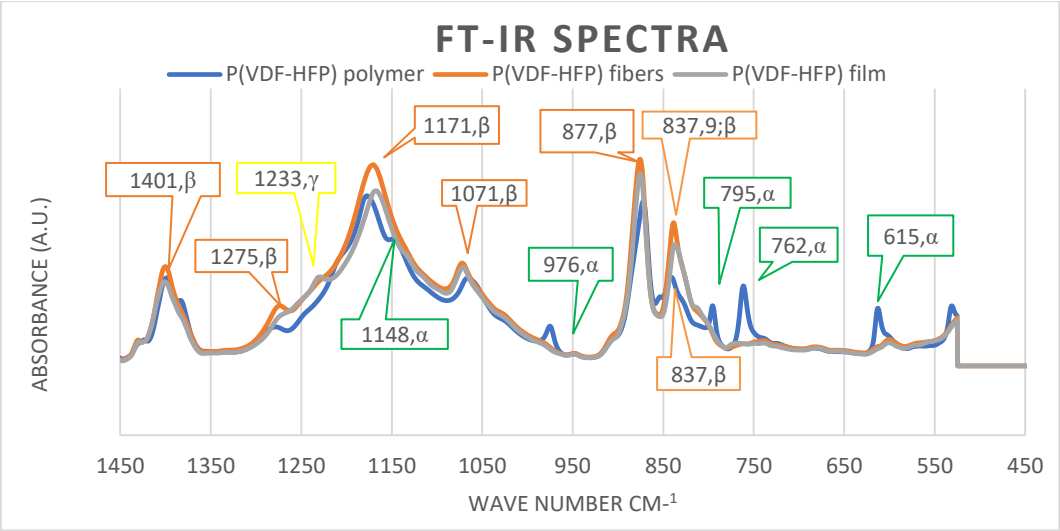

Figure 3.22: Zoom of the region 550 cm^{-1}-1450 cm^{-1} of the FT-IR spectra of P(VDF-HFP) in the form of pellets, casted film and electrospun fibers

In figure 3.22 some peaks related to the α phase of the commercial raw polymer as those at 615, 762, 795, 976, 1148 cm^{-1} can be found [43], but they disappear in the fibers sample.
The β phase characteristic of P(VDF) is revealed by the peaks in proximity of 840 cm^{-1}, 877 cm^{-1}, 1071 cm^{-1}, 1171 cm^{-1}, 1275 cm^{-1} and 1401 cm^{-1}. Their presence can be found in all spectra of P(VDF-HFP) (raw material, film and fibers) but they are increased in fibers.[43] Analysing the γ phase, in the polymer sample as pellets there aren't characteristic peaks, but in P(VDF-HFP) film we observe a little peak at 1233 cm^{-1} in film sample which is demolishing in fibers.
Therefore, P(VDF-HFP) nanofibers produced by the electrospinning technique seem to be in favor of β phase due to the large mechanical elongation to which the polymer is subjected. [43] FT-IR results thus confirm the XRD data.

3.2.2.2 ATR spectra of P(VDF-TrFE-HFP)

Figure 3.23 compares the FT-IR spectra of the raw polymer P(VDF-TrFE-HFP) and of the fibers obtained from it under the best conditions of electrospinning.

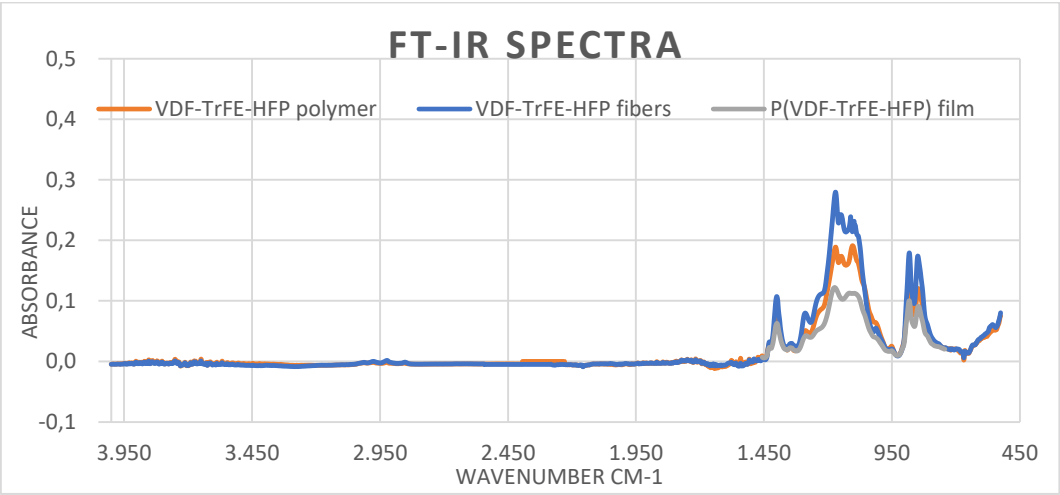

Figure 3.23: FT-IR spectra of P(VDF-TrFE-HFP) in the form of pellets, casted film and electrospun fibers

Moreover, we apply a zoom on the initial part of the spectra from 550 to 1400 cm^{-1} in order to have a precise figure of the differences between the fibers and the raw polymer and to be able to identify the crystalline phases that are present in the sample.

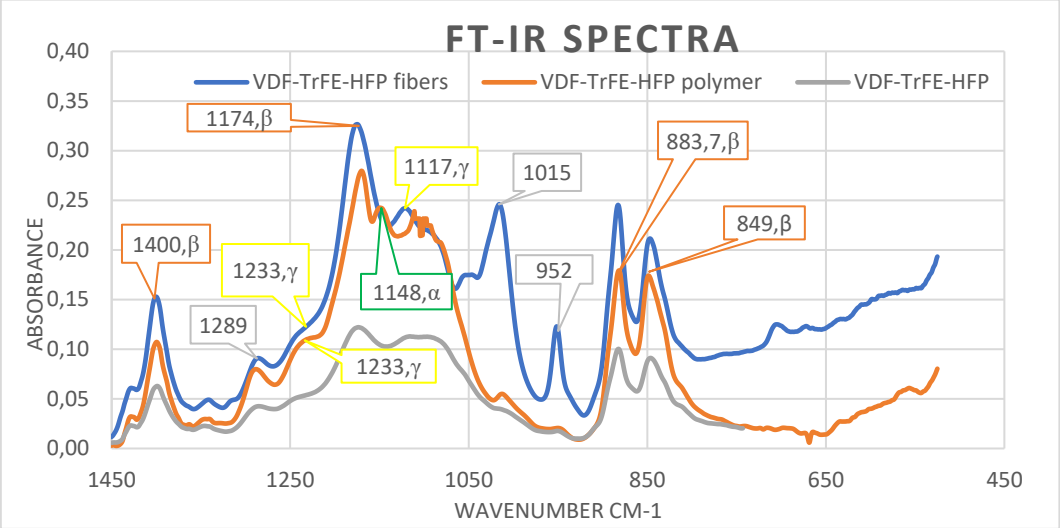

Figure 3.24: Zoom of the region 550 cm^{-1}-1450 cm^{-1} of the FT-IR spectra of P(VDF-TrFE-HFP) in the form of pellets, casted film and electrospun fibers

The two bands at 1288 and 850 cm^{-1} are assigned to CF_2 and CH_2 of the all-trans conformation of the crystalline ferroelectric (FE) phase of poly(VDF-co-TrFE) chains.[32]
Figure 3.24 shows that in both spectra of P(VDF-TrFE-HFP) the β phase can be detected through the peaks at 849 cm^{-1}, 884 cm^{-1}, 1174 cm^{-1}, 1289 and 1400 cm^{-1}. The α phase instead is present only in the bulk polymer with the peak at 1148 cm^{-1}. Confirming XRD data, there is not α phase in PVDF-TrFE-HFP fibers, where the main phases are β and γ for PVDF-TrFE. The peak related to γ phase is slightly present in neat polymer and film, at 1233 cm^{-1} the reduction of peak underlining the presence in polymers rather than the fibers.
In the following the FT-IR spectrum of a P(VDF-TrFE-HFP) casted film obtained from a solution is also investigated in order to assure that the electrospinning process is the only affecting the changing of the crystalline phases of PVDF co-polymers.

In addition some peaks of solvent (DMSO) in the P(VDF-TrFE-HFP) fibers can be seen: they thus represent the insufficient vaporization of solvent during the electrospinning (950.7 cm^{-1} and 1019.2/1015.3 cm^{-1}). As it will be shown below, the presence of solvent is lightly evident also in D-TGA analysis where we find a mass loss linked to the evaporation of solvent.

3.2.2.3 ATR spectra of P(VDF-TrFE-MAF)

The terpolymers prepared by terpolymerization of VDF, TrFE and MAF in solution are mainly composed of poly (VDF-alt-MAF) alternating chains and pure poly (VDF-co-TrFE) copolymer chains. As a consequence, their crystalline properties should be similar to that of poly (VDF-co-TrFE) copolymers, while poly (VDF-alt-MAF) alternating copolymer is amorphous. Figure 3.25 shows the spectra of P(VDF-TrFE-MAF) bulk polymer and fibers, which are very similar to P(VDF-TrFE-HFP) but both the FT-IR spectra display an additional absorption band at 1740 cm^{-1} assigned to the carbonyl bond of the carboxylic acid of MAF. [32]

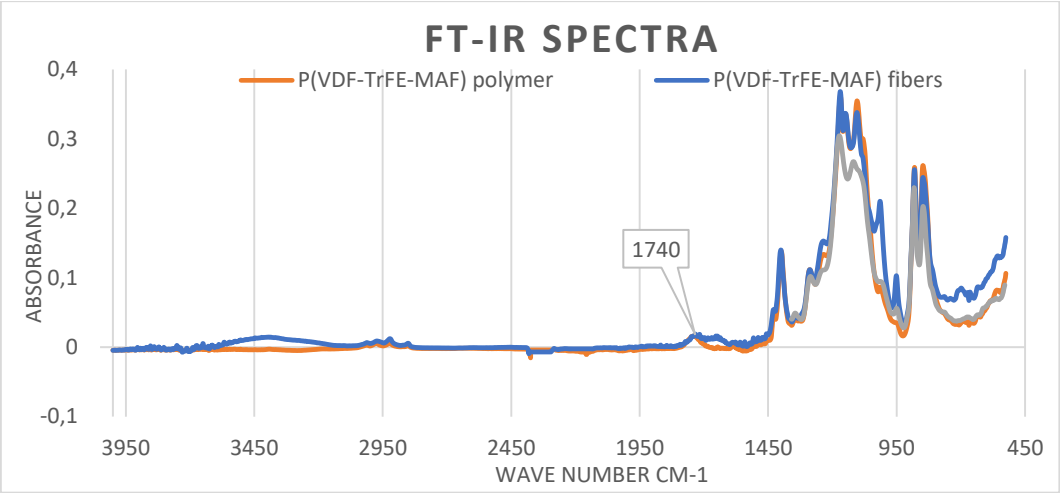

Figure 3.25: FT-IR spectra P (VDF-TrFE- MAF) in the form of pellets, casted film and electrospun fibers

Figure 3.26 shows the zoom of the spectra from 1400 to 550 cm^{-1} to get an accurate representation of the differences between the fibers and the polymer and to identify the presence of one phase rather than another in the samples.

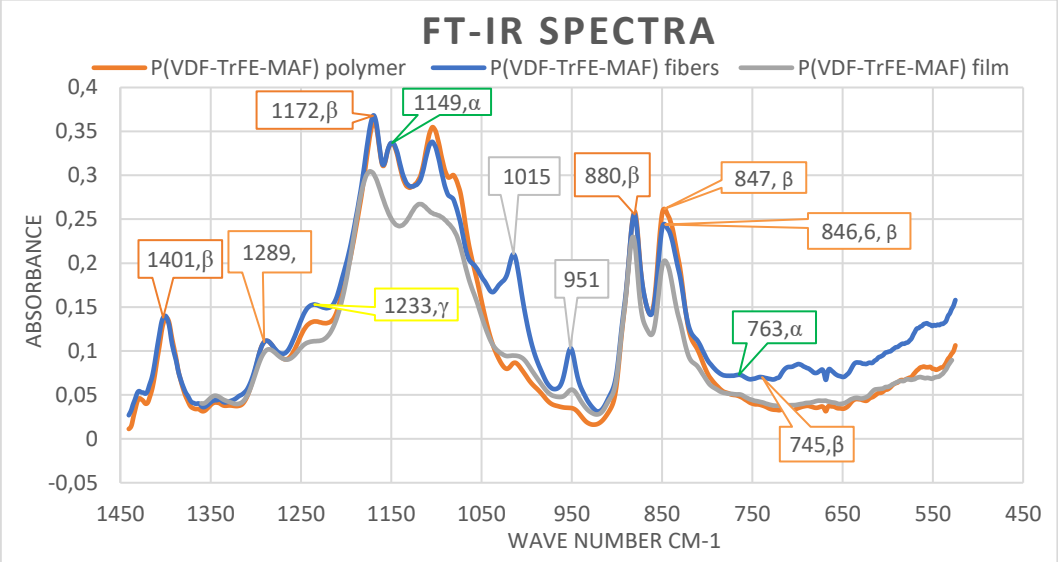

Figure 3.26: Zoom of the region 550 cm^{-1}-1450 cm^{-1} of the FT-IR spectra of P(VDF-TrFE-MAF) in the form of pellets, casted film and electrospun fibers

In figure 3.26 we find characteristic peaks of β phase at 847, 880, 1172, 1289, 1401 cm^{-1} noticeable in both spectra. Moreover we find the α phase as peak at 1149 cm^{-1} in both forms of the polymer and at 763 cm^{-1} less evident for the fibers. The only peak for γ phase is remarkable at 1233 cm^{-1}. Therefore, also for P(VDF-TrFE-MAF), the α phase is not really pronounced and the γ phase decreases in the fibers samples.
The peaks around 840 cm^{-1} appear in both samples and represent the absorbance for the β phase, which is much stronger than that of the α phase.
Film and fibers shows some peaks of DMSO solution in the P(VDF-TrFE-MAF) fibers: this again represent the insufficient vaporization of solvent (950.71 cm^{-1} and in 1019.7/1014.4 cm^{-1}). These results are evident also in the D-TGA analysis where we find a sample weight decrease linked to the degradation of solvent, more marked than in P(VDF-TrFE-MAF).

In conclusion, P(VDF-HFP) copolymer shows a high presence of α phase in raw polymer but this phase disappears with the process of electrospinning, as indeed this phase cannot be found in the fibers samples. The most important thing is the presence of β phase in both P(VDF-HFP) spectra but more accentuated in fibers. P(VDF-HFP) microfibers produced by the electrospinning technique seem to be in favor of β phase due to the large mechanical elongation to which the polymer is subjected.
Analyzing instead the copolymers containing TrFE, P(VDF-TrFE-HFP) and P(VDF-TrFE-MAF), the general behaviour related to the presence of P(VDF) is mainly found with an accentuated β phase presence in the fibers due to the great mechanical elongation during electrospinning. In addition, we find two characteristic peaks at 1288 and 850 cm^{-1} assigned to CF_2 and CH_2 related to the crystalline FE phase of the polychain (VDF-co-TrFE), values found in both spectra of copolymers with TrFE.
Moreover, P(VDF-TrFE-MAF) FT-IR spectra both as polymer and fiber show an absorption band at 1740 cm^{-1} assigned to MAF's carboxylic acid carbonylic bond.

3.3 Thermal properties of polymer before and after electrospinning.

3.3.1 DSC

In this section we analyse by DSC the melting and crystallization behaviour of the three samples as raw materials and as fibers after electrospinning.

1. *DSC results for P(VDF-HFP)*

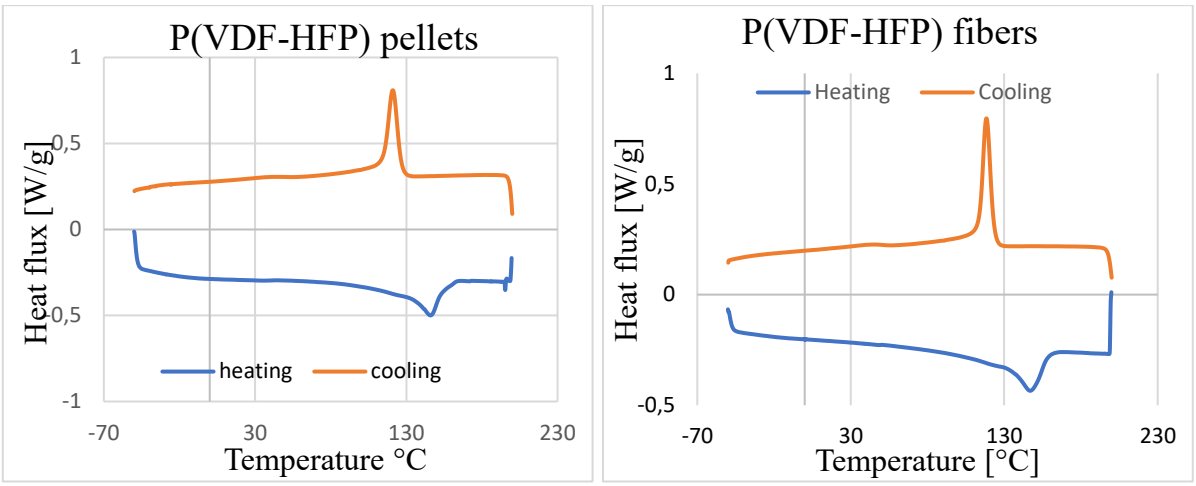

Figure 3.27: DSC characterization of P(VDF-HFP)

In figure 3.27 we show the DSC thermograms of P(VDF-HFP) as pellets and as fibers. For the pellets sample, we individuate a peak of melting at 145.5 °C (from the integration of the peak we have an enthalpy of |37.43 J/g|) and a peak of crystallization at 121.05 °C with an enthalpy of 22.38 J/g.
Analysing the P(VDF-HFP) as fibers, we find a peak of melting at 147.08 °C and a peak of crystallization at 118.48 °C.
We know that the enthalpy of crystallization of pure P(VDF) is 104.7 J/g. [45][47]
From this value the percentage of crystallinity can be calculated: the crystallinity percentage of P(VDF-HFP) before electrospinning as a polymer is about 21.42 %, instead the percentage of crystallinity for P(VDF-HFP) fibers is 20.66%.
In table 3.10 the main results given by DSC about the polymer as powder and as fibers after electrospinning are collected.

P(VDF-HFP) pellets	*Melting peak*	*Crystallization peak*	**P(VDF-HFP) fibers**	*Melting peak*	*Cristallization peak*
Temperature	145.5°C	121.05 °C	*Temperature*	147.08°C	118.48°C
Enthalpy	-37.43 J/g	22.38 J/g	*Enthalpy*	-21.64 J/g	21.1 J/g
Crystallinity	*21.42%*		*Crystallinity*	*20.66%*	

Table 3.10: Summary of DSC results on P(VDF-HFP) comparing commercial polymer and fibers

2. *DSC results for P(VDF-TrFE-HFP):*

The DSC thermograms of the P(VDF-TrFE-HFP) copolymer are reported in figure 3.28. Two peaks can be seen for both the heating and cooling curve, corresponding to the Curie and

melting/crystallization transitions. Right before its melting, the sample loses its ferroelectric properties becoming paraelectric. During the following cooling ramp, the sample recrystallizes and comes back to the ferroelectric state, below the Curie temperature. The Curie temperature is characteristic of the ferroelectric (FE) behaviour of the terpolymer and depends on the morphology (size, amount) of the FE domains. [32]
Analysing the DSC thermogram of P(VDF-TrFE-HFP) as raw polymer shown in figure 3.30, following the heating curve two different peaks can be identified:

- the peak T_C at 52.71 °C, which represents the T related to Curie transition, relative to the TrFE present in the copolymer; from the integration under the curve an enthalpy of |6.27 J/g| is calculated;
- the peak T_m at 143.43 °C relative to the P(VDF-TrFE-HFP) peak of melting, from the integration under the curve we have an enthalpy of |19.14 J/g|.

Analyzing the cooling curve we find:

- the peak T_C at 47.76°C, which represents the Curie temperature, relative to the TrFE present in the copolymer; from the integration under the curve an enthalpy of |6.57 J/g| is calculated;
- the peak T_{CR} at 119.2 °C relative to the P(VDF-TrFE-HFP) peak of crystallization, from the integration under the curve we have an enthalpy of |19.11 J/g|.

In the same way we analyse the P(VDF-TrFE-HFP) sample as fibers. Following the heating curve we identify:

- the peak T_C at 52.28°C, which represents the T related to Curie transition, relative to the TrFE present in the copolymer; from the integration under the curve an enthalpy of |5.95 J/g| is calculated;
- the peak T_m at 142.90°C relative to the P(VDF-TrFE-HFP) peak of melting, from the integration under the curve we have an enthalpy of |16.28 J/g|.

Analyzing the cooling curve of fibers we find:

- the peak T_C at 48.55°, which represents the Curie temperature, relative to the TrFE present in the copolymer; from the integration under the curve an enthalpy of |5.23 J/g| is calculated;
- the peak T_{CR} at 120.17°C relative to the P(VDF-TrFE-HFP) peak of crystallization, from the integration under the curve we have an enthalpy of |17.73 J/g|.

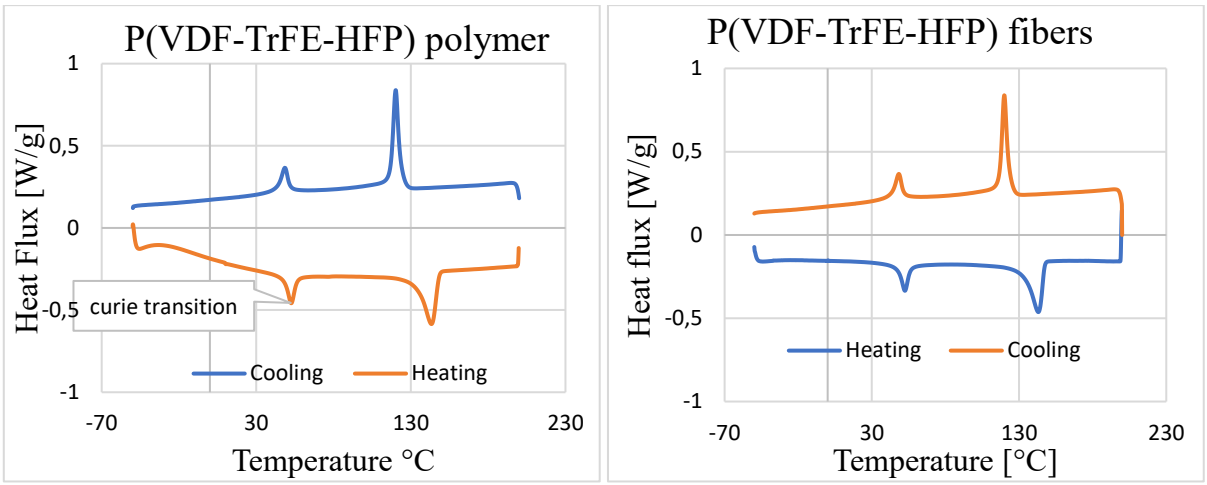

Figure 3.28: DSC Characterization of P(VDF-TrFE-HFP)

Analyzing the DSC results of the P(VDF-TrFE-HFP) both as polymer and as fibers after electrospinning we report in table 3.11 all the main information.
The value of the enthalpy corresponding to 100% crystalline P(VDF-TrFE-HFP) (65/31/4) copolymer is $\Delta H_{m0.\ P(VDF-TrFE-HFP)} = 30.7$ J/g [30] so we obtain a percentage of crystallinity of 47.09 %.
In this case after electrospinning using the same $\Delta H_{m0.,}$ we have a crystallinity of 42.82 % for P(VDF-TrFE-HFP) fibers.

PVDF-TrFE-HFP polymer	*Heating curve*	*Cooling curve*	**PVDF-TrFE-HFP fibers**	*Heating curve*	*Cooling curve*
Temperature	Curie Transition T_C: 52.71 °C	Curie Transition T_C: 47.76°C	*Temperature*	Curie Transition T_C: 52.28°C	Curie Transition T_C: 48.55°C
	Melting peak T_m: 143.43°C	Crystallization peak T_{CR}: 119.2°C		Melting peak T_m: 142.90°C	Crystallization peak T_{CR}: 120.17°C
Enthalpy	H_C: -6.27 J/g H_m: -19.14 J/g	H_C: 6.57 J/g H_{CR}: 19.11 J/g	*Enthalpy*	H_C: - 5.95 J/g H_m: -16.28 J/g	H_C: 5.23 J/g H_{CR}: 17.73 J/g
Crystallinity	*47,09%*		*Crystallinity*	*42,82%*	

Table 3.11: Summary of DSC results on P(VDF-TrFE-HFP) comparing polymer and fibers

3. *DSC results for P(VDF-TrFE-MAF):*

In figure 3.29 we show the DSC thermogram of P(VDF-TrFE-MAF) as raw polymer, in this case following the heating curve we identify two different peaks:

- the peak T_C at 65.91 °C, represents the T related to Curie transition, relative to the TrFE present in the copolymer and from the integration under the curve an enthalpy of |9.34 J/g| is calculated;
- the peak T_m at 147.31°C relative to the P(VDF-TrFE-MAF) peak of melting, from the integration under the curve we have an enthalpy of |19.47 J/g|.

Analyzing the cooling curve we find:

- the peak T_C at 59.04 °C, represents the Curie T, relative to the TrFE present in the copolymer and from the integration under the curve an enthalpy of |6.77 J/g| is calculated;
- the peak T_{CR} at 129.46°C relative to the P(VDF-TrFE-MAF) peak of crystallization, from the integration under the curve we have an enthalpy of |21.11 J/g|.

In the same way we analyse the P(VDF-TrFE-MAF) as fibers. Following the heating curve we identify:

- the peak T_C at 65.55°C, represents the T related to Curie transition, relative to the TrFE present in the copolymer and from the integration under the curve an enthalpy of |3.33 J/g| is calculated;
- the peak T_m at 147.21°C relative to the P(VDF-TrFE-MAF) peak of melting, from the integration under the curve we have an enthalpy of |7.89 J/g|.

Analyzing the cooling curve of fibers we find:

- the peak T_C at 59.58°, represents the CurieT, relative to the TrFE present in the copolymer and from the integration under the curve an enthalpy of |3.65 J/g| is calculated;
- the peak T_{CR} at 130.39°C relative to the P(VDF-TrFE-MAF) peak of crystallization, from the integration under the curve we have an enthalpy of |18.29 J/g|.

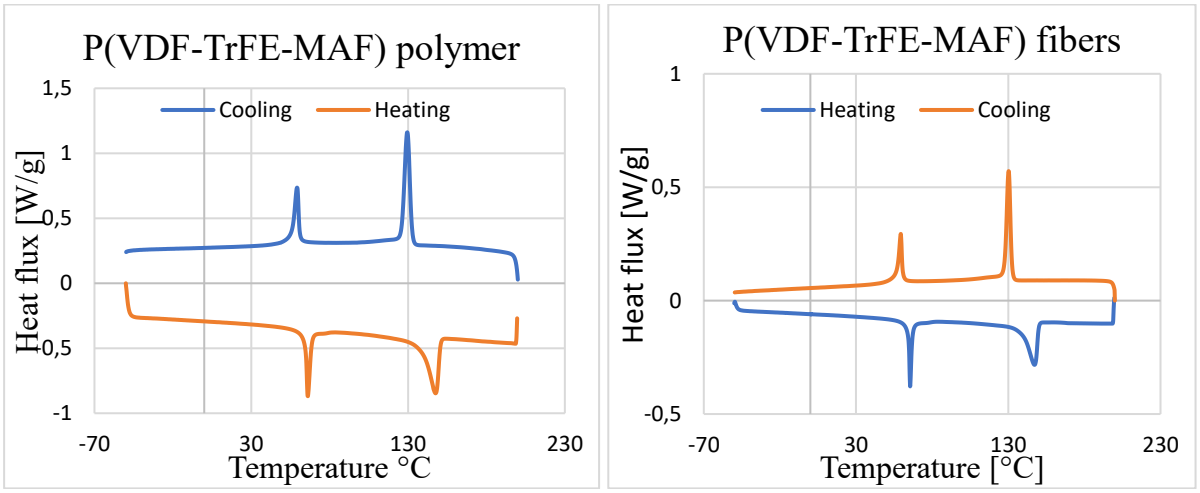

Figure 3.29: DSC characterization of P(VDF-TrFE-MAF)

Analyzing the DSC results of the P(VDF-TrFE-MAF) both as polymer and as fibers after electrospinning we report in table 3.12 all the main information.
Considering the peaks related to P(VDF-TrFE-MAF) we note that the behaviour remains similar to P(VDF-TrFE-HFP) as well as the overall crystallinity. In fact, the poly(VDF-co-TrFE) copolymer chains are not affected by the presence of alternating poly(VDF-alt-MAF) copolymer chains, which are amorphous. [31] For this reason the value of the enthalpy corresponding to 100% crystalline P(VDF-TrFE-MAF) (66/32/2) copolymer is ΔH_{m0} P(VDF−TrFE) = 42 J/g, [28] related only to P(VDF-co-TrFE). A percentage of crystallinity of 50.26 % is thus obtained for the terpolymer. Instead considering the polymer after

electrospinning and using the same ΔH_{m0}, a crystallinity of 43.55 % for P(VDF-TrFE-MAF) fibers is calculated.

PVDF-TrFE-MAF polymer	*Heating curve*	*Cooling curve*	**PVDF-TrFE-MAF fibers**	*Heating curve*	*Cooling curve*
Temperature	Curie Transition T_C: 65.91 °C	Curie Transition T_C: 59.04 °C	*Temperature*	Curie Transition T_C: 65.55°C	Curie Transition T_C: 59.58°C
	Melting peak T_m: 147.31°C	Crystallization peak T_{CR}: 129.46°C		Melting peak T_m: 147.21°C	Crystallization peak T_{CR}: 130.39°C
Enthalpy	H_C: - 9.34 J/g H_m:-19.47 J/g	H_C: 6.77 J/g H_{CR}: 21.11 J/g	*Enthalpy*	H_C: - 3.33 J/g H_m: -7.89 J/g	H_C: 3.65 J/g H_{CR}: 18.29 J/g
Crystallinity	*50,26%*		*Crystallinity*	*43,55%*	

Table 3.12: summary of DSC results on P(VDF-TrFE-MAF) comparing polymer and fibers

Analysing the three copolymers, it can be deduced that the percentage of crystallinity undergoes a slight reduction after electrospinning.

3.3.2 TGA

This section shows the TGA thermograms under nitrogen of poly(VDF-HFP), poly(VDF-co-TrFE) and poly(VDF-ter-TrFE-ter-MAF) copolymers before and after electrospinning to analyse the different thermal behaviour of the materials under thermal degradation.
As expected, these fluoropolymers, both as bulk polymers and fibers, are very stable and show only significant degradation above 400 °C.
Due to the differences in the samples, they could decompose at different temperatures. Compared to P(VDF-HFP), a lower degradation was observed for P(VDF-TrFE-HFP), whereas P(VDF-TrFE-MAF) seems to have a lower degradation temperature mainly in fiber form.

1. *TGA results for P(VDF-HFP)*

In Figure 3.30 the TGA results for P(VDF-HFP) are processed: it is possible to observe that the fibers start to degrade at 329.2 °C, a lower temperature than the original pellets, which have a T of starting degradation close to 400°C.

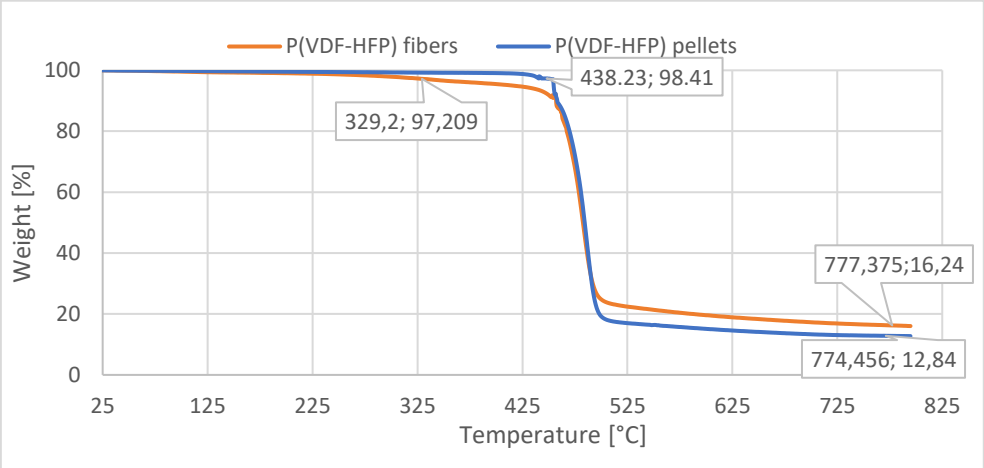

Figure 3.30:TGA thermograms under nitrogen at 10 °C/min of P(VDF-HFP) pellets and P(VDF-HFP) fibers

Figure 3.31 shows the first derivative of the TGA thermograms, indicating the temperature corresponding to the maximun degradation rate: this temperature is lower for the raw polymer than for the fibers.

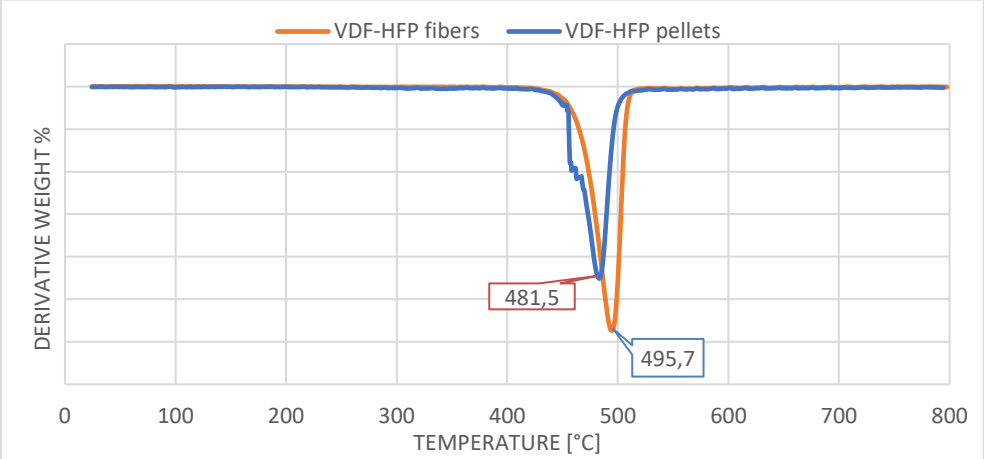

Figure 3.31: D-TGA of P(VDF-HFP)

2. *TGA results for P(VDF-TrFE-HFP)*

Instead, in figure 3.32, we have the comparison of the thermograms for P(VDF-TrFE-HFP) before and after electrospinning and in this case we observe a lower temperature of starting degradation for fibers (around 300 °C) than for raw polymer.

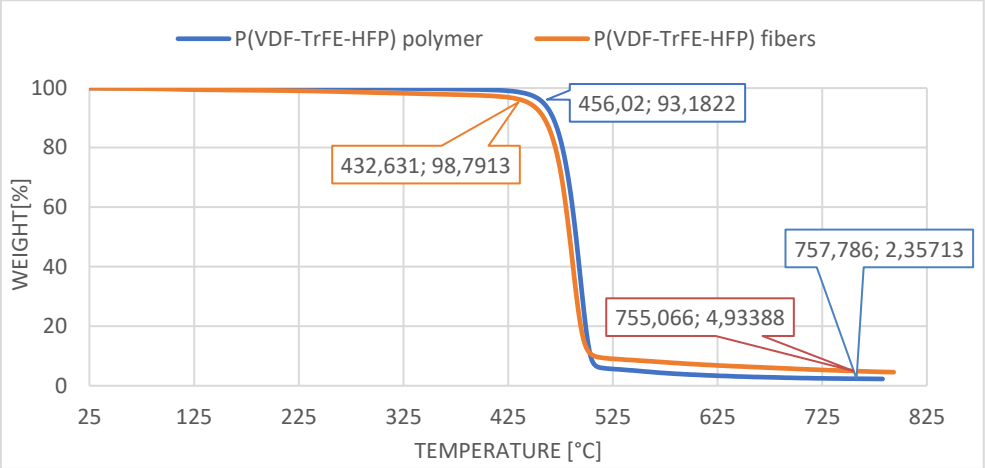

Figure 3.32: TGA thermograms under nitrogen at 10 °C/min of P(VDF-TrFE-HFP) polymer and P(VDF-TrFE-HFP) fibers

In this case, figure 3.33, the temperature corresponding to the maximum degradation rate is slightly lower for the P(VDF-TrFE-HFP) fiber sample than for the raw polymer.

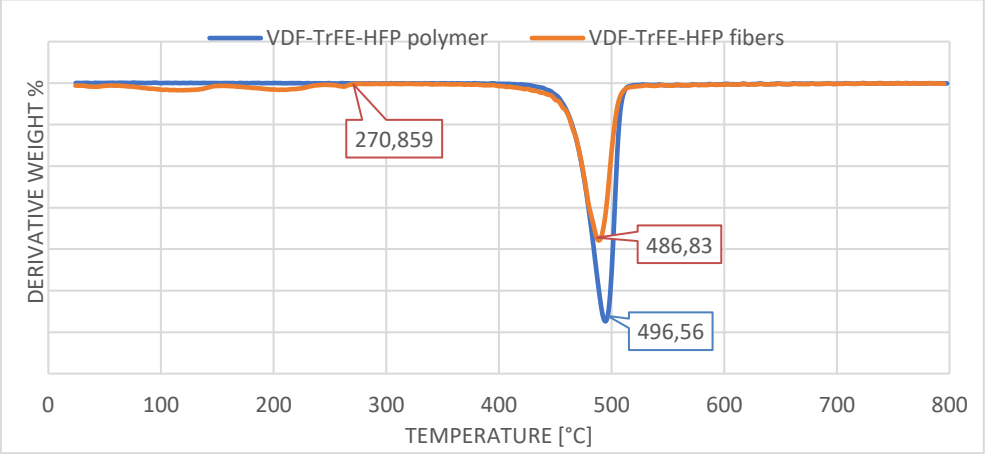

Figure 3.33: D-TGA of P(VDF-TrFE-HFP)

3. *TGA results for P(VDF-TrFE-MAF)*

From these results in figure 3.34, we can assume that P(VDF-TrFE-HFP) copolymer shows a similar degrading behaviour in both forms, but as fibers it has a slightly lower degradation temperature.

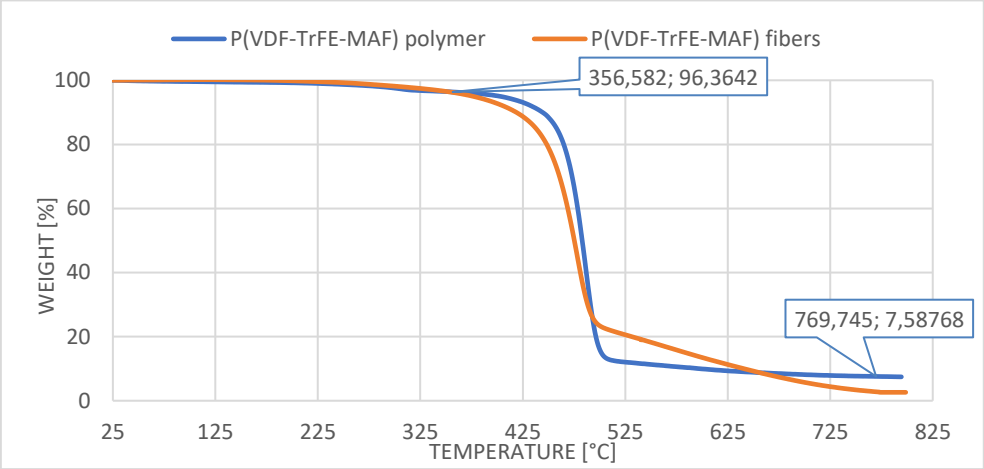

Figure 3.34: TGA thermograms under nitrogen at 10 °C/min. of P(VDF-TrFE-MAF) polymer and P(VDF-TrFE-MAF) fibers

In figure 3.34 the thermograms of P(VDF-TrFE-MAF) are reported. In this case the fibers seem to start to degrade at a lower temperature compared to the raw polymer, about 350 °C, this degradation could be due to a quantity of solvent still present in the fibers not completely evaporated from the solution.

The temperature corresponding to the maximum degradation rate is very similar for the bulk copolymer and its fibers (figure 3.35).

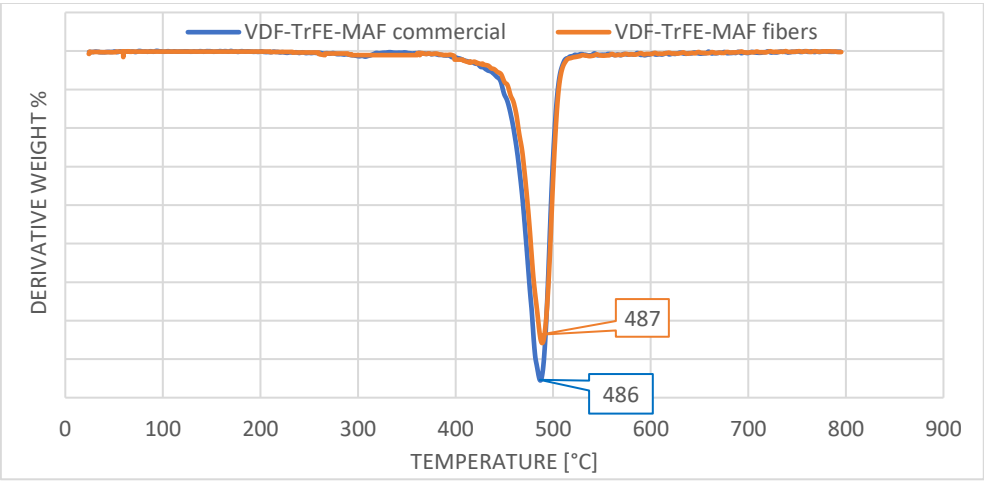

Figure 3.35: D-TGA of P(VDF-TrFE-MAF)

The results obtained from the TGA analyses are summarized in table 3.13, in order to better evaluate the different thermal behavior of the three investigated copolymers in two different forms (bulk and fibers). In particular, in table 3.13 the degradation temperature at which the sample loses 5% and 10% of its weight, the amount of residual material at the end of the thermal degradation (residue) and the temperature corresponding to the maximum degradation rate (i.e., the degradation peak of the D-TGA graphs) are reported.

Samples	T[°C] at 5%	T[°C] at 10%	Residue	T related to maximum degradation rate[°C]
POLYMERS				
P(VDF-HFP)	455.2	458.5	12.82%	481.5
P(VDF-TrFE-HFP)	456.3	467.5	2.35%	496.6
P(VDF-TrFE-MAF)	403.3	435	7.55%	486
FIBERS				
P(VDF-HFP)	418.5	458	16.24%	496
P(VDF-TrFE-HFP)	433	461.4	4.93%	487
P(VDF-TrFE-MAF)	401.7	430.9	7.56%	487

Table 3.13 : Summary of general information from TGA analysis related to polymers and fibers (before andafter electrospinning)

P(VDF-HFP) and P(VDF-TrFE-HFP) show a very similar thermodegradation behavior, although the final residue is much higher for P(VDF-HFP) copolymer. Instead P(VDF-TrFE-MAF) starts to degrade at lower temperatures, due to the presence of the MAF moiety in the copolymer structure.

Comparing the copolymers in the bulk form and in the fibers form, the latter show a slightly lower thermal resistance. This degradation could be due to a small quantity of solvent still present in the electrospun fiber membranes, which has not completely evaporated from the solution during the electrospinning process. This result is also confirmed by FT-IR analyses.

3.4 Stress-strain tests

In this section the mechanical properties of the fibrous membranes are studied. The electrospun fibrous membranes of the three polymers obtained from the best electrospinning conditions are analyzed by tensile test (tensile speed of 5 mm/min) at room temperature. The Young's modulus from the initial linear regime of stress vs. strain curve and the elongation at the breaking point are obtained. Young's modulus measures the resistance of a material to elastic deformation (recoverable) under load, it depends on characteristic of the material but also on how it is loaded and the shape and size of the component. The first stage of the curve represents the linear elastic region. The stress is proportional to the strain that is obeys the general Hooke's law and the slope is Young's modulus:

$$Young's\ modulus : \frac{stress}{strain}$$

Figure 3.36 represents the mechanical behaviour of P(VDF-HFP) fiber membranes.

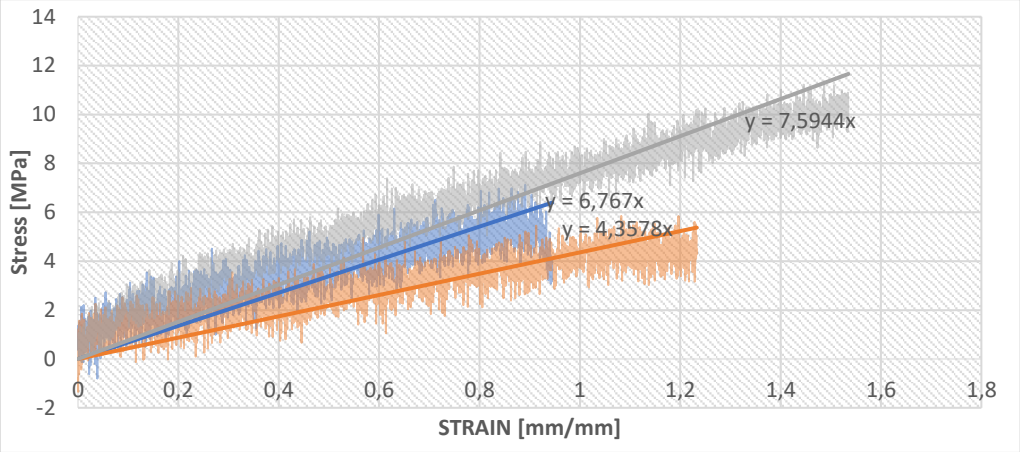

Figure 3.36 : Stress-strain diagram of P(VDF-HFP) fibers

The slope of the curve reflects the Young's Module. The average value for the Young's modulus of P(VDF-HFP) fibers is found 7.18± 3.63 MPa.

Figure 3.37 represents the mechanical behaviour of P(VDF-TrFE-HFP) fiber membranes.

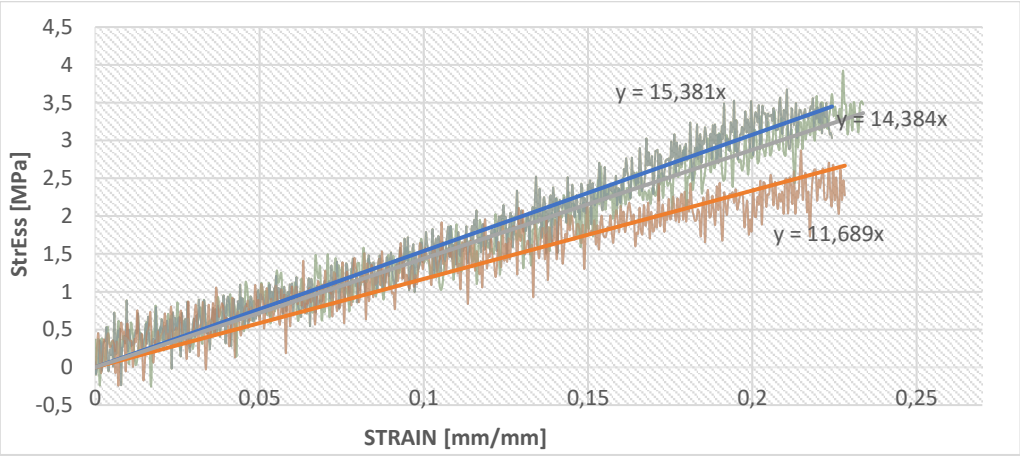

Figure 3.37: Stress-strain diagram of P(VDF-TrFE-HFP) fibers

In the case of the copolymer P(VDF-TrFE-HFP) the Young's modulus is 14.88± 1.23 MPa.

The figure 3.38 represents the mechanical behaviour of P(VDF-TrFE-MAF) fibers:

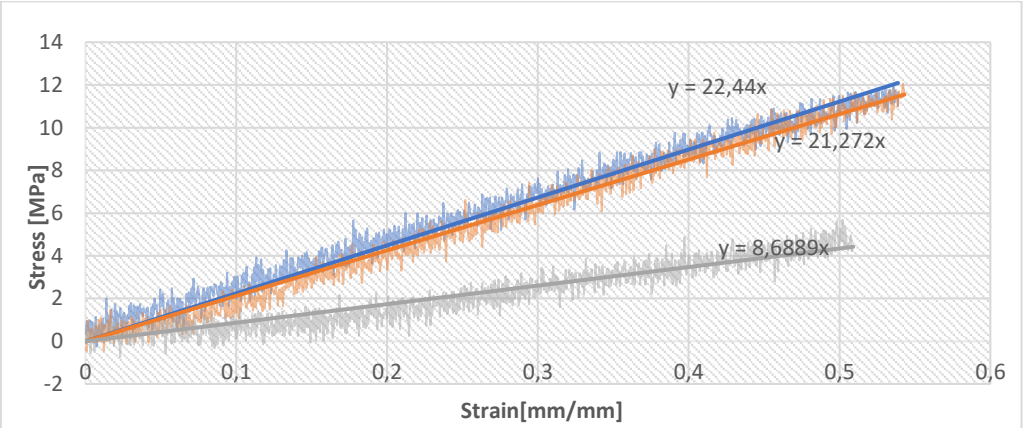

Figure 3.38: Stress-strain diagram of P(VDF-TrFE-MAF) fibers

In the case of the copolymer P(VDF-TrFE-MAF) the Young's modulus is 21.86 ± 3.49 MPa.

In the table 3.14 we report all the mechanical information about the three copolymers.

MECHANICAL TESTS		
FIBERS	***Young's modulus E*** *[MPa]*	***R max***
P(VDF-HFP)	7.18± 3.63 MPa	$1.2\pm 0.3\ \frac{mm}{mm}$
P(VDF-TrFE-HFP)	14.88± 1.23 MPa	$0.25\frac{mm}{mm}$
P(VDF-TrFE-MAF)	21.86± 3.49 MPa	$0.5\pm 0.1\ \frac{mm}{mm}$

Table 3.14 : Mechanical characteristics

The tensile test results of the electrospun fibrous membranes of the three polymers are reported in figure 3.39 for comparison. P(VDF-TrFE-MAF) fibers have the highest Young's modulus and therefore, the higher the Young's modulus value the less deformable the material is.

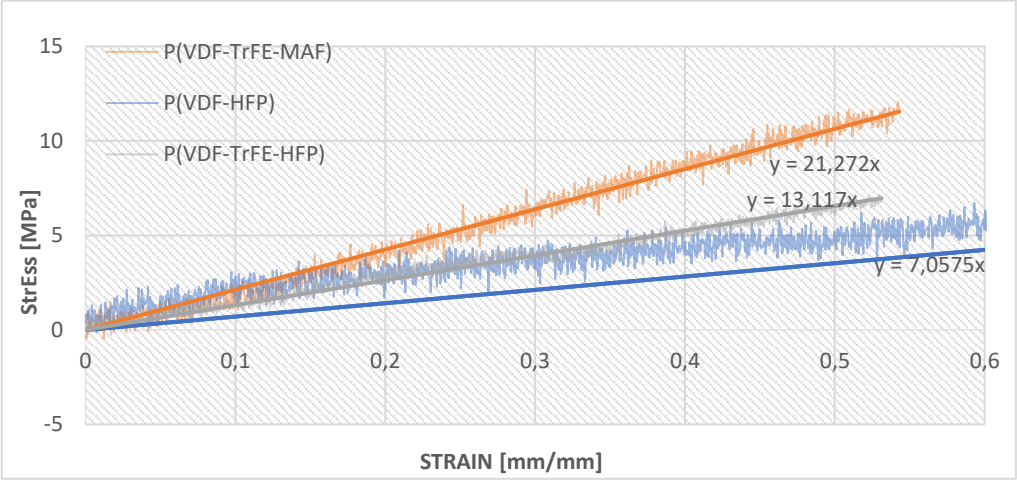

Figure 3.39: Mechanical comparison between three copolymers

3.5 Contact angle measurements

The wettability of the fiber membranes and of the polymer films was assessed by contact angle measurements with water and hexadecane.
Figure 3.40 shows a water droplet on a fibrous membrane of P(VDF-HFP).

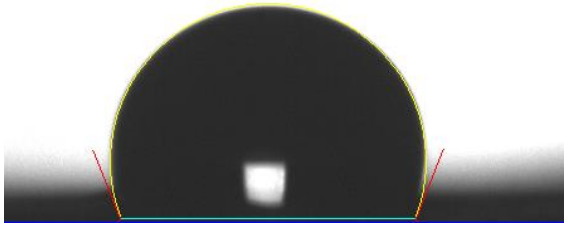

Figure 3.40: Representative figure of contact angle measurements of a drop of water on P(VDF-HFP) fibers membrane.

The measured contact angle is θ_w=111 °. This result indicates the hydrophobicity of the P(VFD-HFP) fibers since the value is higher than 90 °, threshold value for hydrophobic behavior.
Instead when hexadecane is used, the droplet is completely absorbed by the fibers of P(VDF-HFP) thus the surface is oleophilic.
If we consider a P(VDF-HFP) film, (after drying in an oven at 40 °C for one day) we find a different behaviour. When water is used (figure 3.41) the material still shows a hydrophobic behavior (the contact angle is 101°). While when hexadecane is used on P(VDF-HFP) film we obtain a contact angle of 26°, as can be seen in figure 3.42.

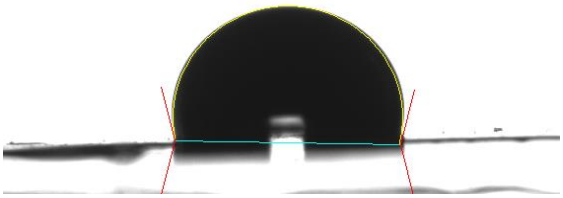

Figure 3.41: Representative figure of contact angle measurements of water on P(VDF-HFP) casted dried film.

Figure 3.42: Contact angle measurements of a P(VDF-HFP) dried film with hexadecane as liquid.

The water contact angle of P(VDF-TrFE-HFP) fibers (figure 3.43) is around θ_w =116°. This result indicates the hydrophobicity of P(VFD-TrFE-HFP) fibers.

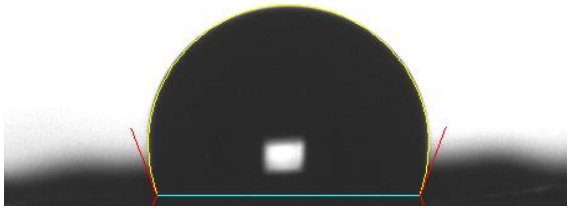

Figure 3.43: Representative figure of contact angle measurements of a drop of water as liquid on P(VDF-TrFE-HFP) fibers.

Instead when using hexadecane the droplet is completely absorbed by the P(VDF-TrFE-HFP) fibers so the surface is oleophilic.

If we consider P(VDF-TrFE-HFP) films (after drying in oven at 40 °C for one day), the contact angle with water is 107.5°, thus it still shows a hydrophobic behavior (figure 3.44).

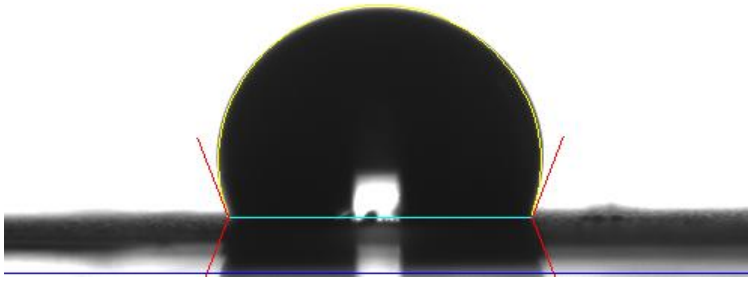

Figure 3.44: Representative figure of contact angle measurements of a drop of water as liquid on P(VDF-TrFE-HFP) dried film.

While when we analyse the hexadecane on P(VDF-TrFE-HFP) film we obtain a contact angle of 41°, a slight wettability, as shown in figure 3.45:

Figure 3.45: Contact angle measurements of a P(VDF-TrFE-HFP) dried film with hexadecane as liquid.

The contact angle using a droplet of water of P(VFD-TrFE-MAF) fiber membranes (figure 3.46) is around θ_w =114.5°; also this copolymer exhibits an hydrophobic but oleophilic surface because also in this case the droplet of hexadecane is completely absorbed.

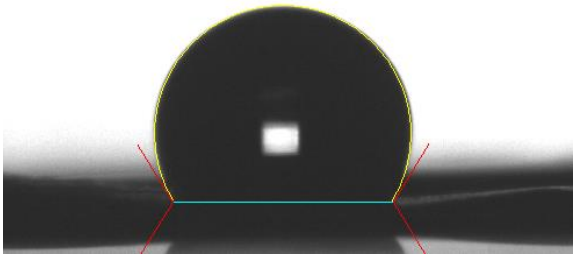

Figure 3.46: Representative figure of contact angle measurements of a drop of water as liquid on P(VDF-TrFE-MAF) fibers.

If we consider P(VDF-TrFE-MAF) films (after drying in oven at 40 °C for one day), the contact angle with water is around 108°; the film still shows a hydrophobic behaviour (figure 3.47).

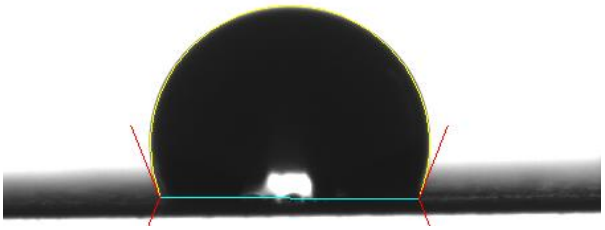

Figure 3.47: Representative figure of contact angle measurements of a drop of water as liquid on P(VDF-TrFE-MAF) dried film.

While when we analyse the hexadecane on P(VDF-TrFE-HFP) film we obtain a contact angle of 40.5°, represented by figure 3.48:

Figure 3.48 : Contact angle measurements of a P(VDF-TrFE-HFP) dried film on the left and P(VDF-TrFE-MAF) dry film on the right with hexadecane as liquid.

In table 3.15 all the information related to the contact angles of the three polymers evaluated on the fibres and the dried films using water and hexadecane as contact liquid respectively are collected. The three copolymers show a similar behavior: they are highly hydrophobic and oleophilic. This behavior is even emphasized (higher contact angle with water and lower contact angle with hexadecane) when the materials are in the form of electrospun fibrous membranes. Therefore an application of the membranes in the field of water/oil separation can be foreseen.

CONTACT ANGLES				
Samples	***Water***		***Hexadecane***	
	Fibers	Dried film	Fibers	Dried film
P(VDF-HFP)	$111° \pm 1°$	$101° \pm 1°$	*0°*	$26° \pm 2°$
P(VDF-TrFE-HFP)	$115.7° \pm 5°$	$107° \pm 5°$	*0°*	$41° \pm 3°$
P(VDF-TrFE-MAF)	$114.5° \pm 5°$	$108° \pm 3°$	*0°*	$40.5° \pm 3°$

Table 3.15: Summary of contact measurement angles related to dried films and fibers

4 Conclusion

In this work fibers from fluorinated copolymers were obtained through electrospinning their solutions. Different spinning conditions were analysed and the best conditions for obtaining microfibers were found using characteristic process parameters: feed rate = 1.5 ml/h, voltage = 15 kV, working distance =15 cm.
Instead related to solution concentration 15% wt of copolymer has been chosen. The electrospinning process was assured thanks to these specific parameters so production of regular fibers can also be obtained.
For the copolymer poly (vinylinedefluoride-co-hexafluoropropylene, poly (VDF-HFP), the average fiber diameter had shown a wider heterogeneus distribution around 2-3 μm and it could reach up to 7 μm.
Instead for poly (vinylidene fluoride - trifluoroethylene –hexafluoropropylene), poly (VDF-TrFE-HFP) and for poly (vinylidene fluoride –trifluoroethylene- (trifluoromethyl)acrylic acid), poly (VDF-TrFE-MAF) the average sizes were homogeneous, so we found all fibers with diameters of 1 μm approximately.
The fibers were collected in the form of mat and subjected to several analyses in order to obtain a characterization of their bulk and surfaces properties. By FTIR and XRD it was assessed the presence of the crystalline β phase related to P(VDF) in all copolymers and its increase after spinning due to the drawing of the material.
By DSC, crystallization and melting points of each material in the form of polymer and fibers were found together with the Curie temperature, i.e. the temperature at which spontaneously a ferroelectric material becomes paraelectric, losing its most interesting electroactive properties.
As far as the thermal decomposition behaviour is concerned, by TGA it was confirmed the excellent thermal stability of the copolymers after spinning.
The electrospun fibrous membranes of the three polymers were also analyzed by tensile tests: data show that the P(VDF-TrFE-MAF) fibers has the highest Young's modulus and therefore, the higher the Young's modulus value, less deformable is the material.
The contact angle measurements with water demonstrated the hydrophobicity of P(VFD) copolymers fibers. Wettability with hexadecane is very high, i.e. the fibers are oleophilic. Therefore the electrospun membranes obtained could be of interest in separation of water-in-oil emulsions.

5 Abbreviations and symbols

- ES: electrospinning
- VDF : vinylidene fluoride
- HFP : Hexafluoropropylene
- P(VDF-HFP): poly (vinylidene fluoride- Hexafluoropropylene)
- TrFE : trifluoroethylene
- P(VDF-TrFE): poly (vinylidene fluoride-co-trifluoroethylene)
- P(VDF-TrFE-HFP) = poly (vinylidene fluoride- trifluoroethylene-Hexafluoropropylene)
- MAF: 2(trifluoromethyl)acrylic
- P(VDF-TrFE-MAF): poly (vinylidene fluoride- trifluoroethylene-2(trifluoromethyl)acrylic)
- DMSO: dimethyl sulfoxide
- FESEM: Field Emission Scanning Electron Microscope
- XRD :X-ray-diffration
- FT-IR: Fourier transform infrared
- DSC: Differential Scanning Calorimetry
- TGA: Thermogravimetric Analysis
- FE: ferroelectric
- PE: paraelectric
- Tc,H_C: Curie conditions
- Tm,Hm: melting conditions
- T_{CR}, $H_{CR:}$ crystallization conditions
- α
- β
- γ
- 2θ
- λ
- d

6 Bibliography

[1] S. Agarwal, S. Horst, and M. Bognitzki, “Electrospinning of fluorinated polymers: Formation of superhydrophobic surfaces,” *Macromol. Mater. Eng.*, vol. 291, no. 6, pp. 592–601, 2006, doi: 10.1002/mame.200600076.

[2] J. Xue, T. Wu, Y. Dai, and Y. Xia, “Electrospinning and electrospun nanofibers: Methods, materials, and applications,” *Chem. Rev.*, vol. 119, no. 8, pp. 5298–5415, 2019, doi: 10.1021/acs.chemrev.8b00593.

[3] N. Bhardwaj and S. C. Kundu, “Electrospinning: A fascinating fiber fabrication technique,” *Biotechnol. Adv.*, vol. 28, no. 3, pp. 325–347, 2010, doi: 10.1016/j.biotechadv.2010.01.004.

[4] M. Alazab, G. R. Mitchell, F. J. Davis, and S. D. Mohan, “Sustainable Electrospinning of Nanoscale Fibres,” *Procedia Manuf.*, vol. 12, no. December 2016, pp. 66–78, 2017, doi: 10.1016/j.promfg.2017.08.009.

[5] X. Shi, W. Zhou, D. Ma, Q. Ma, and D. Bridges, “Review Article Electrospinning of Nanofibers and Their Applications for Electrospinning of Nanofibers and Their Applications for,” vol. 2015, no. May, 2015, doi: 10.1155/2015/140716.

[6] K. S. Athira, P. Sanpui, and K. Chatterjee, “Fabrication of Poly(Caprolactone) Nanofibers by Electrospinning,” *J. Polym. Biopolym. Phys. Chem.*, vol. 2, no. 4, pp. 62–66, 2014, doi: 10.12691/jpbpc-2-4-1.

[7] X. Shi *et al.*, “Electrospinning of Nanofibers and Their Applications for Energy Devices,” *J. Nanomater.*, vol. 2015, 2015, doi: 10.1155/2015/140716.

[8] S. V. Fridrikh, J. H. Yu, M. P. Brenner, and G. C. Rutledge, “Controlling the Fiber Diameter during Electrospinning,” *Phys. Rev. Lett.*, vol. 90, no. 14, p. 4, 2003, doi: 10.1103/PhysRevLett.90.144502.

[9] S. H. Tan, R. Inai, M. Kotaki, and S. Ramakrishna, “Systematic parameter study for ultra-fine fiber fabrication via electrospinning process,” *Polymer (Guildf).*, vol. 46, no. 16, pp. 6128–6134, 2005, doi: 10.1016/j.polymer.2005.05.068.

[10] D. W. Shin, M. D. Guiver, and Y. M. Lee, “Hydrocarbon-Based Polymer Electrolyte Membranes: Importance of Morphology on Ion Transport and Membrane Stability,” *Chem. Rev.*, vol. 117, no. 6, pp. 4759–4805, 2017, doi: 10.1021/acs.chemrev.6b00586.

[11] O. S. Yördem, M. Papila, and Y. Z. Menceloğlu, “Effects of electrospinning parameters on polyacrylonitrile nanofiber diameter: An investigation by response surface methodology,” *Mater. Des.*, vol. 29, no. 1, pp. 34–44, 2008, doi: 10.1016/j.matdes.2006.12.013.

[12] M. A. Alfaro De Prá, R. M. Ribeiro-do-Valle, M. Maraschin, and B. Veleirinho, “Effect of collector design on the morphological properties of polycaprolactone electrospun fibers,” *Mater. Lett.*, vol. 193, pp. 154–157, 2017, doi: 10.1016/j.matlet.2017.01.102.

[13] F. Topuz, B. Satilmis, and T. Uyar, “Electrospinning of uniform nanofibers of Polymers of Intrinsic Microporosity (PIM-1): The influence of solution conductivity

and relative humidity," *Polymer (Guildf).*, vol. 178, no. June, p. 121610, 2019, doi: 10.1016/j.polymer.2019.121610.

[14] A. Bauer, K. Lee, C. Song, Y. Xie, J. Zhang, and R. Hui, "Pt nanoparticles deposited on TiO2 based nanofibers: Electrochemical stability and oxygen reduction activity," *J. Power Sources*, vol. 195, no. 10, pp. 3105–3110, 2010, doi: 10.1016/j.jpowsour.2009.11.107.

[15] J. Xie, M. R. MacEwan, W. Z. Ray, W. Liu, D. Y. Siewe, and Y. Xia, "Radially aligned, electrospun nanofibers as dural substitutes for wound closure and tissue regeneration applications," *ACS Nano*, vol. 4, no. 9, pp. 5027–5036, 2010, doi: 10.1021/nn101554u.

[16] S. Sankar, C. S. Sharma, S. N. Rath, and S. Ramakrishna, "Electrospun nanofibres to mimic natural hierarchical structure of tissues: application in musculoskeletal regeneration," *J. Tissue Eng. Regen. Med.*, vol. 12, no. 1, pp. e604–e619, 2018, doi: 10.1002/term.2335.

[17] J. Zhang *et al.*, "Selective Endothelial Cell Adhesion via Mussel-Inspired Hybrid Microfibrous Scaffold," *ACS Appl. Nano Mater.*, vol. 1, no. 4, pp. 1513–1521, 2018, doi: 10.1021/acsanm.8b00017.

[18] X. F. Wu and A. L. Yarin, "Recent progress in interfacial toughening and damage self-healing of polymer composites based on electrospun and solution-blown nanofibers: An overview," *J. Appl. Polym. Sci.*, vol. 130, no. 4, pp. 2225–2237, 2013, doi: 10.1002/app.39282.

[19] Y. S. Lee, G. Collins, and T. Livingston Arinzeh, "Neurite extension of primary neurons on electrospun piezoelectric scaffolds," *Acta Biomater.*, vol. 7, no. 11, pp. 3877–3886, 2011, doi: 10.1016/j.actbio.2011.07.013.

[20] F. Peng, X. Yu, and M. Wei, "In vitro cell performance on hydroxyapatite particles/poly(L-lactic acid) nanofibrous scaffolds with an excellent particle along nanofiber orientation," *Acta Biomater.*, vol. 7, no. 6, pp. 2585–2592, 2011, doi: 10.1016/j.actbio.2011.02.021.

[21] B. Ameduri, "From vinylidene fluoride (VDF) to the applications of VDF-Containing polymers and copolymers: Recent developments and future trends," *Chem. Rev.*, vol. 109, no. 12, pp. 6632–6686, 2009, doi: 10.1021/cr800187m.

[22] Q. M. Zhang, V. Bharti, and X. Zhao, "Giant electrostriction and relaxor ferroelectric behavior in electron- irradiated poly(vinylidene fluoride-trifluoroethylene) copolymer," *Science (80-.).*, vol. 280, no. 5372, pp. 2101–2104, 1998, doi: 10.1126/science.280.5372.2101.

[23] L. Ruan, X. Yao, Y. Chang, L. Zhou, G. Qin, and X. Zhang, "Properties and applications of the β phase poly(vinylidene fluoride)," *Polymers (Basel).*, vol. 10, no. 3, pp. 1–27, 2018, doi: 10.3390/polym10030228.

[24] C. Yu *et al.*, "Functionalized Polyvinylidene Fluoride Electrospun Nanofibers and Applications," *Intech*, vol. i, no. tourism, p. 13, 2012, doi: 10.1016/j.colsurfa.2011.12.014.

[25] S. Abbrent, J. Plestil, D. Hlavata, J. Lindgren, J. Tegenfeldt, and Å. Wendsjö,

"Crystallinity and morphology of PVdF-HFP-based gel electrolytes," *Polymer (Guildf).*, vol. 42, no. 4, pp. 1407–1416, 2001, doi: 10.1016/S0032-3861(00)00517-6.

[26] "Chemical-structures-of-vinylidene-fluoride-VF2-tetrafluoroethylene-TFE_fig1_232072692 @ www.researchgate.net." .

[27] J. C. Wang, Y. P. Jiang, Y. J. Lin, S. H. Chan, and M. C. Wu, "Trifluoroethylene bond enrichment in P(VDF-TrFE) copolymers with enhanced ferroelectric behaviors by plasma fluorination on bottom electrode," *J. Taiwan Inst. Chem. Eng.*, vol. 107, pp. 152–160, 2020, doi: 10.1016/j.jtice.2019.11.005.

[28] X. Wang, C. Xiao, H. Liu, Q. Huang, and H. Fu, "Fabrication and properties of PVDF and PVDF-HFP microfiltration membranes," *J. Appl. Polym. Sci.*, vol. 135, no. 40, 2018, doi: 10.1002/app.46711.

[29] A. Roy, B. Dutta, and S. Bhattacharya, "Electroactive phase nucleation and non-isothermal crystallization kinetics study in [DEMM][TFSI] ionic liquid incorporated P(VDF-HFP) co-polymer membranes," *J. Mater. Sci.*, vol. 51, no. 17, pp. 7814–7830, 2016, doi: 10.1007/s10853-016-9978-4.

[30] Y. Li *et al.*, "Stretching-Induced Relaxor Ferroelectric Behavior in a Poly(vinylidene fluoride-co-trifluoroethylene-co-hexafluoropropylene) Random Terpolymer," *Macromolecules*, vol. 50, no. 19, pp. 7646–7656, 2017, doi: 10.1021/acs.macromol.7b01205.

[31] "The chemical formula of PVDF T rFE random copolymer www.researchgate.net." .

[32] T. Soulestin, P. Marcelino Dos Santos Filho, V. Ladmiral, T. Lannuzel, F. Domingues Dos Santos, and B. Améduri, "Ferroelectric fluorinated copolymers with improved adhesion properties," *Polym. Chem.*, vol. 8, no. 6, pp. 1017–1027, 2017, doi: 10.1039/c6py02063a.

[33] N. Jia, Q. He, J. Sun, G. Xia, and R. Song, "Crystallization behavior and electroactive properties of PVDF, P(VDF-TrFE) and their blend films," *Polym. Test.*, vol. 57, pp. 302–306, 2017, doi: 10.1016/j.polymertesting.2016.12.003.

[34] "www.sigmaaldrich.com." .

[35] P. E. Cassidy, "Well Architectured Fluoropolymers: Synthesis, Properties and Applications By Bruno Améduri and Bernard Boutevin (Ecole Nationale Supérieure de Chemie de Montpellier). Elsevier Ltd: Oxford. 2004. xviii + 481 pp. $189.00. ISBN 0-08-044388-5.," *J. Am. Chem. Soc.*, vol. 127, no. 9, pp. 3233–3234, 2005, doi: 10.1021/ja040989f.

[36] B. Améduri, B. Boutevin, and G. Kostov, "Fluoroelastomers: Synthesis, properties and applications," *Prog. Polym. Sci.*, vol. 26, no. 1, pp. 105–187, 2001, doi: 10.1016/S0079-6700(00)00044-7.

[37] X. Wang, C. Xiao, H. Liu, Q. Huang, J. Hao, and H. Fu, "Poly(vinylidene fluoride-hexafluoropropylene) porous membrane with controllable structure and applications in efficient oil/water separation," *Materials (Basel).*, vol. 11, no. 3, 2018, doi: 10.3390/ma11030443.

[38] M. M. Nasef, H. Saidi, and K. M. Dahlan, "Comparative investigations of radiation-

grafted proton-exchange membranes prepared using single-step and conventional two-step radiation-induced grafting methods," *Polym. Int.*, vol. 60, no. 2, pp. 186–193, 2011, doi: 10.1002/pi.2925.

[39] N. Golzari, J. Adams, and S. Beuermann, "Inducing β phase crystallinity in block copolymers of vinylidene fluoride with methyl methacrylate or styrene," *Polymers (Basel).*, vol. 9, no. 8, 2017, doi: 10.3390/polym9080306.

[40] PANalytical, "X ' Pert 3 Powder Let materials work for you Advancing materials research."

[41] S. Dalle Vacche *et al.*, "High diffusion barrier and piezoelectric nanocomposites based on polyvinylidene fluoride-trifluoroethylene copolymer and hydrophobized clay," *J. Polym. Sci. Part B Polym. Phys.*, vol. 55, no. 24, pp. 1828–1836, 2017, doi: 10.1002/polb.24432.

[42] Y. Toshiharu, T. Masayoshi, and S. Jun-Ichi, "Transition behavior and dielectric properties in trifluoroethylene and vinylidene fluoride copolymers," *Polym. J.*, vol. 12, no. 4, pp. 209–223, 1980, doi: 10.1295/polymj.12.209.

[43] X. Cai, T. Lei, D. Sun, and L. Lin, "A critical analysis of the α, β and γ phases in poly(vinylidene fluoride) using FTIR," *RSC Adv.*, vol. 7, no. 25, pp. 15382–15389, 2017, doi: 10.1039/c7ra01267e.

[44] "P(VDF-HFP) dati Montpellier.pdf." .

[45] S. Hietala *et al.*, "Structural investigation of radiation grafted and sulfonated poly(vinylidene fluoride), PVDF, membranes," *J. Mater. Chem.*, vol. 7, no. 5, pp. 721–726, 1997, doi: 10.1039/a607675k.

[46] M. Shehzad and T. Malik, "Antiferroelectric Behavior of P(VDF-TrFE) and P(VDF-TrFE-CTFE) Ferroelectric Domains for Energy Harvesting," *ACS Appl. Energy Mater.*, vol. 1, no. 6, pp. 2832–2840, 2018, doi: 10.1021/acsaem.8b00478.

[47] S. Ramesh and S. C. Lu, "Effect of lithium salt concentration on crystallinity of poly(vinylidene fluoride-co-hexafluoropropylene)-based solid polymer electrolytes," *J. Mol. Struct.*, vol. 994, no. 1–3, pp. 403–409, 2011, doi: 10.1016/j.molstruc.2011.03.065.